

Magnetism and dynamics of oxide interfaces (electronic theory)

Dissertation

zur Erlangung des akademischen Grades
doctor rerum naturalium (Dr. rer. nat.)

vorgelegt der
Mathematisch-Naturwissenschaftlich-Technischen Fakultät
(mathematisch-naturwissenschaftlicher Bereich)
der Martin-Luther-Universität Halle-Wittenberg

von

Herrn Oleksandr Ney

geb. am 25.06.1976 in Odessa

Gutachterin/Gutachter:

1. Prof. Dr. W. Hübner (Uni-Kaiserslautern)
2. Prof. Dr. I. Mertig (Uni-Halle)
3. Prof. Dr. O. Eriksson (Uppsala University)

Halle (Saale)

urn:nbn:de:gbv:3-000006255

[<http://nbn-resolving.de/urn/resolver.pl?urn=nbn%3Ade%3Agbv%3A3-000006255>]

Tag der mündlichen Prüfung:
14. Nov. 2003

Contents

1	Introduction	5
2	Crystal Field Theory	7
2.1	Hamiltonian	8
2.2	Crystal field for different symmetries	10
2.3	Wavefunctions	16
2.4	Calculation of matrix elements	19
2.4.1	One-electron operator	19
2.4.2	Two-electron operator	20
2.4.3	Interaction with Nucleus and Kinetic Energy	20
2.4.4	Coulomb Interaction	21
2.4.5	Interaction with Crystal Field	22
2.4.6	Spin-orbit interaction	26
2.5	One-electron case	27
2.6	Many electrons	28
3	Crystal Field Theory: Results for NiO	35
4	Crystal Field Theory: Results for CoO	47
5	Crystal Field Theory: Results for FeO	53
6	Second harmonic generation	57
6.1	Macroscopic theory	57
6.2	Magnetic symmetry	59
6.2.1	Magnetic point groups	59
6.2.2	Magnetic point groups. Bulk <i>fcc</i>	60
6.2.3	Magnetic point groups. (001) surface <i>fcc</i>	61
6.2.4	Symmetry of the tensors	62
6.3	Microscopic theory	66
7	SHG Results	69

4

CONTENTS

8 Conclusions 75

9 Supplementary materials 79

Bibliography 79

Chapter 1

Introduction

The current speed of magnetic recording is of the order of nanoseconds, i.e. close to a single precession cycle of the magnetization (Larmor frequency). Achieving a significantly higher speed will require completely new approaches, such as hybrid or optical recording. In order to overcome the deficiencies of the contemporary computer memories and read-write heads of hard disks, both permanent and dynamic, new designs like magnetic random access memories (MRAMs) are under development [1]. They will eliminate the mechanical motion and the hierarchical structure of the contemporary memories and simplify the design of the CPUs. One of the most important components of these MRAMs are tunnelling magnetoresistance (TMR) devices, where the read-out current passing through the device depends on the relative magnetization of two ferromagnetic layers. The central layer of such a trilayer structure consists of an oxide sandwiched between a soft and a hard magnetic layer (often a ferro-/antiferromagnetic exchange-bias system). Therefore, the performance of these future devices depends heavily on the properties of oxides. Besides, one of the ferromagnetic layers is “pinned” by an antiferromagnet (exchange bias). Thus, the investigation of antiferromagnetic (AF) oxides (also of their spin dynamics) is of technological importance. As a further development, nano-oxide structures are proposed in order to replace the whole exchange-biased system of the tunnel junction.

For these applications it is necessary to develop a technique in order to investigate AF oxide surfaces and buried interfaces. Besides, already the preparation of TM oxide films is a challenge and requires a method to characterize the structure and magnetism of these materials. Such a technique can be optical second harmonic generation (SHG), since conventional linear optics is blind for antiferromagnetism. SHG has already proven as a versatile technique for the investigation of ferromagnetism at surfaces. The sensitivity of this technique to volume *antiferromagnetism* has been shown experimentally [2] and explained theoretically [3]. The sensitivity of SHG to *surface* antiferromagnetism has been predicted theoretically [4, 5].

Excited states in TM oxides have always been difficult to access theoretically due to the highly correlated $3d$ electrons. The localized nature of these optically active states makes them more amenable to theoretical methods usually applied for small clusters rather

than to band-structure approaches commonly used for extended solids. In our approach, these pronounced local-symmetry features are addressed by allowing for the full spherical symmetry of the Hamiltonian of a free ion and subsequently lowering the symmetry by the ligand field of the surface. The correlations are taken into account by coupling two, three, and four holes in the $3d$ and $4s$ shells. This significant extension of our previous results for the two-hole configuration [4, 6, 7] permits us to compute the electronic many-body structure of the majority of TMOs, in particular also CoO and FeO and their surfaces, thus demonstrating the versatility of our theoretical methods. Previous results of our calculations, allowing already for some technologically important predictions (fast spin dynamics accompanied by a long lasting coherence, laser-driven remagnetization), were presented in [6]. The system addressed in that earlier work was a prototypical Ni^{++} ion on NiO (001). Now we can address electronic configurations of various materials with similar structure. In this work, for the sake of consistency, we treat one surface orientation [(001)], one spin structure of the cubic AF oxides NiO, CoO, and FeO.

The field of nonlinear optics has been attracting a lot of attention from both experimental and theoretical points of view. One of the most intensively studied processes is the Sum Frequency Generation and in particular Second Harmonic Generation. The first observation of Second Harmonic Generation by Franken et al. in 1961 [8] followed the development of pulsed lasers having high intensity of the outgoing light. The first experimental observation of SHG from a metal surface was made by Brown et al. [9].

At the present time, optical SHG promised as a powerful tool which being sensitive to magnetism may give an information about magnetic ordering of the sample. However, the investigation of femtosecond spin-dynamics of antiferromagnets is still in its infancy.

Here, we will also describe the electronic theory of a pump-and-SHG-probe experiment on NiO (001). During such an experiment, the sample is excited by a strong laser pulse, and then (with a variable delay of several tens to hundreds of femtoseconds) the second - probe - pulse is issued. The SHG response of the excited sample to this second pulse is monitored and can reveal the dynamic properties of the sample.

Taking into account the arguments mentioned above, we formulate the main aims of this work as follows:

- To get the proper description of the electronic structure of the transition metal monoxides NiO, CoO, and FeO by means of Crystal Field Theory;
- To describe the magnetic states of these systems with the help of magnetic point groups;
- To compute the optical properties of those systems under the influence of an externally applied laser light.

Chapter 2

Crystal Field Theory

One of the main features of transition metal oxides, which makes them difficult to describe theoretically, is the strong localization of their $3d$ -electrons. There is a powerful method allowing to deal with such systems is the Ligand Field Theory (LFT) (which is also known as Crystal Field Theory (CFT) if the surrounding ligands are replaced by the point charges). This theory helps to find the eigenstates and corresponding energy levels on the basis of the known symmetry of the system. Although the theory is well described in many of the textbooks as an example, it is usually restricted to the one-electron case or many-electrons for low lying levels only and an extension of it to the whole set of many-electron states for the given electronic configuration is either omitted or just sketched. In this work we would like to fill this gap and, highlighting the problems arising there, present the way to overcome those.

The CFT, being a perturbation theory, may be used in different ways. One particular realization is based on the assumption about the influence of spin-orbit coupling (SOC) and field of ligands (LF) on the system. The CFT theory describes the following systems:

- A Free ion without SOC (spherical symmetry, gas phase)
- B Ion with SOC
- C Ion with SOC placed in the field of ligands (strong SOC, weak LF)
- D Ion surrounded by ligands
- E Ion surrounded by ligands with SOC (strong LF, weak SOC)

Depending on the relative strength of an SOC and the LF one may neglect the smaller interaction and choose between the incomplete schemes $A \rightarrow B$ or $A \rightarrow D$, or implement one of the complete LFT schemes $A \rightarrow C$ or $A \rightarrow E$.

The atomic states may be calculated within either LS - or jj -coupling. In the first case orbital (\mathbf{l}) and spin (\mathbf{s}) angular momenta of the electrons are combined independently giving the state, characterized by the set of quantum numbers L, M, S, S_z , or in spectroscopical

notation $^{2S+1}L_M^{S_z}$. In the second one, the spin momentum \mathbf{s} of each electron is coupled to its own orbital momentum \mathbf{l} giving a resultant momentum $\mathbf{j} = \mathbf{l} + \mathbf{s}$ and then all the \mathbf{j} -s are combined to give the state of the atom, which is characterized in this case by the set of quantum numbers J, J_z .

If symmetry of the system is lowered by some interaction, its state is defined by irreducible representations of angular momenta in the given symmetry. Interaction with the ligand field does not depend on the spin degree of freedom of electrons. Thus, states of ions in the media are characterized by the set of quantum numbers Γ, S, S_z , where Γ denotes irreducible representations of orbital angular momenta in given point symmetry group (for the O_h group Γ may be $A_{1g}(1)$, $A_{2g}(1)$, $E_g(2)$, $T_{1g}(3)$, $T_{2g}(3)$, $A_{1u}(1)$, $A_{2u}(1)$, $E_u(2)$, $T_{1u}(3)$, or $T_{2u}(3)$; for the C_{4v} group it is $A_1(1)$, $A_2(1)$, $B_1(1)$, $B_2(1)$, or $E(2)$; the number in parentheses shows the degeneracy of the representation). The changing of degeneracy of spherically symmetric levels and the occurrence of corresponding multiplets are governed by Group Theory.

Because strong SOC appears to be important for heavy ions only, its impact on transition-metal ions is assumed to be small compared with LF. However, the inclusion of SOC matters in the optical spectra for such systems changing the selection rules.

The flow chart of our realization of CFT is shown on Fig. 2.1. The ionic model was treated by Racah in his four classic papers [10, 11, 12, 13]. In particular, he defined the tensor operator and developed an appropriate tensor algebra, which replaces the “diagonal sum method” (developed by Slater in [14]) for calculating the energy levels. The fractional parentage coefficients (CFP) introduced by him have been widely used up to the present time. However, his theory for pure ions is difficult to apply for ions situated in the solid material. Although both Racah’s and Slater’s methods exactly describe free ions, they become too complicated for lower symmetries, when states having the same set of quantum numbers may appear more than once in the configuration. In such cases one may get with those methods the sum of corresponding energies only; in order to extract the energies themselves one has to compute the whole Hamiltonian matrix and diagonalize it afterwards. The wavefunctions of the system have to reflect its symmetry. As a starting point we use the linear combination of Slater’s determinants (so called cubic harmonics), which allows to label the levels. However, they are only approximate in the sense, that they give a block-diagonal form of the Hamiltonian matrix. These blocks have to be diagonalized to obtain the exact wavefunction of the system, which completely describes metal ions in different environments.

2.1 Hamiltonian

In CFT one tries to find the solution of the Schrödinger equation with the Hamiltonian

$$\hat{H} = \hat{H}_0 + \hat{H}_C + \hat{H}_{CF} + \hat{H}_{SO}, \quad (2.1)$$

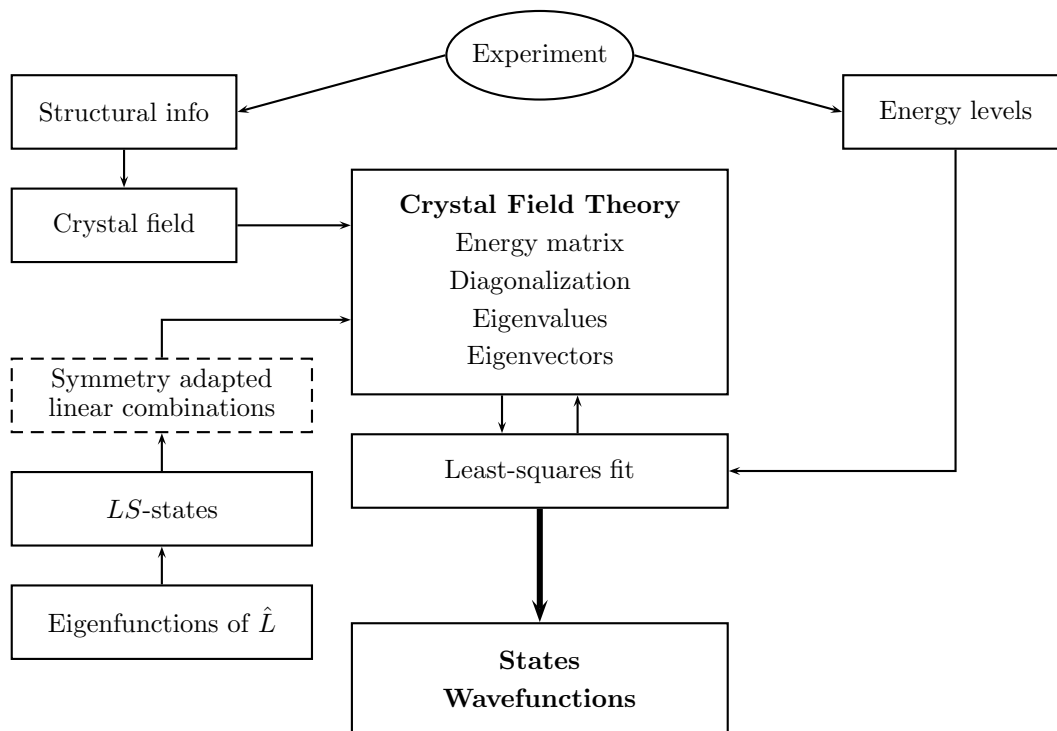


Figure 2.1: Flow chart for Crystal Field Theory

where \hat{H}_0 describes a spherically symmetric interaction, \hat{H}_C is the Coulomb interaction, \hat{H}_{CF} is the interaction with crystal field, and \hat{H}_{SO} is the spin-orbit interaction.

The first term \hat{H}_0 includes the kinetic energy of the particles and their interaction with the nucleus and can therefore be omitted

$$\hat{H}_0 = \sum_{i=1}^N -\frac{1}{2}\Delta_i + \hat{V}_N(\vec{r}_i) \quad (2.2)$$

since it only shifts the whole configuration (we are not interested in the absolute energies, rather in their differences, which give the information about allowed optical transitions between levels formed in the given electronic configurations).

The second term \hat{H}_C describes a pair interaction between the electrons and may be expressed as follows:

$$\hat{H}_C = \sum_{i=1}^{N-1} \sum_{j>i}^N \frac{1}{r_{12}}. \quad (2.3)$$

The third term is responsible for the interaction of the electrons with surrounding ligands. It strongly depends on the symmetry of the system. In this work we consider two symmetries of the crystal, of which the first is O_h and appears in the bulk monoxide, and the second one is C_{4v} which reflects the symmetry of the (001) surface (perfect bulk termination is assumed).

The fourth term describes the spin-orbit interaction derived from the Dirac equation and may be written as

$$\hat{H}_{SO} = \xi(r)\mathbf{l} \cdot \mathbf{s}, \quad (2.4)$$

where $\xi(r)$ is

$$-\frac{e\hbar^2}{2m^2c^2} \frac{1}{r} \frac{dU(r)}{dr} \quad (2.5)$$

with a spherically symmetric potential $U(r)$ for the electron.

Now let us express the electrostatic potential produced by surrounding oxygen ions for the MeO (where Me=Ni,Co,Fe) system. For the sake of consistency we treat those oxygen ions as point charges and consider only one electron with hydrogen-like wavefunctions (see Fig. 2.2). The extension to many-electron cases will be discussed later.

2.2 Crystal field for different symmetries

In this work we deal with two basic symmetries O_h and C_{4v} which describe bulk and (001) surface of *fcc* crystals respectively. Within CFT these symmetries are delineated by one metal ion and six or five surrounding point charges, as depicted in the Fig. 2.2.

In principle, if we would be interested in the calculations of the radial behavior for the wavefunction of the system, it is necessary to include spatial distribution of ligand electrons extended towards the metal ion, which makes the CFT treatment much more complicated.

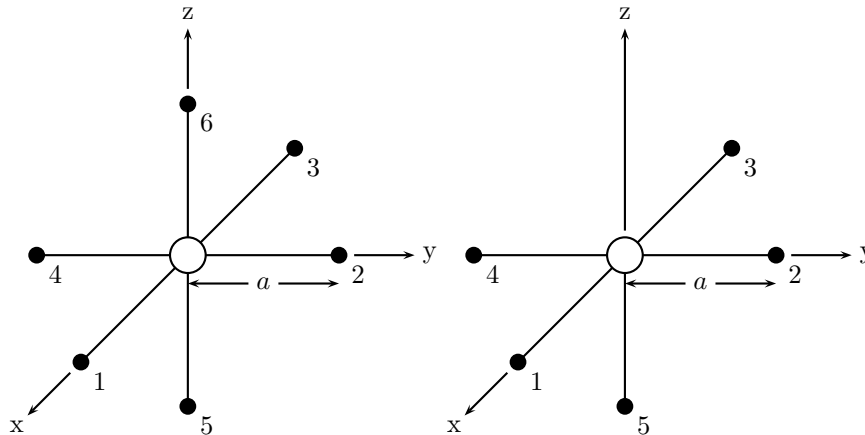


Figure 2.2: Metal ion surrounded by point-charges; the left panel represents O_h symmetry, while the right one reflects the (001) surface of an *fcc* material. \bullet $-Ze$ point charge. \circ metal ion.

Since in this work we are able to omit the radial parts by fitting the appearing integrals, this spatial distribution may be omitted (see [15], p.130), which allows to simplify the treatment without any loss in accuracy (the equivalence of surrounding ligands found in equivalent directions holds for both cases).

Thus it is the key issue of CFT to find an expression for the field produced by point charges which possess a given symmetry. The point charges are assumed to be fixed on equal distances a from the central ion, thus giving an octahedral environment in the bulk or cut octahedral environment on the (001) surface.

The contribution of the surroundings to the electron potential energy is expressed as

$$V_{CF}(\vec{r}) = \sum_{i=1}^{N_s} \frac{Ze^2}{|\vec{R}_i - \vec{r}|}, \quad (2.6)$$

where \vec{r} is the electron coordinate and \vec{R}_i is the position vector of the i -th point charge, and summation is made over all the point charges ($N_s = 5$ or 6).

The perturbation V_{CF} is small compared with electron-nucleus and electron-electron Coulomb interactions. In what follows (2.6) may be expanded in terms of the Legendre polynomials:

$$V_{CF}(\vec{r}) = Ze^2 \sum_{i=1}^{N_s} \sum_{k=0}^{\infty} \frac{r_{<}^k}{r_{>}^{k+1}} P_k(\cos \omega_i), \quad (2.7)$$

in which $r_{<}$ and $r_{>}$ are the lesser and the greater of a and r respectively, and ω_i is the angle between vectors \vec{R}_i and \vec{r} . The strong localization of electronic orbitals in transition metal oxides allows to replace to a good approximation $r_{>}$ and $r_{<}$ in (2.7) by a and r

respectively, which gives

$$V_{CF}(\vec{r}) = Ze^2 \sum_{i=1}^{N_s} \sum_{k=0}^{\infty} a^{-1} \left(\frac{r}{a}\right)^k P_k(\cos \omega_i). \quad (2.8)$$

In the equation above the Legendre polynomials may be expanded using the addition theorem for spherical harmonics:

$$P_k(\cos \omega_i) = \frac{4\pi}{2k+1} \sum_{m=-k}^k Y_{km}(\theta\phi) Y_{km}^*(\theta_i\phi_i), \quad (2.9)$$

where the $Y_{km}(\theta\phi)$'s are the spherical harmonics, and (r, θ, ϕ) and (a, θ_i, ϕ_i) are the polar coordinates of \vec{r} and \vec{R}_i , respectively. Here, $Y_{km}^*(\theta_i\phi_i)$ is the complex conjugate of $Y_{km}(\theta_i\phi_i)$ and is equal to $(-1)^m Y_{k-m}(\theta_i\phi_i)$.

From (2.8) and (2.9), V_c is given as a function of the electron coordinate \vec{r} as follows:

$$V_{CF}(\vec{r}) = \sum_{k=0}^{\infty} \sum_{m=-k}^k r^k q_{km} C_m^{(k)}(\theta\phi), \quad (2.10)$$

where

$$q_{km} = \left(\frac{4\pi}{2k+1}\right)^{1/2} \frac{Ze^2}{a^{k+1}} \sum_{i=1}^{N_s} Y_{km}^*(\theta_i\phi_i), \quad (2.11)$$

and

$$C_m^{(k)}(\theta\phi) = \left(\frac{4\pi}{2k+1}\right)^{1/2} Y_{km}(\theta\phi). \quad (2.12)$$

Since $(\theta_1\phi_1)$, $(\theta_2\phi_2)$, \dots , $(\theta_6\phi_6)$ are known to be (the 6-th point charge is missing on the surface)

$$\left(\frac{\pi}{2}0\right), \left(\frac{\pi}{2}\frac{\pi}{2}\right), \left(\frac{\pi}{2}\pi\right), \left(\frac{\pi}{2}\frac{3\pi}{2}\right), (\pi 0), (00),$$

respectively, the q_{km} 's are given as

$$q_{k0} = \left(\frac{2}{2k+1}\right)^{1/2} \frac{Ze^2}{a^{k+1}} \left[\Theta_{k0}(0) + 4\Theta_{k0}\left(\frac{\pi}{2}\right) + \Theta_{k0}(\pi) \right], \quad (2.13)$$

$$q_{km} = \left(\frac{2}{2k+1}\right)^{1/2} \frac{Ze^2}{a^{k+1}} \Theta_{km}\left(\frac{\pi}{2}\right) \times \left[1 + \exp\left(i\frac{m\pi}{2}\right) + \exp(im\pi) + \exp\left(i\frac{3m\pi}{2}\right) \right], (m : \text{even} \neq 0) \quad (2.14)$$

$$q_{km} = 0 (m : \text{odd}), \quad (2.15)$$

in which Θ_{km} is defined by

$$Y_{km}(\theta\phi) = (2\pi)^{-1/2}\Theta_{km}(\theta)e^{im\phi}. \quad (2.16)$$

The explicit forms of Θ_{km} 's are given in Table 9.3. By inserting the explicit forms of Θ_{km} into (2.13)-(2.15), the explicit form of $V_c(\vec{r})$ is obtained from (2.13)-(2.15) and (2.10) for the bulk material as follows:

$$V_{CF}(\vec{r}) = \frac{6Ze^2}{a} + \frac{7Ze^2}{2a^5}r^4 \left\{ C_0^{(4)}(\theta\phi) + \left(\frac{5}{14}\right)^{1/2} [C_4^{(4)}(\theta\phi) + C_{-4}^{(4)}(\theta\phi)] \right\} + \dots \quad (2.17)$$

In this work we found higher terms in this expression. However, terms with $k > 4$ are not important in our case since integrals of the product of three spherical harmonics (which appear later)

$$\iint Y_{l_1 m_1}^* Y_{km} Y_{l_2 m_2} \sin \theta d\theta d\phi \quad (2.18)$$

which is proportional to the Clebsch-Gordan coefficient $C_{k0l_20}^{l_10}$ vanish if the triangle rule ($|l_1 - l_2| \leq k \leq l_1 + l_2$) is not satisfied. For 3d-electrons $l_1 = l_2 = 2$ which restricts the value of k to 0 - 4; while for 4s-electrons $l_1 = l_2 = 0$ leaving $k = 0$ only.

The first term in (2.17) represents the potential energy of the electron located at the position of the nucleus and elevates all the energy levels of the atom by the same amount, $6Ze^2/a$. The other terms split some of the degenerate energy levels as will be shown later. The field giving rise to the potential energy whose angular dependence is given as (2.17) is called a cubic field. This angular dependence is due to the geometrical arrangement of the point charges as shown in Fig. 2.2.

In the case of bulk material each metal ion is surrounded by six oxygen ions positioned

in the octahedra corners. The field produced by these charges has the following form:

$$V_{CFb}^0(r, \theta, \phi) = \frac{Ze^2}{a} 6C_0^{(0)}(\theta, \phi), \quad (2.19)$$

$$V_{CFb}^4(r, \theta, \phi) = r^4 \frac{Ze^2}{a^5} \left(\frac{7}{2} C_0^{(4)}(\theta, \phi) + \frac{\sqrt{70}}{4} (C_{-4}^{(4)}(\theta, \phi) + C_4^{(4)}(\theta, \phi)) \right), \quad (2.20)$$

$$V_{CFb}^6(r, \theta, \phi) = r^6 \frac{Ze^2}{a^7} \left(\frac{3}{4} C_0^{(6)}(\theta, \phi) - \frac{3\sqrt{14}}{8} (C_{-4}^{(6)}(\theta, \phi) + C_4^{(6)}(\theta, \phi)) \right), \quad (2.21)$$

$$V_{CFb}^8(r, \theta, \phi) = r^8 \frac{Ze^2}{a^9} \left(\frac{99}{32} C_0^{(8)}(\theta, \phi) + \frac{3\sqrt{154}}{32} (C_{-4}^{(8)}(\theta, \phi) + C_4^{(8)}(\theta, \phi)) + \frac{3\sqrt{1430}}{64} (C_{-8}^{(8)}(\theta, \phi) + C_8^{(8)}(\theta, \phi)) \right), \quad (2.22)$$

$$V_{CFb}^{10}(r, \theta, \phi) = r^{10} \frac{Ze^2}{a^{11}} \left(\frac{65}{64} C_0^{(10)}(\theta, \phi) - \frac{\sqrt{1430}\sqrt{3}}{64} (C_{-4}^{(10)}(\theta, \phi) + C_4^{(10)}(\theta, \phi)) - \frac{\sqrt{24310}}{128} (C_{-8}^{(10)}(\theta, \phi) + C_8^{(10)}(\theta, \phi)) \right), \quad (2.23)$$

where the coefficients $C_m^{(k)}$ are defined in (2.12). During the calculation of the energy matrix integrals over angles θ and ϕ are computed exactly, while the integration over r leads to few integrals only and their values may be found if some experimental energies are known.

Because of the highest symmetry of the system (O_h) all terms containing r in odd power and the term with r^2 vanish; the first (in the case of $3d$ -electrons with $l = 2$ this is the only one) term which defines multiplet levels is V_{CFb}^4 . Since the term V_{CFb}^0 does not depend on r , there is now splitting for s and p electrons. Higher terms might be important for rare-earth metals when the state of the system is defined by an incomplete $4f$ -shell with electrons having $l = 3$. For these systems the splitting of levels in the cubic field is defined by both V_{CFb}^4 and V_{CFb}^6 .

Removing one point charge (at the position z) leads to additional terms in the equation

for the crystal field:

$$V_{CFs}^0(r, \theta, \phi) = \frac{Ze^2}{a} 5C_0^{(0)}(\theta, \phi), \quad (2.24)$$

$$V_{CFs}^1(r, \theta, \phi) = r \frac{Ze^2}{a^2} (-C_0^{(1)}(\theta, \phi)), \quad (2.25)$$

$$V_{CFs}^2(r, \theta, \phi) = r^2 \frac{Ze^2}{a^3} (-C_0^{(2)}(\theta, \phi)), \quad (2.26)$$

$$V_{CFs}^3(r, \theta, \phi) = r^3 \frac{Ze^2}{a^4} (-C_0^{(3)}(\theta, \phi)), \quad (2.27)$$

$$V_{CFs}^4(r, \theta, \phi) = r^4 \frac{Ze^2}{a^5} \left(\frac{5}{2} C_0^{(4)}(\theta, \phi) \right. \\ \left. + \frac{\sqrt{70}}{4} (C_{-4}^{(4)}(\theta, \phi) + C_4^{(4)}(\theta, \phi)) \right), \quad (2.28)$$

$$V_{CFs}^5(r, \theta, \phi) = r^5 \frac{Ze^2}{a^6} (-C_0^{(5)}(\theta, \phi)), \quad (2.29)$$

$$V_{CFs}^6(r, \theta, \phi) = r^6 \frac{Ze^2}{a^7} \left(-\frac{1}{4} C_0^{(6)}(\theta, \phi) \right. \\ \left. - \frac{3\sqrt{14}}{8} (C_{-4}^{(6)}(\theta, \phi) + C_4^{(6)}(\theta, \phi)) \right), \quad (2.30)$$

$$V_{CFs}^7(r, \theta, \phi) = r^7 \frac{Ze^2}{a^8} (-C_0^{(7)}(\theta, \phi)), \quad (2.31)$$

$$V_{CFs}^8(r, \theta, \phi) = r^8 \frac{Ze^2}{a^9} \left(\frac{67}{32} C_0^{(8)}(\theta, \phi) \right. \\ \left. + \frac{3\sqrt{154}}{32} (C_{-4}^{(8)}(\theta, \phi) + C_4^{(8)}(\theta, \phi)) \right. \\ \left. + \frac{3\sqrt{1430}}{64} (C_{-8}^{(8)}(\theta, \phi) + C_8^{(8)}(\theta, \phi)) \right), \quad (2.32)$$

$$V_{CFs}^9(r, \theta, \phi) = r^9 \frac{Ze^2}{a^{10}} (-C_0^{(9)}(\theta, \phi)), \quad (2.33)$$

$$V_{CFs}^{10}(r, \theta, \phi) = r^{10} \frac{Ze^2}{a^{11}} \left(\frac{1}{64} C_0^{(10)}(\theta, \phi) \right. \\ \left. - \frac{\sqrt{1430}\sqrt{3}}{64} (C_{-4}^{(10)}(\theta, \phi) + C_4^{(10)}(\theta, \phi)) \right. \\ \left. - \frac{\sqrt{24310}}{128} (C_{-8}^{(10)}(\theta, \phi) + C_8^{(10)}(\theta, \phi)) \right). \quad (2.34)$$

Although the terms having the odd power of r already appear in this symmetry, they do not contribute to the energy levels in the system (the integral (2.18) vanishes for $l_1 + l_2 + k = \text{odd}$). Crystal field splitting in case of C_{4v} symmetry is completely defined by the terms V_{CFs}^2 and V_{CFs}^4 .

2.3 Wavefunctions

CFT is based on the assumption that the angular dependence of basis functions is similar to that for hydrogen wavefunctions. However, radial behavior is not known and may either be calculated by other theories analytically or integrals which involve this dependence have to be fitted to give the *a priori* known energy levels of the system. Such an assumption makes it possible to split the variables and write the one-electron basis function in the form

$$\psi_{nlms_z} = R_{nl}(r)\Theta_{lm}(\theta)\Phi_m(\phi)\chi_{s_z}(s), \quad (2.35)$$

where $n = 0, 1, \dots$, $l = 0, 1, \dots, n - 1$, $m = -l, \dots, l$, $s_z = -1/2, +1/2$ denote principal, orbital, magnetic, and spin quantum numbers respectively.

Many-particle wavefunctions may be constructed in two equivalent ways: (1) in the form of Slater determinants with symmetry-adapted components (linear combinations of one-electron hydrogen-like wavefunctions), or (2) in the form of linear combinations of Slater determinants each of them containing pure one-electron hydrogen-like wavefunctions. In both cases linear combinations describe correlation effects due to the pair Coulomb interaction between electrons and the interaction with the field of ligands.

The way to construct the wavefunctions consists of three steps: (1) an “approximate” wavefunction for the spherically symmetric ion is set up by means of *LS*-algebra, (2) the projection technique is used to adapt those wavefunctions to the lower symmetry of the system, and (3) having diagonalized the energy matrix we are able to find the eigenfunctions of the Hamiltonian. In order to fit the radial integrals the step (3) is repeated to give the best convergence of the Hamiltonian eigenvalues to the known energies.

Since the one-electron wavefunctions are simple hydrogen-like ones, we begin with the electronic configuration $3d^84s^0$ (corresponding hole configuration $3d^24s^2$), which is the ground state configuration of Ni^{++} in NiO ¹. We have to note that the inclusion of a fully occupied shell (as $4s^2$ here) only shifts the zero of energy but does neither affect the energies of the individual states differently nor does it affect the symmetry of the wavefunctions. Thus it suffices to consider partially occupied shells only.

The correlation of *d*-electrons couples the two holes in the *d*-shell of the ion, in the limit of weak spin-orbit coupling, by an *LS* coupling (neglecting the spin-orbit coupling (SOC)). The resulting coupled states have quantum numbers which are expressed as

$$\begin{aligned} L_z &= l_{z,1} + l_{z,2} \\ S_z &= s_{z,1} + s_{z,2} \end{aligned} \quad (2.36)$$

Here, the $l_{z,i}$ and $s_{z,i}$ ($i = 1, 2$) denote the *z*-components of orbital and spin momenta of the *i*-th hole, respectively. From Eq. (2.36) it becomes clear that the orbital momentum of the coupled state constructed from two *d*-holes can be 0, 1, 2, 3, or 4, which is conventionally labelled by the spectroscopic symbols as *S*, *P*, *D*, *F*, and *G*. The resulting spin can be equal

¹Throughout this work, we assume a transfer of an integer number of electrons to the oxygen atom.

to 0 or 1, in other words each of these states can have a singlet or triplet spin multiplicity. Since the two holes are indistinguishable, the Pauli principle forbids two identical holes to produce a coupled state. This limitation leaves us with the following set of two-hole states: 1S , 3P , 1D , 3F , and 1G . These spherical-symmetry adapted states are produced from simple products of d-holes with the use of Clebsch-Gordan algebra

$$\begin{aligned}
& \{d_{l=2,s=1/2} \otimes d_{l=2,s=1/2}\}_{L,M,S,S_z} \\
= & \sum_{m_1,m_2,s_{z1},s_{z2}} C_{2,m_1,2,m_2}^{LM} \cdot C_{1/2,s_{z1},1/2,s_{z2}}^{SS_z} \\
& \cdot d_{2,m_1,1/2,s_{z1}} \cdot d_{2,m_2,1/2,s_{z2}}
\end{aligned} \tag{2.37}$$

followed by a Gram-Schmidt orthonormalization procedure. As a result we obtain orthonormal wavefunctions for these spherical states, expressed as linear combinations of simple antisymmetric products of d -hole wavefunctions (Slater's determinants).

The Hamiltonian commutes with all components of the resultant angular momenta \mathbf{L} and \mathbf{S} , therefore there is no matrix component connecting states with different values \mathbf{L}^2 , \mathbf{S}^2 , L_z , and S_z . Note, that the energy of the $3d^24s^2$ and $3d^24s^0$ configurations does not depend on the values of L_z and S_z which means that the states are degenerate.

Coming to the states having more than two electrons we use a step-by-step procedure, in which at each step one nl particle is added to the previously found LS -states and use of (2.37) provides us with new set of levels. This is employed to find the wavefunctions for spherically symmetric Co^{2+} and Fe^{2+} . Note that for these configurations the levels having the same quantum numbers and eigenfunctions of the Hamiltonian appear by the diagonalization procedure.

If one goes to the lower symmetry the wavefunctions have to be adapted to this symmetry. In our case lowering of the system symmetry from spherical to cubic assumes a change of degeneracy of resultant orbital magnetic momentum L . This is governed by Group Theory, which gives irreducible representations of angular momentum for each point group symmetry. In particular, for O_h this changing is incorporated by means of so-called cubic harmonics. To find them we employ a projection technique, which is given by the operator

$$\widehat{\mathcal{P}}_{\lambda k}^{(j)} = \frac{l_j}{h} \sum_R \Gamma^{(j)}(R)_{\lambda k}^* \widehat{P}_R, \tag{2.38}$$

where: l_j - dimension of j -th representation, h - order of the group (for O_h $h = 48$), sum over all symmetry operations R in the group, $\Gamma^{(j)}(R)_{\lambda k}^*$ - complex conjugate to the $\lambda k - th$ element of the $j - th$ irreducible representation of the $R - th$ symmetry operation, P_R - symmetry operator.

The group O_h contains 10 classes, i.e. we have 10 irreducible representations ($A1_u$, $A2_u$, E_u , $T1_u$, $T2_u$, $A1_g$, $A2_g$, E_g , $T1_g$ and $T2_g$).

Irreducible representations of any point groups are matrices, the traces of are given in the character tables for corresponding group:

\mathbf{R}^3	E	$3C_2$	$8C_3$	$6C_4$	$6C'_2$	I	$3\sigma_2$	$8S_3$	$6S_4$	$6\sigma'_2$
S ($l=0$)	1	1	1	1	1	1	1	1	1	1
P ($l=1$)	3	-1	0	1	-1	-3	1	0	-1	1
D ($l=2$)	5	1	-1	-1	1	5	1	-1	-1	1
F ($l=3$)	7	-1	1	-1	-1	-7	1	-1	1	1
G ($l=4$)	9	1	0	1	1	9	1	0	1	1
H ($l=5$)	11	-1	-1	1	-1	-11	1	1	-1	1
I ($l=6$)	13	1	1	-1	1	13	1	1	-1	1

\mathbf{O}_h	E	$3C_2$	$8C_3$	$6C_4$	$6C'_2$	I	$3\sigma_2$	$8S_3$	$6S_4$	$6\sigma'_2$
A_{1u}	1	1	1	1	1	-1	-1	-1	-1	-1
A_{2u}	1	1	1	-1	-1	-1	-1	-1	1	1
E_u	2	2	-1	0	0	-2	-2	1	0	0
T_{1u}	3	-1	0	1	-1	-3	1	0	-1	1
T_{2u}	3	-1	0	-1	1	-3	1	0	1	-1
A_{1g}	1	1	1	1	1	1	1	1	1	1
A_{2g}	1	1	1	-1	-1	1	1	1	-1	-1
E_g	2	2	-1	0	0	2	2	-1	0	0
T_{1g}	3	-1	0	1	-1	3	-1	0	1	-1
T_{2g}	3	-1	0	-1	1	3	-1	0	-1	1

\mathbf{C}_{4v}	E	$2C_4$	C_2	$2\sigma_v$	$2\sigma_d$
A_1	1	1	1	1	1
A_2	1	1	1	-1	-1
B_1	1	-1	1	1	-1
B_2	1	-1	1	-1	1
E	2	0	-2	0	0

Comparison of these tables gives us the following level splitting for cubic and surface environments (note that $3d$ -states are even under space inversion):

\mathbf{R}^3	\mathbf{O}_h
S	A_{1g}
P	T_{1g}
D	$E_g + T_{2g}$
F	$A_{2g} + T_{1g} + T_{2g}$
G	$A_{1g} + E_g + T_{1g} + T_{2g}$
H	$E_g + 2T_{1g} + T_{2g}$
I	$A_{1g} + A_{2g} + E_g + T_{1g} + 2T_{2g}$

O_h	C_{4v}
A_{1g}	A_1
A_{2g}	B_1
E_g	$A_1 + B_1$
T_{1g}	$A_2 + E$
T_{2g}	$B_2 + E$
A_{1u}	A_2
A_{2u}	B_2
E_u	$A_2 + B_2$
T_{1u}	$A_1 + E$
T_{2u}	$B_1 + E$

Applying the projection technique to the wavefunctions gives us basis functions for the cubic symmetry; only angular parts of wavefunctions are presented, because the projection operator does not change their radial parts since

$$\widehat{\mathcal{P}}_{\lambda k}^{(j)} R_{nl} Y_{lm} = R_{nl} \widehat{\mathcal{P}}_{\lambda k}^{(j)} Y_{lm}. \quad (2.39)$$

Having these wavefunctions incorporated into CFT we get the block-diagonal form of the energy matrix. Diagonalization of these blocks is discussed later.

Cubic harmonics are also applicable in the case of C_{4v} symmetry. If the blocks are not diagonalized afterwards, one gets an approximate solution (for perturbation due to the uncompensated field of the point charge at the position $-z$). If this is followed by the diagonalization procedure for the blocks (which is the case in this work) the results are exact (within our model).

We would like to note, that the projection operator (2.38) may be used to get the wavefunctions for direct splitting $R_3 \rightarrow C_{4v}$, without calculation of intermediate bulk states. However, it is not important since we finally get completely diagonal energy matrix with its eigenfunctions.

2.4 Calculation of matrix elements

Employing CFT requires calculations of matrix elements between wavefunctions in form of Slater's determinants for various operators. Since operators considered in this work are either one- or two-electron operators, we would like to give the expressions for them.

2.4.1 One-electron operator

The simplest case is one-electron operator $\hat{F} = \sum_i \hat{f}(\vec{r}_i)$. Action of such an operator is completely defined by the wavefunction of one electron only. This part of the treatment concerns the kinetic energy of the electrons $\sum_{i=1}^N -\frac{1}{2}\Delta$, their interaction with the nucleus

$\sum_{i=1}^N V_n(\vec{r}_i)$, and crystal-field terms $\sum_{i=1}^N V_{CF}(\vec{r}_i)$. Extension of these operator to many-body wavefunctions is straightforward and gives following results [16]

$$(\Phi_A|\hat{F}|\Phi_B) = \pm \sum_{i=1}^N (a_i|\hat{f}|a_i), \quad (2.40)$$

$$(\Phi_A|\hat{F}|\Phi_B) = \pm (a_k|\hat{f}|b_l), \quad (2.41)$$

$$(\Phi_A|\hat{F}|\Phi_B) = 0, \quad (2.42)$$

of which the first equation describes the case when Φ_A and Φ_B are the same (except for possible permutation), the second one is used if two Slater determinants $\Phi_A = a_1, a_2, \dots, a_k, \dots, a_N$ and $\Phi_B = b_1, b_2, \dots, b_l, \dots, b_N$ have one pair of different particles only (the \pm sign is determined by the number of permutations to bring b_j into coincidence with a_i , except $a_k \neq b_l$); the integral is zero for Slater determinants Φ_A and Φ_B which differ by more than one pair of occupied functions.

2.4.2 Two-electron operator

There are pair electronic interactions, one of them being the Coulomb interaction (2.3). In the most general form the pair interaction is expressed as $\hat{G} = \sum_{i>j} \hat{g}(i, j)$ and depends on the wavefunctions of two electrons. For such operators there are four possible cases:

$$(\Phi_A|\hat{G}|\Phi_B) = \pm \sum_{k>t} \{(a_k a_t|\hat{g}|a_k a_t) - (a_k a_t|\hat{g}|a_t a_k)\} \quad (2.43)$$

$$(\Phi_A|\hat{G}|\Phi_B) = \pm \sum_t \{(a_k a_t|\hat{g}|b_l a_t) - (a_k a_t|\hat{g}|a_t b_l)\} \quad (2.44)$$

$$(\Phi_A|\hat{G}|\Phi_B) = \pm \{(a_k a_l|\hat{g}|b_m b_n) - (a_k a_l|\hat{g}|b_n b_m)\} \quad (2.45)$$

$$(\Phi_A|\hat{G}|\Phi_B) = 0. \quad (2.46)$$

Equation (2.43) is valid if the wavefunctions Φ_A and Φ_B are exactly the same ($a_i = b_i$ for all i), equation (2.44) should be used for wavefunctions which differ in one particle only ($a_i = b_i$ for all i , except $a_k \neq b_l$), the third equation (2.45) is used for wavefunctions Φ_A and Φ_B which differ in two particles ($a_i = b_i$ for all i , except $a_k \neq b_m$ and $a_l \neq b_n$); as it is seen from (2.46) the two-particle operator vanishes for wavefunctions which differ by more than two pairs of particles. Here again \pm sign in front of right-hand side is given by the parity of the particular permutation which bring Φ_A and Φ_B into coincidence.

2.4.3 Interaction with Nucleus and Kinetic Energy

The interaction of electrons with nucleus and their kinetic energies are given by the expression

$$U(a; b) = \delta(m_a, m_b)\delta(s_z^a, s_z^b)I(n_a, l_a; n_b, l_b). \quad (2.47)$$

However, this interaction is the same for all the diagonal matrix elements and has no effect on the individual levels. The only effect is to shift the initial position of the energy. This allows us to omit this term in the following consideration.

2.4.4 Coulomb Interaction

Coulomb interaction (2.3) in the Hamiltonian matrix describes pair interactions between the electrons. Strictly speaking, this interaction may be broken up into three parts: (1) electron pairs within closed shells, (2) electron pairs with one electron in closed shell, and (3) electron pairs within open shells. Cases (1) and (2) are subject to Unsöld's theorem (whenever a sub-shell is filled or half-filled, the total wavefunction squared gives the spherically symmetric spatial probability distribution for the atom's electrons) and do not lead to any splitting when summed over all occupied states. This leaves the entire splitting to be related to the part

$$\begin{aligned} (\Phi_A | \hat{H}_C | \Phi_B) &= \sum_{i=1}^{N-1} \sum_{j>i}^N \frac{1}{r_{12}} \\ &= \sum_{i=1}^{N-1} \sum_{j>i}^N [J(a, b) - K(a, b)] \end{aligned} \quad (2.48)$$

in which summation is made only over the electrons not in closed shells. Symbols $J(a, b) = (ab | \hat{q} | ab)$ and $K(a, b) = (ab | \hat{q} | ba)$ denote direct and exchange integrals of the Coulomb interaction respectively. This interaction is an origin of multiplet splitting for the spherically symmetric ions, but is also required for ions placed in the field of ligands.

As it is already shown each two-electron operator may be reduced to the form $(ab | \hat{q} | cd)$. Substitutions of (2.35) into (2.48) gives

$$(ab | q | cd) = \iint a^*(1) b^*(2) \left(\frac{e^2}{r_{12}} \right) c(1) d(2) \, d\tau_1 \, d\tau_2, \quad (2.49)$$

where a , b , c , and d denote wavefunctions $\psi_{n_a, l_a, m_a, s_z^a} \dots \psi_{n_d, l_d, m_d, s_z^d}$ respectively; τ_1 and τ_2 are the integration variables. The integration is performed over six spatial coordinates and summed over two spin coordinates. The spin sum gives unity if simultaneously $s_z^a = s_z^c$ and $s_z^b = s_z^d$ and zero otherwise.

Conventional expansion of $1/r_{12}$ gives

$$\frac{1}{r_{12}} = \frac{1}{(r_1^2 + r_2^2 - 2r_1 r_2 \cos \omega)^{1/2}} = \sum_{k=0}^{\infty} \frac{r_{<}^k}{r_{>}^{k+1}} P_k(\cos \omega) \quad (2.50)$$

where $r_{<}$ and $r_{>}$ are the lesser and greater of $|r_1|$, $|r_2|$ and ω is the angle between \vec{r}_1 and \vec{r}_2 . Next, it is possible to expand $P_k(\cos \omega)$ using the addition theorem for spherical

harmonics (2.9). Integration of the resulting expression over ϕ 's merely gives δ functions which assure conservation of L_z and precludes $m_a + m_b = m_c + m_d$. The remaining integral may be expressed in terms of c^k symbols as follows

$$(a, b|\hat{q}|c, d) = \delta(s_z^a, s_z^c)\delta(s_z^b, s_z^d)\delta(m_a + m_b, m_c + m_d) \\ \times \sum_{k=0}^{\infty} c^k(l_a, m_a, l_c, m_c)c^k(l_d, m_d, l_b, m_b)R^k(n_a, l_a, n_b, l_b, n_c, l_c, n_d, l_d). \quad (2.51)$$

The quantities R^k are radial integrals which depend on the particular form for the radial wavefunctions. The definition is just

$$R^k(n_a, l_a, n_b, l_b, n_c, l_c, n_d, l_d) \\ = e^2 \int_0^{\infty} \int_0^{\infty} \frac{r_{\leq}^k}{r_{>}^{k+1}} R_1(n_a, l_a)R_2(n_b, l_b)R_1(n_c, l_c)R_2(n_d, l_d) dr_1 dr_2. \quad (2.52)$$

Since an analytical expression for $R_{n,l}(r)$ is not known within CFT, these integrals can not be calculated and their values are fitted to some data available from independent experiments or theories. However, usually there are few of such integrals (3 for systems consisting of $3d$ particles only). Such a simplification is due to the fact that these integrals appear multiplied by coefficients c^k for which the triangle rule must be satisfied as well as the condition $k + l_1 + l_2 = \text{even}$. The linear combinations of these integrals are also known as Racah parameters, while the integrals themselves are called Slater integrals. Thus it is possible to find their numerical values without touching the question about the behavior of $R_{n,l}(r)$ itself.

2.4.5 Interaction with Crystal Field

Since expressions for the crystal field for both the bulk and (001) surface of an *fcc* crystal are already defined (see (2.19) and (2.24)) and their extension to many-electron wavefunctions is settled (see (2.40)) we may now proceed to find the Hamiltonian matrix elements for the interaction of the ion with surrounding ligands. For the interaction with the electrostatic field produced by ligands is a one-particle operator, we derive expressions for $3d$ - and $4s$ -particles which form incomplete shells of the system under consideration.

This task is reduced to integrals of the form

$$\langle \psi_1 | \hat{V}_{CF} | \psi_2 \rangle = \int \psi_{n_1, l_1, m_1, s_z^1}^* \hat{V}_{CF} \psi_{n_2, l_2, m_2, s_z^2} d\tau, \quad (2.53)$$

where the crystal field is given either by (2.19)...(2.23) for the bulk environment or by (2.24)...(2.34) for the (001) surface.

Substitution of (2.35) and (2.10) into (2.53) gives the result

$$\begin{aligned} \langle \psi_1 | \hat{V}'_{CF} | \psi_2 \rangle = & \delta(s_z^1, s_z^2) \sum_{k=0}^{\infty} \sum_{m=-k}^k q_{km} \int r^k R_1(n_1, l_1, r) R_2(n_2, l_2, r) r^2 dr \\ & \int Y_{l_1, m_1}^*(\theta\phi) C_m^{(k)}(\theta\phi) Y_{l_2, m_2}(\theta\phi) \sin\theta d\theta d\phi. \end{aligned} \quad (2.54)$$

This formula contains the threefold integration over spatial coordinates, which may be easily reduced to the product of two Clebsch-Gordan coefficients for the angular part and one radial integral. The resulting expression for the interaction with crystal field is

$$\begin{aligned} \langle \psi_1 | \hat{V}'_{CF} | \psi_2 \rangle = & \delta(s_z^1, s_z^2) \\ & \sum_{k=0}^{\infty} \sqrt{\frac{4\pi}{2k+1}} q_{km} \sqrt{\frac{(2k+1)(2l_2+1)}{4\pi(2l_1+1)}} C_{k0l_20}^{l_10} C_{km_l_2m_2}^{l_1m_1} R^k(n_1 l_1 n_2 l_2). \end{aligned} \quad (2.55)$$

Here the expression for integral of product of three spherical harmonics over the solid angle [17] has been used

$$\int_0^{2\pi} d\phi \int_0^{\pi} \sin\theta d\theta Y_{l_1 m_1} Y_{l_2 m_2} Y_{l_3 m_3}^* = \sqrt{\frac{(2l_1+1)(2l_2+1)}{4\pi(2l_3+1)}} C_{l_10l_20}^{l_30} C_{l_1m_1l_2m_2}^{l_3m_3}. \quad (2.56)$$

Integration over ϕ gives non-zero only when

$$m_1 + m_2 = m_3 \quad (2.57)$$

and in addition the triangle rule must be fulfilled

$$|l_1 - l_2| \leq l_3 \leq l_1 + l_2 \quad (2.58)$$

Relation (2.58) tells us that the matrix elements of the bulk crystal field V'_{CFb} between the p -states are vanishing (since $l_1 = l_2 = 1$ and $k = 0, 4, 6, \dots$), resulting in the absence of the cubic field splitting of the p -levels, while for the surface $k = 0, 1, 2, \dots$ and p -levels are splitted by the crystal field. Equation (2.58) also shows that, in calculating the matrix elements of V'_{CF} between the nd -states, the terms proportional to r^k ($k > 4$) in V_c give a vanishing contribution, since for $3d$ -particles $l_1 = l_2 = 2$ and $n_1 = n_2$. Such restrictions allow to introduce another notation

$$c^k(l_1 m_1, l_2 m_2) = \int d\phi \sin\theta d\theta Y_{l_1 m_1}^*(\theta\phi) C_m^{(k)}(\theta\phi) Y_{l_2 m_2}(\theta\phi), \quad (2.59)$$

where the coefficients $c^k(l_1 m_1, l_2 m_2)$ are known as Gaunt's coefficients and tabulated once and for all [18]. Some of them are presented in Table 9.1.

Bulk environment. The non-vanishing integrals for the bulk crystal are given by the first two terms in the expansion of V_{CFb} , namely

$$\hat{V}_{CFb} = \hat{V}_{CFb}^0 + \hat{V}_{CFb}^4, \quad (2.60)$$

which is due to the restrictions imposed by the triangle rule for the coefficients $c^k(l_1 m_1, l_2 m_2)$ as it is just shown. Next, the first term of \hat{V}_{CFb} which is independent of the electron coordinate appears in all the diagonal matrix elements. To make the following arguments simple we leave out the first term of V_{CFb} and shift the origin of the energy by $6Ze^2/a$. Therefore, in what follows, we shall deal with V'_{CFb} given by

$$V'_{CF} = V_{CF} - \frac{6Ze^2}{a}. \quad (2.61)$$

This also means that there is no crystal-field splitting of $4s$ -levels for both bulk and surface environments and we may restrict our attention to the $3d$ -levels only.

Now let us calculate the matrix elements in (2.55) with $n_1 = n_2 = 3$ and $l_1 = l_2 = 2$. For the bulk environment the electrostatic potential has a form

$$V'_{CFb} = V_{CFb}^4 = \frac{7Ze^2}{2a^5} r^4 (C_0^{(4)} + \sqrt{\frac{5}{14}} (C_{-4}^{(4)} + C_4^{(4)})), \quad (2.62)$$

or in a more convenient form

$$\frac{2a^5 V'_{CFb}}{7Ze^2} = r^4 (C_0^{(4)} + \sqrt{\frac{5}{14}} (C_{-4}^{(4)} + C_4^{(4)})). \quad (2.63)$$

Incorporating the equation (2.19) into (2.55) we make independent integrations over solid angle $\iint \sin\theta d\theta d\phi$ and over the radial part $\int dr$. Within CFT method (hydrogen-like angular behavior of the basis wavefunctions) the angular integrals are calculated exactly using the expression (2.56) while the integrals over radial parts will be fitted later to the known energies of the particular system. Note, that first Clebsch-Gordan coefficient C_{a0b0}^{c0} vanishes if $a + b + c = 2g + 1$ (odd) and is equal to

$$C_{a0b0}^{c0} = \frac{(-1)^{g-c} \sqrt{2c+1} g!}{(g-a)!(g-b)!(g-c)!} \left[\frac{(2g-2a)!(2g-2b)!(2g-2c)!}{(2g+1)!} \right]^{1/2} \quad (2.64)$$

otherwise (the sum $a + b + c$ is even), g is positive integer. From the these equations we have: $C_{0020}^{20} = 1$, $C_{4020}^{20} = \sqrt{2/7}$, $C_{2020}^{20} = -\sqrt{2/7}$.

Results of this integration are

m_1	m_2	$\langle \phi_{3dm_1} V_{CFb}^4 \phi_{3dm_2} \rangle$ $\langle r^4 \rangle_{3d} \frac{7Ze^2}{2a^5}$
m_1	m_2	$C_{4020}^{20} \left(C_{402m_2}^{2m_1} + \sqrt{\frac{5}{14}} (C_{4-42m_2}^{2m_1} C_{442m_2}^{2m_1}) \right)$
± 2	± 2	1/21
± 1	± 1	-4/21
0	0	2/7
± 2	∓ 2	5/21

Because the dependence $\langle r \rangle^k$ is not known *a priori* only ratios of these integrals matter. They can also be presented in the conventional form (this form is used if the cubic environment only is introduced in the calculations)

$$\langle \phi_{nd\pm 2} | V_c^0 | \phi_{nd\pm 2} \rangle = Dq, \quad (2.65)$$

$$\langle \phi_{nd\pm 1} | V_c^0 | \phi_{nd\pm 1} \rangle = -4Dq, \quad (2.66)$$

$$\langle \phi_{nd0} | V_c^0 | \phi_{nd0} \rangle = 6Dq, \quad (2.67)$$

$$\langle \phi_{nd\pm 2} | V_c^0 | \phi_{nd\mp 2} \rangle = 5Dq, \quad (2.68)$$

where

$$D = 35Ze^2/4a^5, \quad (2.69)$$

$$q = (2/105)\langle r^4 \rangle_{3d}, \quad (2.70)$$

and

$$\langle r^m \rangle_{nd} = \int dr r^{2+m} |R_{nd}(r)|^2. \quad (2.71)$$

It should be remarked that D in (2.69) depends upon point-charges, and that q in (2.70) reflects the properties of the electron of the central atom. The physical meaning of D may easily be understood if V_{CFb}^4 is reexpressed in the form

$$V_{CFb}^4 = D(x^4 + y^4 + z^4 - \frac{3}{5}r^4) + \dots \quad (2.72)$$

(001) surface environment. A similar treatment is used to get the matrix elements of crystal-field interaction for the case of (001) surface. However in this case the electrostatic environmental potential V_{CFs} has more complicated structure due to the lower symmetry of the system. Again, omitting 4s-levels and cutting the sum

$$V_{CFs} = V_{CFs}^0 + V_{CFs}^1 + \dots$$

at the $k = 4$ we may write down a simplified form of V_{CFs}' as follows (keeping in mind that odd terms do not contribute to the energy due to the restrictions $l_1 + l_2 + k = (\text{even})$)

$$V_{CFs}' = -r^2 \frac{Ze^2}{a^3} C_0^{(2)} + r^4 \frac{Ze^2}{a^5} \left(\frac{5}{2} C_0^{(4)} + \frac{\sqrt{70}}{4} (C_{-4}^{(4)} + C_4^{(4)}) \right). \quad (2.73)$$

or in more convenient form

$$\frac{V_{CFs}'}{Ze^2} = -\frac{1}{a^3} r^2 C_0^{(2)} + \frac{5}{2a^5} r^4 (C_0^{(4)} + \sqrt{\frac{7}{10}} (C_{-4}^{(4)} + C_4^{(4)})),$$

The corresponding angular integrals are calculated in the same way as for the bulk and are

Table 2.6: Non-zero energy matrix elements for one $3d$ -particle placed in a field with either O_h or C_{4v} symmetry

m_1	m_2		$\frac{Ze^2}{a}$	$\frac{1}{7} \frac{Ze^2}{a^3} \langle r_{3d}^2 \rangle$	$\frac{1}{42} \frac{Ze^2}{a^5} \langle r_{3d}^4 \rangle$
± 2	± 2	bulk	6	0	7
		surface	5	2	5
± 1	± 1	bulk	6	0	-28
		surface	5	-1	-20
0	0	bulk	6	0	42
		surface	5	-2	30
± 2	∓ 2	bulk	0	0	35
		surface	0	0	35

m_1	m_2	$\langle \phi_{ndm_1} V_c^2 \phi_{ndm_2} \rangle$ $\langle r^2 \rangle_{3d} \frac{-Ze^2}{a^3}$	$\langle \phi_{ndm_1} V_c^4 \phi_{ndm_2} \rangle$ $\langle r^4 \rangle_{3d} \frac{5Ze^2}{2a^5}$
m_1	m_2	$C_{2020}^{20} C_{202m_2}^{2m_1}$	$C_{4020}^{20} \left(C_{402m_2}^{2m_1} + \sqrt{\frac{7}{10}} (C_{4-42m_2}^{2m_1} C_{442m_2}^{2m_1}) \right)$
± 2	± 2	$-2/7$	$1/21$
± 1	± 1	$1/7$	$-4/21$
0	0	$2/7$	$2/7$
± 2	∓ 2	0	$1/3$

It is worth to note that in case of bulk crystal-field splitting is completely defined by one parameter only, while on the surface one needs two parameters (apart from the zeroth-order term which is the same for all the terms and shifts the origin of the energy).

Before going further we have to say that zeroth-order terms for bulk and surface environments relate to each other with ratio $5/6$, which is used in the comparison of these two symmetries of the same system. The results for both bulk and surface environments may be summarized and are given in Table 2.6. This result shows a deep interrelation between bulk and surface splitting of the same material and was not presented before. As we will show later the values of parameters we got from two independent fits (for bulk and surface) are very close to each other, confirming the applicability of CFT to transition metal oxides.

2.4.6 Spin-orbit interaction

The spin-orbit interaction is proportional to the $l \cdot s$ which can be expressed as

$$l \cdot s = l_z s_z + \frac{l_+ s_- + l_- s_+}{2}, \quad (2.74)$$

where the operators are defined for any angular momentum lm (for the spin $l = 1/2$, $m = \pm 1/2$) as:

$$l_z \phi_{lm}(\vec{r}) = m \phi_{lm}(\vec{r}), \quad (2.75)$$

$$l_{\pm} \phi_{lm}(\vec{r}) = [l(l+1) - m(m \pm 1)]^{1/2} \phi_{l, m \pm 1}(\vec{r}). \quad (2.76)$$

For $3d$ -particles one gets the following matrix of $l \cdot s$:

$$\begin{array}{cc|c} \psi_{\pm 2}^{\uparrow} & \psi_{\pm 2}^{\downarrow} & -1 \\ \psi_{\pm 2}^{\downarrow} & \psi_{\pm 2}^{\uparrow} & 1 \\ \psi_{\pm 1}^{\uparrow} & \psi_{\pm 1}^{\downarrow} & -0.5 \\ \psi_{\pm 1}^{\downarrow} & \psi_{\pm 1}^{\uparrow} & 0.5 \\ \psi_{-2}^{\uparrow} & \psi_{-1}^{\downarrow} & 1 \\ \psi_{-1}^{\downarrow} & \psi_{-2}^{\uparrow} & 1 \\ \psi_2^{\downarrow} & \psi_1^{\uparrow} & 1 \\ \psi_1^{\uparrow} & \psi_{-2}^{\downarrow} & 1 \\ \psi_{-1}^{\uparrow} & \psi_0^{\downarrow} & \sqrt{6}/2 \\ \psi_0^{\downarrow} & \psi_{-1}^{\uparrow} & \sqrt{6}/2 \\ \psi_1^{\downarrow} & \psi_0^{\uparrow} & \sqrt{6}/2 \\ \psi_0^{\uparrow} & \psi_1^{\downarrow} & \sqrt{6}/2 \end{array}$$

The splitting of the levels resulting from the spin-orbit coupling depends on both the symmetry of the system and the total spin momentum S . For the symmetries of our interest (O_h and C_{4v}) the splitting of the triplets ($S = 1$) in NiO is

O_h	O_h with SOC	C_{4v}	C_{4v} with SOC
${}^3A_{1g} = \Gamma_1^+$	Γ_4	${}^3A_1 = \Gamma_1$	$\Gamma_2 + \Gamma_5$
${}^3A_{2g} = \Gamma_2^+$	Γ_5	${}^3A_2 = \Gamma_2$	$\Gamma_1 + \Gamma_5$
${}^3E_g = \Gamma_3^+$	$\Gamma_4 + \Gamma_5$	${}^3B_1 = \Gamma_3$	$\Gamma_4 + \Gamma_5$
${}^3T_{1g} = \Gamma_4^+$	$\Gamma_1 + \Gamma_3 + \Gamma_4 + \Gamma_5$	${}^3B_2 = \Gamma_4$	$\Gamma_3 + \Gamma_5$
${}^3T_{2g} = \Gamma_5^+$	$\Gamma_2 + \Gamma_3 + \Gamma_4 + \Gamma_5$	${}^3E = \Gamma_5$	$\Gamma_1 + \Gamma_2 + \Gamma_3 + \Gamma_4 + \Gamma_5$

and may be extended to other symmetries. The way to construct it is: (1) define the irreducible representations of the orbital momentum \vec{L} in the given point symmetry group; (2) define the irreducible representations of the spin momentum \vec{S} in the given point symmetry group; (3) form the direct product $\mathcal{D}^{(L)} \times \mathcal{D}^{(S)}$.

2.5 One-electron case

The simplest case of CFT is one-particle case, when one electron only is considered. This starting part does not only give the ideas, which the CFT is based on, but is also required when one goes to many-particle cases.

Using results presented before we already may write the Hamiltonian for one $3d$ -particle moving in the potential produced by surrounding point charges. Since at this stage the Coulomb interaction is not present, the energy matrix is formed by the effect of all other interactions and has a form:

$$\begin{pmatrix} 6A + 7C & 0 & 0 & 0 & 35C \\ 0 & 6A - 28C & 0 & 0 & 0 \\ 0 & 0 & 6A + 42C & 0 & 0 \\ 0 & 0 & 0 & 6A - 28C & 0 \\ 35C & 0 & 0 & 0 & 6A + 7C \end{pmatrix},$$

for the bulk system and

$$\begin{pmatrix} 5A + 2B + 5C & 0 & 0 & 0 & 35B \\ 0 & 5A - B - 20C & 0 & 0 & 0 \\ 0 & 0 & 5A - 2B + 30C & 0 & 0 \\ 0 & 0 & 0 & 5A - B - 20C & 0 \\ 35B & 0 & 0 & 0 & 5A + 2B + 5C \end{pmatrix},$$

for the surface, where letters A , B , and C denote zeroth-, second-, and fourth-order contributions of the crystal field to the energy of the electron. The bases of these matrices are arranged in the ascending order of m .

Since both matrices have off-diagonal terms connecting the states with $m_a = +2$, $m_b = -2$ we have to solve secular equations in order to find the eigenvalues of the Hamiltonian. This task is straightforward and leads to the result

$$\begin{array}{ll} O_h & C_{4v} \\ \epsilon_{1,2,3} = 6A - 28C & \epsilon_{1,2} = 5A - B - 20C \\ \epsilon_{4,5} = 6A + 42C & \epsilon_3 = 5A - 2B + 30C \\ & \epsilon_4 = 5A + 2B - 30C \\ & \epsilon_5 = 5A + 2B + 40C \end{array}$$

The first column represents the well known fact that $3d$ -particles in a cubic bulk field form two states - a three-fold degenerate t_{2g} and a doubly degenerate e_g . On the surface we observe further splitting when four different states are formed, of which one is doubly degenerated (e_g) and other three have multiplicity one (a_1 , b_1 , and b_2).

2.6 Many electrons

The results of the previous section now have to be expanded to case of more than one particle. There are two equivalent ways doing this.

In the first case one may employ the already calculated one-particle states. Knowing the energies it is possible to find the eigenfunctions corresponding to them. These one-particle

eigenfunctions may be arranged in the single Slater determinant to give the many-particle wavefunctions of the system. For instance, in the case of two $3d$ -electrons (which form one of the five states $t_{2g}^1, t_{2g}^2, t_{2g}^3, e_g^1$, and e_g^2 omitting the spin degree of freedom) the following 45 states may be formed (number in parentheses shows the multiplicity of the state): $t_{2g}t_{2g}$ gives 15 states $^1A_{1g}(1)$, $^1E_g(2)$, $^1T_{2g}(3)$, and $^3T_{1g}(9)$; $e_g e_g$ gives 6 states $^1A_{1g}(1)$, $^1E_g(2)$, and $^3A_{2g}(3)$; and finally $t_{2g}e_g$ gives 24 states $^1T_{1g}(3)$, $^1T_{2g}(3)$, $^3T_{1g}(9)$, and $^3T_{2g}(9)$. Such way of doing this is used in [15]. Although it is possible to derive this scheme for C_{4v} symmetry, we do not do it here since we use the second method.

The other way of inclusion many-body states is to keep the basis of hydrogen-like orbitals and implement symmetry-adapted linear combinations of Slater determinants. In this way the wavefunction has a form

$$\Phi = \sum_k \alpha_k \Phi_k, \quad (2.77)$$

where Φ_k 's are the Slater determinants

$$\Phi_k = (N!)^{-1/2} \sum_P (-1)^P P \psi(r_1, \dots, r_N), \quad (2.78)$$

$$= (N!)^{-1/2} \begin{pmatrix} u_1(1) & u_2(1) & \dots & u_N(1) \\ u_1(2) & u_2(2) & \dots & u_N(2) \\ \dots & \dots & \dots & \dots \\ u_N(1) & u_N(1) & \dots & u_N(N) \end{pmatrix} \quad (2.79)$$

and p denotes the number of binary permutations in the permutation P . The method is easily expandable to a many-particle electronic configuration using general formulas in dealing with one- and two-particle operators. Another advantage of this method is that one-particle matrix elements are already calculated and may be used directly. However to form proper linear combinations of Slater determinants it is necessary to derive cubic harmonics for any level which is accomplished by projection operator.

It is of basic importance that none of these two methods gives energies and eigenfunctions for levels appearing more than once in the configuration. The Hamiltonian matrix has a block-diagonal form (see chapter 7 section 3) with blocks being formed by the levels with the same set of quantum numbers. Thus it is critical to diagonalize this matrix to find the eigenstates of this system. The main problem coming out at this point is the fitting of the energy levels to given values. For NiO, the Hamiltonian matrix $E_{i,j}$ has a size 45×45 and the task seems to be trivial (there is a lot of programs which can do it). However it is not so. Actually the interaction is defined by the rank 3 matrix $E_{i,j,k}$ of size $45 \times 45 \times k$ (number of parameters) which can not be diagonalized analytically. However once the parameters are fitted the matrix may be given as $E_{i,j} = \sum_k E_{i,j,k}$, where i and j denote states and k runs over CFT parameters and is diagonalized easily. Thus the difficulty is to modify standard CFT in order to remove off-diagonal elements. This is done by using Powell's non-linear least-squares method [19].

To the best of our knowledge the complete diagonalization of block-diagonal matrices of many-body states in CFT was never done before. Some authors neither computed nor even mention this point [20]; some other authors neglected their contribution because methods they use do not allow this (however they found the whole energy matrix for rare-earth metals and regarded those elements being small) [21].

Off-diagonal elements of the energy matrix appear already for the spherically symmetric Co^{2+} ion, when two 2D levels are formed within the $3d^7$ electronic configuration. It is possible to construct different wavefunctions on the base of Clebsch-Gordan algebra. For example, the equation (2.37) gives us wavefunctions c^2D and d^2D , while a^2D_2 and b^2D_2 are taken from [22]:

state	[1,9,10]	[4,7,9]	[3,8,9]	[3,7,10]	[5,6,9]	[5,7,8]
$a^2D_2^\uparrow$	$-\frac{1}{2}$	$+\frac{1}{2}$	$-\frac{1}{2}$		$+\frac{1}{2}$	
$b^2D_2^\uparrow$	$-\sqrt{\frac{25}{84}}$	$-\sqrt{\frac{9}{84}}$	$-\sqrt{\frac{1}{84}}$	$+\sqrt{\frac{16}{84}}$	$-\sqrt{\frac{9}{84}}$	$-\sqrt{\frac{24}{84}}$
$c^2D_2^\uparrow$	$+\sqrt{\frac{8}{15}}$		$+\sqrt{\frac{2}{15}}$	$-\sqrt{\frac{2}{15}}$		$+\sqrt{\frac{3}{15}}$
$d^2D_2^\uparrow$	$+\sqrt{\frac{1}{70}}$	$-\sqrt{\frac{25}{70}}$	$+\sqrt{\frac{9}{70}}$	$+\sqrt{\frac{4}{70}}$	$-\sqrt{\frac{25}{70}}$	$-\sqrt{\frac{6}{70}}$

Both two sets of basis functions are eigenfunctions of operator \hat{L} and are connected to each other by the expressions

$$c^2D_2^\uparrow = -\sqrt{\frac{3}{10}}a^2D_2^\uparrow - \sqrt{\frac{7}{10}}b^2D_2^\uparrow,$$

$$d^2D_2^\uparrow = -\sqrt{\frac{7}{10}}a^2D_2^\uparrow + \sqrt{\frac{3}{10}}b^2D_2^\uparrow.$$

which simply represent the unitary rotations matrix.

The energy matrices for these two sets have block-diagonal forms with 2×2 blocks: (for convenience Slater integrals are denoted as $A = F_0 - 49F_4 = F^0 - F^4/9$, $B = F_2 - 5F_4 = (9F^2 - 5F^4)/441$, and $C = 35F_4 = 5F^4/63$):

$$\begin{array}{l} \text{a} \\ \text{b} \end{array} \begin{array}{|c|c|} \hline \text{a} & \text{b} \\ \hline 3A + 7B + 7C & 3\sqrt{21}B \\ \hline 3\sqrt{21}B & 3A + 3B + 3C \\ \hline \end{array}$$

for the first set and

$$\begin{array}{l} \text{c} \\ \text{d} \end{array} \begin{array}{|c|c|} \hline \text{c} & \text{d} \\ \hline 3A + \frac{84}{5}B + \frac{21}{5}C & \frac{8}{5}\sqrt{21}B + \frac{2}{5}\sqrt{21}C \\ \hline \frac{8}{5}\sqrt{21}B + \frac{2}{5}\sqrt{21}C & 3A - \frac{34}{5}B + \frac{29}{5}C \\ \hline \end{array}$$

for the second one. It is already seen that diagonal elements are different which means that eigenfunctions of \hat{L} are not the eigenfunctions of our Hamiltonian and the diagonal sum rule can not be used for this configuration. However $aa+bb = cc+dd = 6A+10B+10C$ e.g. the diagonal sum rule gives the correct sum of energies for two 2D levels, but their values should be found from the secular equation.

Having calculated the whole blocks of the energy matrix we may now diagonalize them in order to find the eigenfunctions of the Hamiltonian.

Both matrices give the same secular equation with its eigenvalues

$$\epsilon = 3F_0 + 5F_2 + 3F_4 \pm \sqrt{193F_2^2 + 8325F_2F_4 - 1650F_4^2},$$

$$\epsilon = 3A + 5B + 5C \pm \sqrt{193B^2 + 8BC + 4C^2}.$$

The corresponding eigenfunctions can be written as

$$\alpha a^2 D_2^\dagger + \beta b^2 D_2^\dagger,$$

$$\alpha c^2 D_2^\dagger + \beta d^2 D_2^\dagger,$$

where coefficients α and β are different for two sets but do give the same final eigenfunctions.

$$\alpha_{ab} = \left[\left(\frac{aa - \epsilon}{ab} \right)^2 + 1 \right]^{-1/2},$$

$$\beta_{ab} = -\frac{aa - \epsilon}{ab} \alpha,$$

$$\alpha_{cd} = \left[\left(\frac{cc - \epsilon}{cd} \right)^2 + 1 \right]^{-1/2},$$

$$\beta_{cd} = -\frac{cc - \epsilon}{cd} \alpha.$$

Such a situation always occurs for O_h and C_{4v} symmetries for the levels characterized by the same set of quantum numbers Γ, S, S_z , as will be shown for NiO later. This is due to the fact that eigenfunctions of orbital angular momenta (cubic harmonics) are not eigenfunctions of the Hamiltonian, however they are used to reduce the task to the diagonalization of the blocks instead of the whole matrix.

It is also possible to show this numerically. To get values of A , B , and C we use the least squares method. Some energies for gas phase Co^{++} are known from experiment [23]:

level	energy	expression
4F	0.0000 eV	$3A-15B$
4P	1.8849 eV	$3A$
2G	2.1051 eV	$3A-11B+3C$
2H	2.8171 eV	$3A-6B+3C$
a^2D	2.8591 eV	$3A+5B+5C \pm \sqrt{193B^2 + 8BC + 4C^2}$

At the first stage we get the parameters from 4 energies (without the “problematic” a^2D level for which the sign before the square root is not defined), then with sign + in the equation 2.6, and finally with sign – in it. The results are:

step	A	B	C	$\sum (E_{exp} - E_{fit})^2$
1	0.632485	0.127334	0.548661	0.003153
2	0.485029	0.027679	0.227420	2.313683
3	0.634003	0.125953	0.519724	0.026151

The parameters above produce the following values of the energy for different levels:

level	Exp. value	Fitted value	$E_{fit} - E_{exp}$	$(E_{exp} - E_{fit})^2$
4F	0.000000	-0.012555	-0.01255	0.000158
4P	1.884900	1.897455	0.01255	0.000158
2G	2.105100	2.142765	0.03766	0.001419
2H	2.817100	2.779435	-0.03766	0.001419
4F	0.000000	1.039903	1.03990	1.081398
4P	1.884900	1.455087	-0.42981	0.184739
2G	2.105100	1.832879	-0.27222	0.074104
2H	2.817100	1.971274	-0.84582	0.715422
a^2D	2.859100	3.367057	0.50795	0.258020
4F	0.000000	0.012711	0.01271	0.000162
4P	1.884900	1.902008	0.01710	0.000293
2G	2.105100	2.075697	-0.02940	0.000865
2H	2.817100	2.705463	-0.11163	0.012463
a^2D	2.859100	2.970320	0.11122	0.012370

This table clearly shows the validity of 3-rd step of our treatment, which allows to find the eigenfunctions for two 2D levels. For two different sets of angular momentum eigenfunctions we get two different sets of α and β parameters

the values of α and β			
Set	ϵ	α	β
ab	2.970320	0.448426	-0.893820
ab	7.290468	0.893820	0.448426
cd	2.970320	0.502211	-0.864745
cd	7.290468	0.864745	0.502211

which do give the same Hamiltonian eigenfunctions

state	[1,9,10]	[4,7,9]	[3,8,9]	[3,7,10]	[5,6,9]	[5,7,8]
EF_{ab}^1	0.263406	0.516784	-0.126689	-0.390095	0.516784	0.477767
EF_{ab}^2	-0.691546	0.300128	-0.495837	0.195709	0.300128	-0.239694
EF_{cd}^1	0.263406	0.516784	-0.126689	-0.390095	0.516784	0.477767
EF_{cd}^2	0.691546	-0.300128	0.495837	-0.195709	-0.300128	0.239694

As that was expected, the eigenfunctions are the same for both ab and cd sets (except for the sign in EF_{ab}^2 and EF_{cd}^2 , which does not play a role since it is always squared). Our results are the same as in [22]².

The conclusion is: application of the diagonal sum method requires a careful treatment of levels, which occur more than once in a configuration. For complicated electronic configurations of spherically symmetric ion and for all the states in the lower symmetry the whole Hamiltonian matrix should be computed and diagonalized.

As the next point, we would like to show the impossibility of analytical diagonalization of the energy matrix. Let us assume that we have 2 functions f_a and f_b which are not the eigenfunctions of the Hamiltonian and produce an energy matrix

$$\begin{pmatrix} aa & ab \\ ab & bb \end{pmatrix}$$

which has off-diagonal elements $ab = ba$.

It is possible to introduce two new functions, defined as ($\alpha^2 + \beta^2 = 1$)

$$f'_a = \alpha f_a + \beta f_b \quad (2.80)$$

$$f'_b = -\beta f_a + \alpha f_b \quad , \quad (2.81)$$

where α and β may be defined from one variable as $\alpha = \cos \phi$ and $\beta = \sin \phi$ considering the transformation of functions as a rotation in some virtual space over the angle ϕ .

Clearly these new function also are the eigenfunctions of the \hat{L} operator. For these functions the matrix of an interaction becomes

$$\begin{pmatrix} \alpha^2 aa + \beta^2 bb + 2\alpha\beta ab & \alpha\beta(bb - aa) + (\alpha^2 - \beta^2)ab \\ \alpha\beta(bb - aa) + (\alpha^2 - \beta^2)ab & \beta^2 aa + \alpha^2 bb - 2\alpha\beta ab \end{pmatrix} \quad (2.82)$$

Suppose that it is possible to find the coefficients α and β which give zero for the off-diagonal elements a' and b' . They may be found from the condition

$$\frac{\alpha\beta}{\alpha^2 - \beta^2} = \frac{ab}{aa - bb}$$

for f'_a and f'_b to be the Hamiltonian eigenfunctions.

For the case discussed before we have:

$$\begin{array}{c} a \\ b \end{array} \begin{array}{c|c} a & b \\ \hline 3A + 7B + 7C & 3\sqrt{21}B \\ 3\sqrt{21}B & 3A + 3B + 3C \end{array}$$

²two misprints are found in [22] p.173. Equation $\alpha^2 D_{2,1/2}^a + \beta^2 D_{2,1/2}^b$ should be $\alpha D_{2,1/2}^a + \beta D_{2,1/2}^b$. Equation $F_4 = (1/144)F^4(nd^2)$ should be $F_4 = (1/441)F^4(nd^2)$

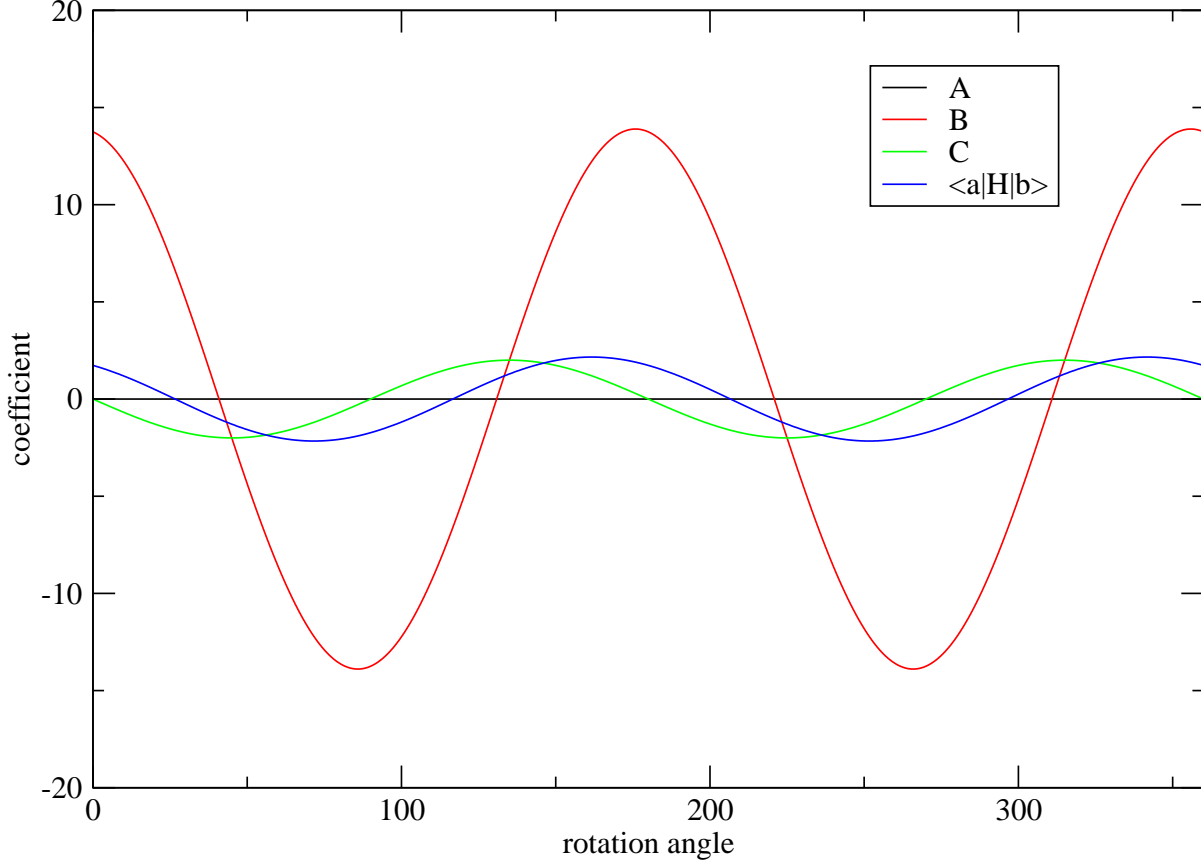


Figure 2.3: Dependence of the off-diagonal element $\langle a'|\hat{H}|b' \rangle$ on the rotation angle

$$\begin{array}{c}
 a' \\
 b'
 \end{array}
 \begin{array}{c}
 \\
 \\
 \end{array}
 \begin{array}{cc}
 & a' & & b' \\
 \left[\begin{array}{cc}
 3A + (3 + 4\alpha^2 + 6\alpha\beta\sqrt{21})B + (3 + 4\alpha^2)C & (-4\alpha\beta + 3\sqrt{21}(\alpha^2 - \beta^2))B - 4\alpha\beta C \\
 (-4\alpha\beta + 3\sqrt{21}(\alpha^2 - \beta^2))B - 4\alpha\beta C & 3A + (3 + 4\beta^2 - 6\alpha\beta\sqrt{21})B + (3 + 4\beta^2)C
 \end{array} \right.
 \end{array}$$

which give the condition

$$\frac{\alpha\beta}{\alpha^2 - \beta^2} = \frac{3\sqrt{21}B}{4B + 4C},$$

showing that the eigenfunctions depend strongly on the values of B and C which are not known *a-priori*.

Figure 2.3 shows the dependence of the $\langle a'D|\hat{H}|b'D \rangle$ matrix element on the rotation angle for $B = 0.125953$ and $C = 0.519724$. It is seen that intersection points of $\langle a'|\hat{H}|b' \rangle$ with the x axis correspond to non-zero contributions of B and C separately and only their sum is zero.

Chapter 3

Crystal Field Theory: Results for NiO

NiO has been attracting enormous attention of physicists for more than 50 years. This monoxide has a simple crystalline structure of NaCl type (an *fcc* lattice with $a = 4.18\text{\AA}$ and shortest metal-oxygen distance 2.08\AA). In the paramagnetic state above the Néel temperature $T_N = 525\text{ K}$ bulk NiO possesses a symmetry of the crystallographic point group O_h , while its undistorted (001) surface is described by C_{4v} one. In the ground state two $4s$ -electrons of each Ni ion are transferred to the surrounding oxygen ions, thus giving the ground state electronic configuration $3d^84s^0$ of the Ni^{2+} ion. The gap of NiO is shown in an XPS-BIS experiment [24] to be about 4 eV. Although NiO is considered in this work as being Mott-Hubbard-like insulator, some authors attribute this material to the charge-transfer insulators [25] or to the intermediate systems [26]. Due to the interaction with the field of oxygen ligands electronic levels existing in the gas phase become splitted. Because the interaction with the field of ligands is spin-independent the resulting levels are defined by the irreducible representations of orbital angular momentum \vec{L} only. Inclusion of spin-orbit coupling leads to the mixing of \vec{L} and \vec{S} momenta. According to the general theory the splitted states of the system are defined in this case via the direct product of the \vec{L} and \vec{S} irreducible representations in the given symmetry. The measured magnetic moments of this system are in range of $M = (1.77 - 2.2 \pm 0.2)\mu_B$ [27, 28, 29, 30] which are comparable to the spin-only moment of an associated Ni^{2+} ion. However, in the nonresonant magnetic X-ray scattering the separation of spin and orbital moment densities, which have different geometrical prefactors in the scattering cross section, can be adjusted by changing either the scattering geometry or the X-ray polarization. In Ref. [29, 30], the orbital magnetic moment in NiO is extracted by the polarization analysis of nonresonant magnetic scattering intensities. A large contribution of the orbital moment to the total magnetic moment was found by this method. Authors also found that the spin and orbital moments in NiO are collinear.

Below the Néel temperature these symmetries are lowered due to the antiferromagnetic ordering of spins of individual metal ions. All possible magnetic symmetries will be

discussed in this work later. Although Group Theory (namely Theory of Corepresentations for magnetic point groups) is able to give the set of levels for any magnetic point group [31, 32], the exchange interaction, which produces them, is intra-site one and can not be incorporated in the CFT where one metal ion only is considered. None of the terms in the CFT Hamiltonian (2.1) depends on the orientation of the resultant spin of the metal ion. If this interaction were constructed and included in the Hamiltonian, we would have complete description of the magnetic state too, but this treatment goes beyond the scope of this work. The splitting of the levels due to magnetic interaction is relatively small and would not affect their energies too much, however it changes the selection rules. Thus, CFT can not be used to get the proper symmetry of magnetic state of the system without deep modifications. However, as we will show later, CFT does discriminate the tensor elements of crystallographic and magnetic origin, which allows to use it for the description of Second Harmonic Generation process.

In this chapter we present the results of our calculations for NiO having symmetries $R(3)$, O_h , and C_{4v} .

It is quite important to note an improvement of our previous calculations [20, 7, 6], where we followed the diagonal sum realization of CFT [33]. The off-diagonal elements of the energy matrix (they appear between different levels, characterized by the same set of quantum numbers L, M, S, S_z) were omitted, which greatly simplifies the calculations, allowing the usage of Clebsch-Gordan algebra for getting the wavefunctions. However, this treatment of CFT is exact only for the levels which appear alone on the given configuration. For levels, appearing more than once, only the sum of their energies may be calculated. In the current work the whole energy matrix is computed and completely diagonalized. This realization required the calculation of at most $45 \times 45 \times 5 = 10125$ matrix elements (actually less because the Hamiltonian matrix is symmetric and $H_{ij} = H_{ji}$) and diagonalization of this matrix on each step of the least-squares procedure for the (001) surface where each energy level is defined by 5 parameters. For comparison, in the diagonal sum method only the diagonal matrix elements H_{ii} have to be computed which gives $45 \times 3 = 135$ elements; fitting of parameters in this case is a much simpler linear least-squares problem.

To fit the radial integrals which enter the CFT we use already available information about the energies of low lying states, which have been obtained in experimental and theoretical works [34, 35, 36, 37, 38, 39, 40, 41, 42, 43, 44]. Unfortunately, the careful analysis of those articles about NiO does not give a unique assignment of energies to corresponding atomic multiplets. The results of different authors may contradict each other, as discussed at the end of this chapter.

In the first step of our calculations we have chosen Ni^{2+} ion to find the values of parameters, which describe the Coulomb interaction between $3d$ -electrons in the metal ion. All input energies of the free Ni^{2+} ion are taken from the gas phase experiment [23], namely ${}^3F = 0.0000$, ${}^1D = 1.7398$, ${}^3P = 2.0658$, and ${}^1G = 2.8652$.

The obtained results for gas phase Ni^{2+} are presented in Table 3.1. Since each of the levels appears only once in this configuration, they are completely characterized by

quantum numbers L, S , which means that L, S are good quantum numbers for the gas phase of Ni^{2+} (which becomes violated for both the bulk and surface of NiO).

Table 3.1: Calculated energies for free Ni^{2+} ion

1S	A	+14B	+126C	7.0677
3P	A	+7B	-84C	2.1276
1D	A	-3B	+36C	1.8370
3F	A	-8B	-9C	0.0000
1G	A	+4B	+C	2.8299
A=1.8933, B=10.8974/49, C=7.1049/441				

In order to test the applicability of CFT to NiO we choose three and four sets of energies for the bulk and (001) surface of NiO respectively, as it is presented in Tab. 3.2. For all of those cases three parameters describing Coulomb interaction are taken from the previous step (Ni^{2+} ion).

When we come to the Ni^{2+} ion in the bulk NiO, orbital quantum numbers L, M behave according to the irreducible representations for the given symmetry group (O_h). Use of cubic harmonics to form symmetry adapted linear combinations of LS -wavefunctions yield a block-diagonal form of the energy matrix with off-diagonal elements between the levels having the same quantum numbers Γ, S, S_z . Thus the energy matrix contains blocks with size 2×2 for levels $^1A_{1g}, ^3T_{1g}, ^1E_g, ^1T_{2g}$ which appear twice in the configuration and exact wavefunctions for other levels appearing alone.

$$\begin{pmatrix} ^1A_{1g}^{2 \times 2} & 0 & 0 & 0 & 0 & 0 & 0 \\ 0 & ^3T_{1g}^{2 \times 2} & 0 & 0 & 0 & 0 & 0 \\ 0 & 0 & ^1E_g^{2 \times 2} & 0 & 0 & 0 & 0 \\ 0 & 0 & 0 & ^1T_{2g}^{2 \times 2} & 0 & 0 & 0 \\ 0 & 0 & 0 & 0 & ^3A_{2g}^{1 \times 1} & 0 & 0 \\ 0 & 0 & 0 & 0 & 0 & ^3T_{2g}^{1 \times 1} & 0 \\ 0 & 0 & 0 & 0 & 0 & 0 & ^1T_{1g}^{1 \times 1} \end{pmatrix}$$

The blocks calculated with cubic harmonics are expressed in terms of two CFT parameters as follows (the parameter E does not exist in the O_h symmetry, but will appear on the surface)

$$^1A_{1g}^{2 \times 2} = \begin{pmatrix} 12D & 68.585713F \\ 68.585713F & 12A + 28D \end{pmatrix}$$

$$^3T_{1g}^{2 \times 2} = \begin{pmatrix} 12D & 28D \\ 28F & 12D - 42F \end{pmatrix}$$

Table 3.2: Energies for bulk and (001) surface of NiO, used in fitting procedure

Bulk NiO				
	[34]	[39]		
	theory	experiment		
	a	b	c	
a^3A_{2g}	0.0000	0.0000	0.0000	
a^3T_{2g}	0.8406	1.0000	1.1000	
a^3T_{1g}	1.4586	1.7200	1.6000	
a^1E_g	1.8474			
a^1T_{2g}	2.5553			
b^3T_{1g}	2.8186			
(001) surface NiO				
	[34]	[39]	[41]	[43]
	theory	experiment	theory	theory
	1	2	3	4
a^3B_1	0.0000	0.0000	0.0000	0.0000
a^3E	0.6500	0.6000	0.4900	0.4600
a^3B_2	1.0000	1.1000	0.8300	0.8300
a^3A_2	1.3000	1.3000		1.0200
b^3E	1.4400		1.8400	1.1700

$${}^1E_g^{2 \times 2} = \begin{pmatrix} 12D + 24F & 69.282032F \\ 69.282032F & 12D + 4F \end{pmatrix}$$

$${}^1T_{2g}^{2 \times 2} = \begin{pmatrix} 12D - 16F & 34.641016F \\ 34.641016F & 12D - 26F \end{pmatrix}$$

while the single levels are

$${}^3A_{2g}^{1 \times 1} = 12D + 84F$$

$${}^3T_{2g}^{1 \times 1} = 12D + 14F$$

$${}^1T_{1g}^{1 \times 1} = 12D + 14F$$

If there were no Coulomb interaction, the equations above might have the following exact solutions:

$$\begin{aligned}
{}^1A_{1ga}^{2 \times 2} & 12D + 84F \\
{}^1A_{1gb}^{2 \times 2} & 12D - 56F \\
{}^3T_{1ga}^{2 \times 2} & 12D + 14F \\
{}^3T_{1gb}^{2 \times 2} & 12D - 56F \\
{}^1E_{ga}^{2 \times 2} & 12D + 84F \\
{}^1E_{gb}^{2 \times 2} & 12D - 56F. \\
{}^1T_{2ga}^{2 \times 2} & 12D + 14F \\
{}^1T_{2gb}^{2 \times 2} & 12D - 56F \\
{}^3A_{2g}^{1 \times 1} & 12D + 84F \\
{}^3T_{2g}^{1 \times 1} & 12D + 14F \\
{}^1T_{1g}^{1 \times 1} & 12D + 14F
\end{aligned} \tag{3.1}$$

However, bringing in the Coulomb interaction, we have to diagonalize the whole energy matrix for all the bulk states. In this case both the spherical Coulomb interaction (see Table 3.1) and the interaction with the crystal field (3.1) lose their simple forms and take a complicated structure which is quite dependent on the values of CFT parameters, which themselves are defined during the fitting process and depend on the employed known energies.

The particular set of the bulk levels energies obtained with CFT is presented in Table 3.3. We have to note again that the expressions are different for different energies used

Table 3.3: Calculated energies for Ni^{2+} ion in the bulk NiO

${}^1A_{1g}$	A	+4.2817B	+4.5211C	+12D	+49.9068F	3.3471
${}^1A_{1g}$	A	+13.7183B	+122.4789C	+12D	-21.9068F	8.1841
${}^3T_{1g}$	A	-7.4659B	-11.6706C	+12D	-30.1270F	1.4075
${}^3T_{1g}$	A	+6.4659B	-81.3294C	+12D	-11.8730F	3.1706
1E_g	A	-1.6150B	+29.0750C	+12D	+75.2445F	2.1356
1E_g	A	+2.6150B	+7.9250C	+12D	-47.2445F	4.1649
${}^1T_{2g}$	A	-2.3288B	+32.6440C	+12D	+3.4402F	2.8722
${}^1T_{2g}$	A	+3.3288B	+4.3560C	+12D	-45.4402F	4.2451
${}^3A_{2g}$	A	-8B	-9C	+12D	+84F	0.0000
${}^3T_{2g}$	A	-8B	-9C	+12D	+14F	0.8168
${}^1T_{1g}$	A	+4B	+C	+12D	+14F	3.6467
A=1.8933, B=10.8974/49, C=7.1049/441, D=0.0720, F=-0.0117						

as input data in CFT.

The situation for the Ni^{2+} ion on (001) surface of NiO is similar to the bulk, namely there are off-diagonal elements in the energy matrix. Here the biggest block has the size 4×4 for level 1A_1 , which appears four times in the $3d^8$ configuration. The Hamiltonian

matrix in this case has the form

$$\begin{pmatrix} {}^1A_1^{4 \times 4} & 0 & 0 & 0 & 0 & 0 & 0 & 0 & 0 \\ 0 & {}^3A_2^{2 \times 2} & 0 & 0 & 0 & 0 & 0 & 0 & 0 \\ 0 & 0 & {}^3E^{3 \times 3} & 0 & 0 & 0 & 0 & 0 & 0 \\ 0 & 0 & 0 & {}^1B_1^{2 \times 2} & 0 & 0 & 0 & 0 & 0 \\ 0 & 0 & 0 & 0 & {}^1B_2^{2 \times 2} & 0 & 0 & 0 & 0 \\ 0 & 0 & 0 & 0 & 0 & {}^1E^{3 \times 3} & 0 & 0 & 0 \\ 0 & 0 & 0 & 0 & 0 & 0 & {}^3B_1^{1 \times 1} & 0 & 0 \\ 0 & 0 & 0 & 0 & 0 & 0 & 0 & {}^3B_2^{1 \times 1} & 0 \\ 0 & 0 & 0 & 0 & 0 & 0 & 0 & 0 & {}^1A_2^{1 \times 1} \end{pmatrix}$$

The corresponding blocks contain energies expressed in terms of three parameters D , E , and F , while the values of parameters A , B , and C are again taken from the first step.

$${}^1A_1^{4 \times 4} = \begin{pmatrix} 10D & 3.34664E & 57.15476F & 9.66092F \\ 3.34664E & 10D+0.85714E+17.14286F & 1.17108E+9.75900F & -0.98974E+61.03417F \\ 57.15476F & 1.17108E+9.75900F & 10D+23.33333F & 3.38062E+0.56344F \\ 9.66092F & -0.98974E+61.03417F & 3.38062E+0.56344F & 10D+1.14286E-0.47619F \end{pmatrix},$$

$${}^3A_2^{2 \times 2} = \begin{pmatrix} 10D+2.8E & 2.4E+20F \\ 2.4E+20F & 10D-0.8E-30F \end{pmatrix},$$

$${}^3A_{2a}^{2 \times 2} = 10D+4E+10F,$$

$${}^3A_{2b}^{2 \times 2} = 10D-2E-40F,$$

$${}^3E_{ab}^{3 \times 3} = \begin{pmatrix} 10D-1.4E & 1.2E-25F & -1.54919E-3.87298F \\ 1.2E-25F & 10D+0.4E-37.5F & 0.77460E+1.93649F \\ -1.54919E-3.87298F & 0.77460E+1.93649F & 10D+17.5F \end{pmatrix},$$

$${}^1B_1^{2 \times 2} = \begin{pmatrix} 10D-0.85714E+22.85714F & 0.98974E+54.43588F \\ 0.98974E+54.43588F & 10D-1.14286E+7.14286F \end{pmatrix},$$

$${}^1B_{1a}^{2 \times 2} = 10D+70F,$$

$${}^1B_{1b}^{2 \times 2} = 10D-2E-40F,$$

$${}^1B_2^{2 \times 2} = \begin{pmatrix} 10D-0.85714E-17.14286F & 0.98974E+19.79487F \\ 0.98974E+19.79487F & 10D-1.14286E-22.85714F \end{pmatrix},$$

$${}^1B_{1a}^{2 \times 2} = 10D,$$

$${}^1B_{1b}^{2 \times 2} = {}_{10D-2E-40F},$$

$${}^1E_{ab}^{3 \times 3} = \begin{pmatrix} 10D+0.42857E-11.42857F & 1.30931E+3.27327F & -0.49487E+33.40384F \\ 1.30931E+3.27327F & 10D-2E+12.5F & 1.13389E+2.83473F \\ -0.49487E+33.40384F & 1.13389E+2.83473F & 10D+0.57143E-21.07143F \end{pmatrix},$$

$${}^3B_1^{1 \times 1} = {}_{10D+70F},$$

$${}^3B_2^{1 \times 1} = {}_{10D},$$

$${}^1A_2^{1 \times 1} = {}_{10D+4E+10F}.$$

The diagonalization of the resulting blocks for given values of the parameters is straightforward and yields the expressions presented in Table 3.4. Comparing the values of pa-

Table 3.4: Calculated energies for Ni^{2+} ion on the (001) surface of NiO

1A_1	A	-0.8495B	+26.9966C	+10D	+2.1604E	+68.4115F	1.9575
1A_1	A	+2.9461B	+9.0198C	+10D		+19.6495F	3.4289
1A_1	A	+3.2207B	+5.5892C	+10D	+0.1671E	-30.4306F	4.1171
1A_1	A	+13.6827B	+122.3943C	+10D	-0.3275E	-17.6304F	8.2003
3A_2	A	-6.2955B	-17.5224C	+10D	+1.1324E	-13.8965F	1.2921
3A_2	A	+5.2955B	-75.4776C	+10D	+0.8676E	-16.1035F	2.9959
3E	A	-7.8512B	-9.7440C	+10D	+0.5185E	+17.9796F	0.6923
3E	A	-7.8591B	-9.7044C	+10D	-0.1848E	-31.4378F	1.4589
3E	A	+6.7103B	-82.5516C	+10D	-1.3337E	-6.5418F	3.3022
1B_1	A	-1.5368B	+28.6841C	+10D	-0.1120E	+63.8410F	2.1428
1B_1	A	+2.5368B	+8.3159C	+10D	-1.8880E	-33.8410F	4.2801
1B_2	A	-2.3719B	+32.8593C	+10D	-0.3170E	-6.3409F	3.0283
1B_2	A	+3.3719B	+4.1407C	+10D	-1.6830E	-33.6591F	4.3737
1E	A	-1.9887B	+30.9433C	+10D	+0.6919E	+9.9930F	2.7445
1E	A	+3.4484B	+3.7580C	+10D	-1.8671E	+4.4950F	3.8709
1E	A	+3.5403B	+3.2987C	+10D	+0.1751E	-34.4880F	4.2071
3B_1	A	-8B	-9C	+10D		+70F	0.0000
3B_2	A	-8B	-9C	+10D			0.9791
1A_2	A	+4B	+C	+10D	+4E	+10F	3.2341
A=1.8933, B=10.8974/49, C=7.1049/441, D=0.1004, E=-0.1087, F=-0.0140							

rameters computed for the Ni^{2+} ion placed inside the bulk and on the (001) surface of NiO

respectively, we see that they are very close to each other. This fact not only shows the interrelation between them, but also supports our assumption about the applicability of CFT to NiO.

The results of different fits are shown in Figure 3.1. Summarizing these, we may conclude that results from [41] deviate from other authors and can not be accepted as input data for CFT. Although other sets give comparable level schemes, it should be noted that values from [43] are in generally lower; ones from [39] give higher energies, and values from [34] lie in between those two. For our further calculation we will employ the states, which come from the fit to the results of Freitag's *et al.* The position of those levels are visualized in Fig. 3.2 where the energies of the levels are shown for the free ion Ni^{2+} ion, the same ion in the bulk NiO and on the (001) surface respectively.

It is worth to note, that the big divergence in results of CFT coming from different input energies, does not violate any of the available data. The point simply is, that CFT is based on the assumptions, which being reasonable themselves, describe the real system to some approximation only (which explains the divergence with experiment), while other theories are based on other key points, which deviate from CFT assumptions. Apart from that there is no unambiguous experimental results even for bulk NiO, for instance the energy of ${}^3T_{2g}$ level lies in range from 1.05 eV in [35] to 1.13 in [38]; the energy of ${}^3T_{1g}$ was measured to be from 1.6 eV in [39, 40, 44] to 1.87 eV in [34]. Different theoretical works give even larger ranges for them: from 0.74 eV in [41] to 1.04 in [34] for ${}^3T_{2g}$ and from 1.40 eV in [42] up to 2.21 eV in [41] for ${}^3T_{1g}$. The situation is even worse for the higher levels of bulk NiO. The same is true for surface energies. The energy of the a^3E state was measured (computed) in the range 0.57-0.60 eV (0.42-0.75 eV), for a^3B_2 it is 1.10-1.12 eV (0.76-1.09 eV), for a^3A_2 1.3-1.75 eV (1.00-1.30 eV). Although such an inconsistency prevents us from providing accurate quantitative data for SHG spectra, it does not change the qualitative predictions about the ability of SHG to give information about the magnetic structure of the system. Depending on the levels, used for the calculation of the SHG response of the system, the nonlinear optical susceptibility tensor may differ in the positions of the peaks, nevertheless keeping the characteristic features.

Results of our calculations of NiO within Crystal Field Theory clearly show that the electronic structure of Ni^{2+} ion is well reproduced in this theory. Although there is no unambiguous information for the energy levels of this ion in the NiO compound, we showed that “the truth lies in the middle” of the wide range of available data. The comparison of data for the Ni ion in the bulk and on the surface validates this model to be an appropriate tool for the description of this material.

The energy levels as well as the corresponding wavefunctions of Ni ion have been computed. Since the knowledge of the wavefunctions allows to find all the observable quantum mechanical quantities for the system, we will apply this data to get the values of $\chi^{(2\omega)}$ tensor, which gives an information about the SHG process for this material.

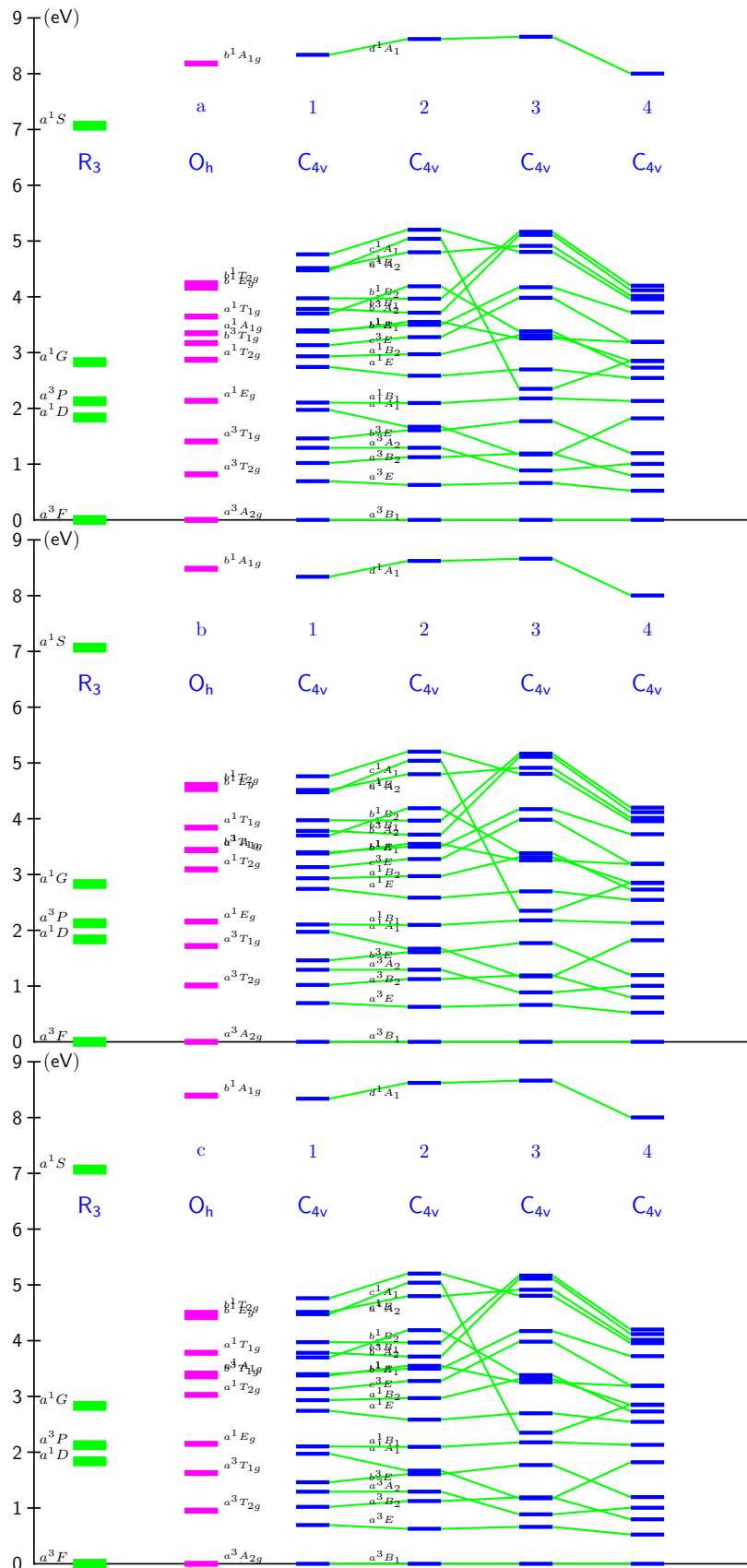


Figure 3.1: Resulting energy levels for NiO fitted to different sets of known energies. The labels a, b, c and 1, 2, 3, 4 correspond to different input sets presented in Table 3.2.

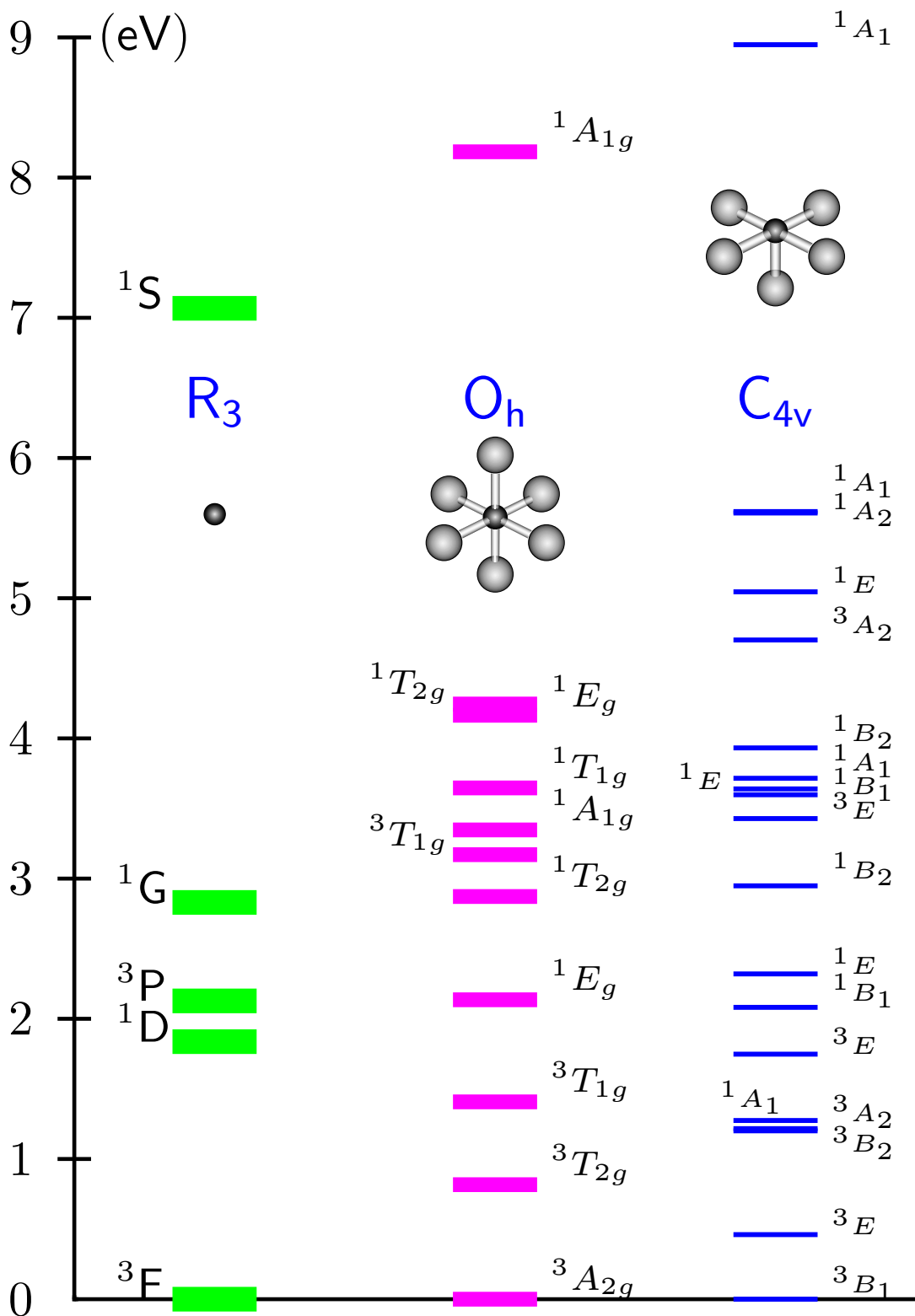


Figure 3.2: Level scheme of Ni^{2+} ion representing the levels for the free ion, bulk, and (001) surface environments of NiO. See also Table 3.5.

Table 3.5: Bulk and (001) Surface energies of NiO

state	energy			
	$\gamma = a$	$\gamma = b$	$\gamma = c$	$\gamma = d$
bulk, $D = 0.0720$, $F = -0.0117$				
$\gamma^1 A_{1g}$	3.3471	8.1841		
$\gamma^3 T_{1g}$	1.4075	3.1706		
$\gamma^1 E_g$	2.1356	4.1649		
$\gamma^1 T_{2g}$	2.8722	4.2451		
$^3 A_{2g}$	0.0000			
$^3 T_{2g}$	0.8168			
$^1 T_{1g}$	3.6467			
(001) surface, $D = 0.1036$, $E = 0.1926$, $F = -0.0146$				
$\gamma^1 A_1$	1.9728	3.3764	4.7614	8.3387
$\gamma^3 A_2$	1.2921	3.7000		
$\gamma^3 E$	0.6945	1.4615	3.1331	
$\gamma^1 B_1$	2.1036	3.7821		
$\gamma^1 B_2$	2.9333	3.9732		
$\gamma^1 E$	2.7424	3.4000	4.5158	
$^3 B_1$	0.0000			
$^3 B_2$	1.0208			
$^1 A_2$	4.4751			

Chapter 4

Crystal Field Theory: Results for CoO

The second transition metal oxide we are interested in is CoO. A strong magnetic Co state is realized in CoO which is an antiferromagnet with $T_N = 289K$. The crystal structure of CoO is similar to that of NiO with the lattice parameter $a = 4.26\text{\AA}$ and the shortest metal-oxygen distance 2.13\AA according to [45]. The magnetic moment of Co measured in [46] is $M = 3.4\mu_B$, which indicates that the orbital moment is only partially quenched because M clearly exceeds the spin magnetic moment alone. Although it was more or less accepted in early days that the gap around 4 eV of NiO, CoO, and FeO arises from Mott-Hubbard localization of electrons in partly filled $3d$ -band, this has not been settled yet. From the comparison of the data of Powell and Spicer [47] for CoO with that of NiO, it is observed that the mean position of the strong rise in the CoO absorption edge occurs at an even higher energy than in NiO which gives the gap more than 4 eV. Shen *et al.* defined a gap in this way of about 6 eV. On the other side, J. van Elp *et al.* calculated [26] the gap in CoO of 2.5 ± 0.3 eV; the authors assigned this value to the minimum in the (broader than in NiO) absorption edge. This is also visible in the data of Pratt and Coelho [48], where the absorption onset occurs between 2.5 and 3.0 eV. Although the gap can not be calculated within CFT, it is possible to make some statements about its origin. Since CFT is based on the assumption about the strong localization of the outermost incomplete shell electrons, this theory anticipates the Mott-Hubbard model to be valid for the material. As we showed, CFT well describes the NiO thus supporting this assumption. Since the gap in CoO is of intermediate character, the localization of $3d$ -electrons is weaker. It is shown in this chapter that CFT does give an acceptable description of this material, while for FeO, discussed in the next chapter, CFT fails to even give the proper ground state symmetry. Thus, we may conclude that CFT results for both NiO and CoO confirm strong localization of $3d$ -electrons thus supporting the validity of the Mott-Hubbard model for these systems.

Similarly to nickel, we consider the Co^{2+} ion as a highly-correlated electron system in which the outermost incomplete shell consists of seven $3d$ -electrons. Equivalently, we treat this system as being composed from three $3d$ -holes. Wavefunctions for the spherically

Table 4.1: The energy levels for Co^{2+} ion having $3d^34s^2$ configuration

hole configurations $3d^34s^0$ and $3d^34s^2$					
state		correction			energy
$E(^2P)$	$= A$	$-6B$	$+3C$		2.6928
$E(^4P)$	$= A$				1.8893
$E(a^2D)$	$= A$	$+5B$	$+5C$	$-\alpha$	2.9576
$E(b^2D)$	$= A$	$+5B$	$+5C$	$+\alpha$	7.2778
$E(^2F)$	$= A$	$+9B$	$+3C$		4.5820
$E(^4F)$	$= A$	$-15B$			0.0000
$E(^2G)$	$= A$	$-11B$	$+3C$		2.0630
$E(^2H)$	$= A$	$-6B$	$+3C$		2.6928
$\alpha = \sqrt{193B^2 + 4C^2 + 8BC}$					
$A = 1.9020, B = 0.1260, \text{ and } C = 0.5197 \text{ for CoO}$					

symmetric cobalt ion are constructed from the already calculated Ni^{2+} wavefunctions by adding one $3d$ -particle to the $3d^8$ LS states by means of Clebsch-Gordan algebra. This method produces an energy matrix of the $120 \times 120 \times 3$, so there are 120 LS -states formed and each of them is expressed in terms of three parameters. Since the symmetry is high and these levels are degenerate, it is possible to decompose them into 8 allowed LS -terms, of which the 2D appears twice. The values of the parameters A , B , and C which describe the Coulomb interaction in CoO have been found from the least-squares fitting to experimentally measured energies $^4F = 0.0000$, $^4P = 1.8849$, $^2G = 2.1051$, $^2H = 2.8171$, and $a^2D = 2.8591$ which are taken from [23]. Knowing the parameters we are able to find the energies of all levels as well as their eigenfunctions, as it is presented in Table 4.1. As we saw before the wavefunctions of two 2D levels are defined by the values of the parameters and can be calculated numerically only (there is no analytical solution). Note that three $3d$ -electrons may form states with spin multiplicity 2 (doublets) or 4 (quartets). As it is seen from this table the highest value of $L = 6$, which requires the cubic harmonics for L up to six to be found. This task is solved by using the projection technique. Although some of them are already tabulated in [49], they can not be used without modification since we deal with a basis of spherical harmonics, while the mentioned work contains expressions in cartesian coordinates.

To make further steps towards the electronic structure of CoO we modify spherically symmetric wavefunctions according to the expressions for cubic harmonics to get symmetry adapted wavefunctions. For the case of bulk CoO it produces the set of ΓSS_z levels with $\Gamma = A_{1g}, \dots, T_{2g}$. Spin degeneracy of each state is either 2 or 4 which corresponds to the total spin moment $S = 1/2$ or $S = 3/2$ respectively. Next, we may compute the Hamiltonian matrix with these approximate trial wavefunctions and find two CFT

parameters, describing the interaction of electrons with the ligand field. The energies used to fit the parameters for CoO are $a^4T_{1g} = 0.0000$, $a^4T_{2g} = 0.6800$, $a^2E_g = 1.9000$, $a^2T_{1g} = 2.5100$, $a^2T_{2g} = 2.5500$, and $a^4A_{2g} = 1.4100$ and are taken from [50]. In the same way as before, substitution of the parameters into the Hamiltonian matrix followed by the diagonalization procedure provides us with the complete description of the Co^{2+} ion placed in the field of six oxygen ions. The biggest block in case bulk CoO has a size 5×5 .

Table 4.2: Bulk and Surface energies of CoO

state	energy									
	$\gamma = a$	$\gamma = b$	$\gamma = c$	$\gamma = d$	$\gamma = e$	$\gamma = f$	$\gamma = g$	$\gamma = h$	$\gamma = i$	$\gamma = j$
bulk, $D = 0.0328$, $F = -0.0096$										
${}^2A_{1g}$	2.6310									
${}^2A_{2g}$	5.1501									
${}^4A_{2g}$	1.2393									
γ^2E_g	1.7612	3.3476	3.6851	7.7981						
γ^2T_{1g}	2.2329	2.8161	3.1293	3.6619	5.0521					
γ^4T_{1g}	0.0000	2.3541								
γ^2T_{2g}	2.2354	3.0758	3.6590	4.9821	7.7899					
${}^4T_{2g}$	0.5681									
(001) surface, $D = 0.0263$, $E = 0.3763$, $F = 0.0093$										
γ^2A_1	2.0786	2.5966	3.7509	4.5481	7.3305					
γ^2A_2	2.1402	2.5112	3.4292	4.2767	5.6167					
γ^4A_2	0.0000	2.4542								
γ^2B_1	2.2688	2.5815	3.4476	5.3264	9.1996					
4B_1	0.3910									
γ^2B_2	2.3464	2.5129	3.2868	5.0355	9.6423					
4B_2	0.2601									
γ^2E	1.9290	2.3562	2.6778	2.8383	3.4782	3.8500	4.4766	5.4669	5.8016	7.9234
γ^4E	0.1370	0.6539	3.2409							

If the Co ion is found on the (001) surface of CoO surrounded by five oxygen ions then the symmetry is further reduced. Now the orbital moment of the system is characterized by $\Gamma = A_1, A_2, B_1, B_2, E$. Using wavefunctions produced with the help of cubic harmonics we get 120 states of the metal ion. The Hamiltonian matrix again has a block-diagonal form with a maximum block size of 10×10 for 2E state. The experimentally known energies for the surface of CoO are $a^4A_2 = 0.0000$, $a^4E = 0.0500$, $a^4B_2 = 0.3500$, and $b^4E = 0.7000$ and are taken from [51]. Having the parameters fitted and the Hamiltonian matrix diagonalized we come to the energy levels and wavefunctions for the (001) surface of CoO. Our results for CoO are not so good as for NiO, but are nevertheless acceptable. Although the convergence

of calculated energies to their experimental values is not perfect, it does give the proper order of levels and acceptable differences between “input” and “output” energies in CFT. In our opinion, these differences show the limited applicability of CFT to CoO.

Both bulk and surface terms for CoO are presented in Table 4.2, where the levels having the same quantum numbers Γ and S are given in rows. For levels appearing more than once in configuration their energies are arranged in columns within the same row.

The multiplet levels of CoO may be visualized in form of the level scheme, as presented in Fig. 4.1.

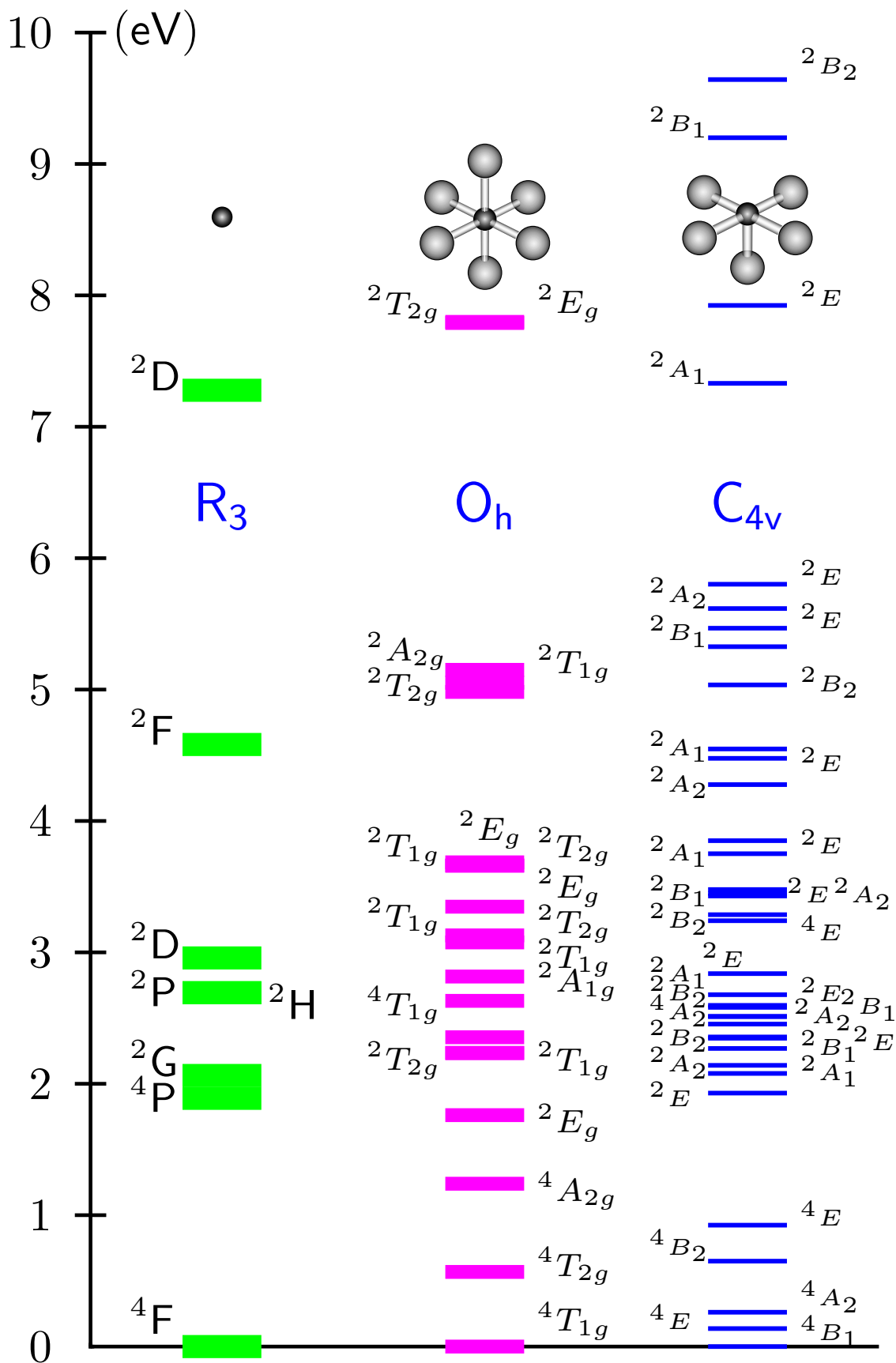


Figure 4.1: Level scheme of Co^{2+} ion representing the levels for the free ion, bulk, and (001) surface environments of CoO

Chapter 5

Crystal Field Theory: Results for FeO

The last material of our interest is Wustite (FeO). The symmetry of this compound above $T_N = 198$ K is $Fm\bar{3}m$ (the point group O_h) with the lattice parameter $a = 4.296\text{\AA}$. The magnetic moment of the metal ion in the FeO is $3.32\mu_B$ [52]. The ground state electronic configuration in FeO is $3d^64s^0$, which gives 210 possible electronic states.

Similarly to CoO, we start our treatment with the free ion Fe^{2+} . The wavefunctions of this system are formed by means of Clebsch-Gordan algebra from the already available eigenfunctions of \vec{L} for the $3d^34s^0$ configuration (they were calculated for Co^{2+} ion) by adding one $3d$ -particle to them. The resulting states may have the total orbital moment $L = 0, \dots, 6$ and the total spin moment $S = 0, 1, 2$ (which corresponds to the spin multiplicity 1, 3, or 5) respectively. In this configuration most of the levels (1S , 3P , 1D , 3F , and 1G) appear twice, which requires the solution of the secular equations to find their energies. Using already known energies for the gas phase of Fe^{2+} ion we are able to compute the CFT parameters, which describe the Coulomb interaction between the $3d$ -electrons, and the wavefunctions of the system. The energies for the free Fe^{2+} ion are again taken from gas phase experiments [23], namely (in eV) $^5D = 0.0000$, $a^3P = 2.4060$, $^3H = 2.4861$, $a^3F = 2.6611$, $^3G = 3.0450$, $^1I = 3.7639$, $^3D = 3.8097$, $a^1G = 3.8296$, $a^1S = 4.3164$, $a^1D = 4.4393$, $^1F = 5.3188$, $b^3P = 6.0939$, $b^3F = 6.2224$, and $b^1G = 7.0949$. The results are presented in Table 5.1. The energies provided by CFT are close to the ones found in experiment, which confirms the validity of our calculations for the free Fe^{2+} ion.

In order to describe the electronic configuration of the Fe^{2+} ion in the bulk monoxide FeO, we form the symmetry adapted linear combinations of the spherically symmetric wavefunctions. In case of FeO, the total orbital moment of the spherically symmetric metal ion may be up to $L = 6$, which requires the cubic harmonics of corresponding order. Once these approximate wavefunctions are formed and the values of parameters describing the Coulomb interaction are calculated, we are ready to find the wavefunctions for bulk FeO. Some of the energies for the bulk FeO are measured in experiment and equal $a^5T_{2g} = 0.0000$, $a^5E_g = 1.0400$, $a^3T_{1g} = 1.7200$, and $a^1A_{1g} = 2.0200$. Using these energies

we compute the whole level scheme for the bulk of FeO. The results are presented in Table 5.2. Unfortunately, the computed levels are not comparable with the values found in experiment. Even the proper symmetry of the ground state cannot be reproduced. Thus we have reached the point where CFT fails. In our opinion, this is due to the smaller number of electrons in the outermost shell. Compared with NiO and CoO, in the FeO the $3d$ -shell (consisting of six electrons) is far from being closed. In this case electronic correlations between these electrons in the bulk material may differ from ones for the free ion. Thus, the parameters describing the Coulomb interaction for the free ion change their values in the bulk material.

The situation for the (001) surface of FeO is similar to that for the bulk. Following our standard scheme and using the experimentally measured energies of Fe^{2+} ion on the (001) surface ($a^5E = 0.0000$, $a^5B_2 = 0.1300$, $a^5A_1 = 0.4700$, and $a^5B_1 = 1.1400$) we could not get the proper description of the system.

Table 5.1: The energy levels for Fe^{2+} ion having $3d^44s^2$ configuration

state	correction				energy
$E(a^1S)$	$= A$	$+10B$	$+10C$	$-\alpha_1$	4.3318
$E(b^1S)$	$= A$	$+10B$	$+10C$	$+\alpha_1$	12.2004
$E(a^3P)$	$= A$	$-5B$	$+5.5C$	$-\alpha_2$	2.6397
$E(b^3P)$	$= A$	$-5B$	$+5.5C$	$+\alpha_2$	6.2114
$E(a^1D)$	$= A$	$+9B$	$+7.5C$	$-\alpha_3$	4.5766
$E(b^1D)$	$= A$	$+9B$	$+7.5C$	$+\alpha_3$	9.3753
$E(^3D)$	$= A$	$-5B$	$+4C$		3.7205
$E(^5D)$	$= A$	$-21B$			0.0000
$E(^1F)$	$= A$		$+6C$		5.2357
$E(a^3F)$	$= A$	$-5B$	$+5.5C$	$-\alpha_4$	2.6912
$E(b^3F)$	$= A$	$-5B$	$+5.5C$	$+\alpha_4$	6.1600
$E(a^1G)$	$= A$	$-5B$	$+7.5C$	$-\alpha_5$	3.7296
$E(b^1G)$	$= A$	$-5B$	$+7.5C$	$+\alpha_5$	7.0017
$E(^3G)$	$= A$	$-12B$	$+4C$		2.9154
$E(^3H)$	$= A$	$-17B$	$+4C$		2.3402
$E(^1I)$	$= A$	$-15B$	$+6C$		3.5104
$\alpha_1 = \sqrt{772B^2 + 16C^2 + 32BC}$					
$\alpha_2 = \sqrt{228B^2 + 2.25C^2 - 6BC}$					
$\alpha_3 = \sqrt{324B^2 + 2.25C^2 + 18BC}$					
$\alpha_4 = \sqrt{153B^2 + 2.25C^2 + 9BC}$					
$\alpha_5 = \sqrt{177B^2 + 2.25C^2 - 3BC}$					
$A = 2.4457$, $B = 0.1150$, and $C = 0.4700$ for Fe^{2+}					

Table 5.2: The energy levels of the Fe^{2+} ion in the bulk and on the (001) surface of FeO. The levels on the (001) surface may be up to 12-fold degenerated, which is denoted by the second line having no label in the first column. For such states corresponding γ -s should be taken from the second row ($\gamma = h, \dots, \gamma = l$).

state	energy						
	$\gamma = a$	$\gamma = b$	$\gamma = c$	$\gamma = d$	$\gamma = e$	$\gamma = f$	$\gamma = g$
	$\gamma = h$	$\gamma = i$	$\gamma = j$	$\gamma = k$	$\gamma = l$		
bulk							
$\gamma^1 A_{1g}$	3.6746	4.4086	5.0467	7.0434	12.5232		
$\gamma^1 A_{2g}$	3.5883	5.6385					
$\gamma^1 E_g$	3.3405	4.1237	4.5732	7.2952	9.8224		
$\gamma^1 T_{1g}$	3.7583	4.4938	5.4945	7.1728			
$\gamma^1 T_{2g}$	3.3231	3.6620	4.0376	5.0623	5.5738	7.6115	9.5921
$^3 A_{1g}$	2.9154						
$\gamma^3 A_{2g}$	2.7763	6.5555					
$\gamma^3 E_g$	2.4009	3.1371	3.9188				
$\gamma^3 T_{1g}$	2.1297	2.5627	2.9154	3.2140	3.4528	6.3101	6.6362
$\gamma^3 T_{2g}$	2.5799	3.0368	3.5077	4.0924	6.5332		
$^5 E_g$	0.0000						
$^5 T_{2g}$	0.4807						
(001) surface							
$\gamma^1 A_1$	2.3422	3.7913	4.0657	4.4777	5.1080	5.4704	7.6124
	7.8681	9.3361	12.7796				
$\gamma^1 A_2$	3.0976	4.2110	5.9807	7.5717			
$\gamma^1 B_1$	3.4613	4.0564	4.5592	5.2987	5.7329	7.6911	9.8059
$\gamma^1 B_2$	3.4558	3.6396	4.4016	4.7426	5.8541	7.2361	10.3288
$\gamma^1 E$	2.8484	3.5139	3.9257	4.3398	4.5911	4.8421	5.5207
	5.8913	7.1254	7.7652	9.9376			
$\gamma^3 A_1$	2.8628	3.3103	3.7119	4.5070			
$\gamma^3 A_2$	2.0447	2.2737	2.8845	3.6621	4.0445	6.7527	6.9618
$\gamma^3 B_1$	2.7265	3.2535	3.7285	4.5696	6.4380		
$\gamma^3 B_2$	1.9895	2.8167	3.3180	3.9018	6.7965		
$\gamma^3 E$	1.7334	2.3276	2.4973	2.7291	3.0232	3.2457	3.3251
	3.9545	4.2097	6.2927	6.4508	7.2204		
$^5 A_1$	0.5584						
$^5 B_1$	1.1653						
$^5 B_2$	0.2184						
$^5 E$	0.0000						

Chapter 6

Second harmonic generation

Selective sensitivity of Second Harmonic Generation to the surfaces of centrosymmetric materials (within the electric-dipole approximation) allows to use this method as a very powerful non-destructive tool for the investigation of the material structure. In magnetic materials SHG may also provide information about magnetic ordering of the surface, as was predicted for ferromagnets by Pan *et. al* [53] and for antiferromagnets by Dähn *et. al* [54]. However, none of the authors presented magnetic point groups in the classical meaning. At this work the classical treatment of magnetic point groups is used, which greatly simplifies the discussion.

Contrary to other techniques as two-photon photoemission (TPPE) or neutron diffraction, SHG allows to extract structural information at different points in the Brillouin's zone of the material. The appropriate choice of the experimental geometry enhances the selectivity of this method. One may choose different incoming-outgoing angle combinations, polarization of photons

6.1 Macroscopic theory

The broadest area of different electromagnetic phenomena is completely covered by Maxwell's equations

$$\nabla \cdot \mathbf{D} = 0 \tag{6.1a}$$

$$\nabla \cdot \mathbf{B} = 0 \tag{6.1b}$$

$$\nabla \times \mathbf{B} = -\frac{1}{c} \frac{\partial \mathbf{B}}{\partial t} \tag{6.1c}$$

$$\nabla \times \mathbf{H} = \frac{1}{c} \frac{\partial \mathbf{D}}{\partial t} \tag{6.1d}$$

In the media possessing spontaneous dielectric and magnetic moments the fields which enter Maxwell's equations relate to each other as

$$\mathbf{D} = \mathbf{E} + 4\pi\mathbf{P} \quad (6.2a)$$

$$\mathbf{B} = \mathbf{H} + 4\pi\mathbf{M} \quad (6.2b)$$

Since the largest electric field encountered in practice (10^6 V/cm) is much smaller than typical value of the internal field in the crystal (10^9 V/cm), it is possible to decompose \mathbf{P} in power of \mathbf{E} which gives a Taylor's series

$$\begin{aligned} P_\alpha(\mathbf{r}, t) = & P_\alpha^{(0)} + \sum_\beta \left(\frac{\partial P_\alpha}{\partial E_\beta} \right)_0 E_\beta + \frac{1}{2!} \sum_{\beta\gamma} \left(\frac{\partial^2 P_\alpha}{\partial E_\beta \partial E_\gamma} \right)_0 E_\beta E_\gamma \\ & + \frac{1}{3!} \sum_{\beta\gamma\delta} \left(\frac{\partial^3 P_\alpha}{\partial E_\beta \partial E_\gamma \partial E_\delta} \right)_0 E_\beta E_\gamma E_\delta + \dots \end{aligned} \quad (6.3)$$

If \mathbf{E} becomes comparable with a typical intra-atomic field, the non-linear terms start to play a role. In particular, second harmonic generation has its origin in the non-linear dielectric polarization $\mathbf{P}^{(2\omega)}$, which is expressed as

$$\mathbf{P}_i^{(2\omega)} = \chi_{ijk}^{(2\omega)} E_j E_k. \quad (6.4)$$

The non-linear second-order susceptibility tensor $\chi_{ijk}^{(2\omega)}$ may have additional symmetry due to the ordered crystalline structure. Thus we have to apply symmetry analysis to this tensor. Such a task is solved by applying the Neumann principle as will be discussed later.

Second-harmonic generation is a non-linear second-order effect. It resides in the non-linear susceptibility tensor $\chi_{ijk}^{(2\omega)}$, defined in (6.4) and therefore does not occur in media which allow spatial inversion.

If there is no absorption in the medium then the tensor elements $\chi_{ijk}^{(2\omega)}$ are real quantities. In addition they satisfy the permutation symmetry relation [55]

$$\chi_{ijk}^{(2)}(-\omega_3; \omega_1, \omega_2) = \chi_{jik}^{(2)}(\omega_1; -\omega_3, \omega_2), \text{ etc.} \quad (6.5)$$

These relations follow from the existence of a thermodynamic potential energy cubic in the electric field amplitude. The order of the indices may be interchanged if the corresponding frequencies are interchanged with them.

In general the $\chi_{ijk}^{(2\omega)}$ tensor is represented in the form of a 6×3 matrix, taking into account the fact that two incoming photons are indistinguishable:

$$\left(\begin{array}{ccc|ccc} \text{xxx} & \text{xyy} & \text{xzz} & \text{xyz}=\text{xzy} & \text{xzx}=\text{xxz} & \text{xyx}=\text{xyy} \\ \text{yxx} & \text{yyy} & \text{yzz} & \text{yzy}=\text{yyz} & \text{yzx}=\text{yxz} & \text{yxy}=\text{yyx} \\ \text{zxx} & \text{zyy} & \text{zzz} & \text{zyz}=\text{zzy} & \text{zxx}=\text{zzx} & \text{zxy}=\text{zyx} \end{array} \right) \quad (6.6)$$

Considering the magnetic crystals, one has to augment the usual space symmetry operations by time-reversal operator. As one of its consequences, there is a change (flip) of magnetic moments [56].

6.2 Magnetic symmetry

Above the Néel temperature transition metal oxides have the sodium chloride (NaCl) structure. The non-magnetic unit cell has the *face-centered cubic* Bravais lattice, which consists of two interpenetrating *fcc* sublattices. In the bulk material each Ni ion is surrounded by six oxygen ions and vice versa. Oxygen ions occupy octahedral sites in the nickel sublattice.

The (001) surface of NiO, as was observed in LEED experiment [57], has almost perfect bulk termination with only 2% relaxation of the outermost layer.

Thus the space symmetry group of paramagnetic NiO is O_h^5 ($F_m^4 \bar{3}_m^2$ or $Fm\bar{3}m$), which gives point symmetry groups O_h ($m\bar{3}m$) and C_{4v} ($4mm$) for bulk and (001) surface respectively.

6.2.1 Magnetic point groups

It is of major importance in the systematic classification and discussion of magnetically ordered crystals that there must exist a symmetry operation which reverts magnetic moments. The physical meaning of this symmetry operation is time-reversal, as that was shown by Landau and Lifschitz [56]. Reversal of magnetic moments under the inversion of time follows from different behaviors of microscopic charges and currents (integration of which gives dielectric polarization and magnetization respectively). Time-reversal operation is denoted throughout as $\underline{1}$. Notations \underline{R} means $R \times \underline{1}$ - usual (proper or improper) symmetry operation R is followed by the time-reversal $\underline{1}$. All the symmetry operations, which belong to any magnetic point group, may be accommodated to one of four classes:

- proper rotation, denoted as R
- improper rotation \bar{R}
- proper rotation, followed by time-reversal \underline{R}
- improper rotation, followed by time-reversal $\bar{\underline{R}}$

This additional symmetry operation allows the complete classification of any magnetic crystal. Similarly to the 230 crystallographic space groups there are 1651 magnetic space groups.

The symmetry of the magnetic crystal is completely defined by its magnetic space group. The 1651 magnetic space groups can be classified as follows[58]:

- 230 *colorless groups* (M). These are the 230 ordinary (Federov) groups for non-magnetic crystals which do not involve the time reversal operator $\underline{1}$. If G is any Federov group then the corresponding colorless (non-magnetic) group is given by

$$M = G.$$

- *230 grey groups* (M_g). These are obtained by associating $\underline{1}$ with each element of the Federov group G , that is

$$M_g = G + \underline{G}.$$

- *674 black and white groups associated with 14 uncolored or ordinary Bravais lattices* (M_{bwO_L}). A black and white magnetic space group belonging to this class is defined by

$$M_{bwO_L} = H + \underline{(G - H)}.$$

The unit cell of magnetic structure is the same as the purely crystallographic one.

- *517 black and white groups associated with the 22 colored Bravais lattices* (M_{bwC_L}). A group belonging to this class is defined by

$$M_{bwC_L} = G + \tau \underline{G}$$

where τ is the extra translation operation introduced when dealing with colored lattices. The unit cell of the magnetic structure has a volume twice that of the crystallographic unit cell.

However, taking into account the historical digression on magnetic groups (presented in [59]), we would like to mention another classification (presented in [60]):

- *230 uncolored patterns*, which correspond to the 230 grey groups in the classification above. These groups are appropriate to diamagnetic and paramagnetic crystals and to some non-pyromagnetic antiferromagnetic crystals;
- *230 monocolored patterns*, which correspond to the 230 colorless groups in the classification above.
- *1191 bicolored patterns*, which correspond to the cases 3 and 4 in the classification above.

The patterns from the second and third classes are appropriate to ferromagnetic and ferrimagnetic crystals, to pyromagnetic antiferromagnetic crystals (i.e. those that can exhibit parasitic ferromagnetism) and to some non-pyromagnetic antiferromagnetic crystals. Such a naming is based on the definition of the time-inversion operation as the operation which changes the colors. With such a definition the difference between *grey* and *uncolored* in the Joshua classification is not clear, because both should not be affected by this operation.

6.2.2 Magnetic point groups. Bulk *fcc*.

In the paramagnetic state the undistorted *fcc* crystal is described by the magnetic point group $\mathbf{m}\bar{\mathbf{3}}\mathbf{m}$ (O_h), which contains 48 symmetry operations.

Table 6.1: Magnetic symmetry point groups, bulk *fcc* crystal

\vec{M} \vec{L}	Ferro-/ferrimagnet Symmetry group		Antiferromagnet Symmetry group	
	International	Schoenflies	International	Schoenflies
$\langle 100 \rangle$	4/mmm	$D_{4h}(C_{4h})$	$4/mmm$	D_{4h}
$\langle 110 \rangle$	mmm	$D_{2h}(C_{2h})$	mmm	D_{2h}
$\langle 111 \rangle$	$\bar{3}m$	$D_{3d}(S_6)$	$\bar{3}m$	D_{3d}
$\langle hk0 \rangle$	$\underline{2}/\underline{m}$	$C_{2h}(C_i)$	$2/m$	C_{2h}
$\langle hhk \rangle$	$\underline{2}/\underline{m}$	$C_{2h}(C_i)$	$2/m$	C_{2h}
$\langle hkl \rangle$	$\bar{1}$	$C_i(C_i)$	$\bar{1}$	C_i

This symmetry is necessarily lower if metal ions possess magnetic moments, aligned parallel to each other. If those magnetic moments oriented along one of four $\langle 100 \rangle$ directions (cube edges), then the point symmetry group becomes **4/mmm**. For magnetic moments oriented along cube-face diagonal ($\langle 110 \rangle$ direction) or cube-body diagonal ($\langle 111 \rangle$) directions the magnetic point groups are **mmm** and **$\bar{3}m$** respectively. If \vec{M} is perpendicular to a cube-edge or to a cube-face diagonal (i.e. for $\langle hk0 \rangle$ or $\langle hhk \rangle$ directions) the magnetic point group is **$\underline{2}/\underline{m}$** . Clearly, there is a primitive case of magnetic point group **$\bar{1}$** for all the others directions.

Antiferromagnetic configurations for the bulk of an *fcc* crystal are similar to those defined above for ferro-/ferrimagnetic configurations. The only difference is that antiferromagnetic bulk *fcc* crystals are symmetric under time-reversal, which means that each symmetry group contains twice as many symmetry operations, as ferromagnetic ones, each of them being augmented by the time-reversal operator. For instance the ferromagnetic configuration with $\vec{M} \parallel \langle hk0 \rangle$ has a symmetry group $C_{2h}(C_i)$, which contains 4 symmetry operations E , \underline{C}_2 , I , and $\underline{\sigma}_h$, while the antiferromagnetic configuration with $\vec{L} \parallel \langle hk0 \rangle$ has a point symmetry group C_{2h} , which contain 8 symmetry operations E , \underline{E} , C_2 , \underline{C}_2 , I , \underline{I} , σ_h and $\underline{\sigma}_h$.

Note that all the symmetry groups, presented in Table 6.1 contain space inversion.

6.2.3 Magnetic point groups. (001) surface *fcc*.

Similar treatment may be applied to the (001) surface of an *fcc* crystal.

In the paramagnetic state the (001) surface of an *fcc* crystal, presented on Fig. 6.1 (only Ni ions are shown), is described by the non-magnetic point-group $4mm$.

This group contains 16 symmetry operations, which are presented in the table 6.3 (for this uncolored group each of them appears twice with and without time-reversal operator).

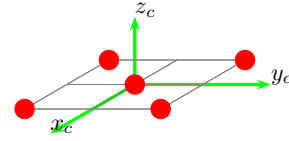
In the ferromagnetic state the presence of uniform magnetization \vec{M} lowers the symme-

Table 6.2: Symmetry operations allowed for bulk *fcc* crystal

O_h $\vec{M} = 0$	$D_{4h}(C_{4h})$ $\vec{M} \parallel [001]$	$D_{2h}(C_{2h})$ $\vec{M} \parallel [110]$	$D_{3d}(S_6)$ $\vec{M} \parallel [111]$	$C_{2h}(C_i)$ $\vec{M} \parallel [120]$	$C_{2h}(C_i)$ $\vec{M} \parallel [112]$	$C_i(C_i)$ $\vec{M} \parallel [hkl]$
E	E	E	E	E	E	E
$3C_2$	$\underline{C}_{2x} \underline{C}_{2y} \underline{C}_{2z}$	\underline{C}_{2z}		\underline{C}_{2z}		
$8C_3$			$C_{3xyz}^+ C_{3xyz}^-$			
$6C_4$	$C_{4z}^+ C_{4z}^-$					
$6C_2'$	$\underline{C}_{2xy} \underline{C}_{2x\bar{y}}$	$C_{2xy} \underline{C}_{2x\bar{y}}$	$\underline{C}_{2\bar{x}y} \underline{C}_{2\bar{y}z} \underline{C}_{2\bar{z}x}$		$\underline{C}_{2x\bar{y}}$	
I	I	I	I	I	I	I
$3\sigma_h$	$\underline{\sigma}_x \underline{\sigma}_y \sigma_z$	$\underline{\sigma}_z$		$\underline{\sigma}_z$		
$8S_6$			$S_{61}^+ S_{61}^-$			
$6S_4$	$S_{4z}^+ S_{4z}^-$					
$6\sigma_d$	$\underline{\sigma}_{xy} \underline{\sigma}_{x\bar{y}}$	$\sigma_{xy} \underline{\sigma}_{x\bar{y}}$	$\underline{\sigma}_{xy} \underline{\sigma}_{yz} \underline{\sigma}_{zx}$		$\underline{\sigma}_{xy}$	
$S_{61}^+ = C_{3xyz}^- \times i, S_{61}^- = C_{3xyz}^+ \times i$						

try. There are three non-primitive cases, namely $\vec{M} \parallel [001]$, $\vec{M} \parallel \langle 100 \rangle$, and $\vec{M} \parallel \langle 110 \rangle$. If case $\vec{M} \parallel [001]$ the point symmetry group is **4mm**, two other cases give rise to the same magnetic point symmetry group **2mm**.

The antiferromagnetic state on the (001) surface may be described by two parameters: the orientation \vec{L} of the antiferromagnetic order parameter and the additional vector \vec{A} which denotes the orientation of ferromagnetic "lines". Totally there are 6 possible magnetic symmetries for an (001) antiferromagnetically ordered surface.

Figure 6.1: *fcc* (001) surface, paramagnetic state

6.2.4 Symmetry of the tensors

Once the magnetic point group of the system is defined, it is possible to simplify the form of different tensors, which describe physical characteristics of this system. Such an analysis is based on the use of the Neumann principle, which assumes equality of tensor elements corresponding to equivalent directions in the crystal. Mathematically this is formulated by the following set of equations

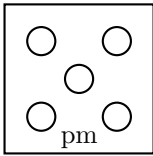
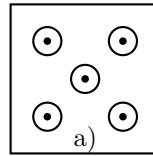
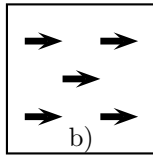
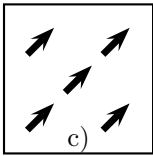
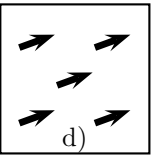
$$d_{ijk\dots n} = \sigma_{ip}\sigma_{jq}\sigma_{kr} \dots \sigma_{nu}d_{pqr\dots u} \quad (6.7a)$$

$$d_{ijk\dots n} = |\sigma|\sigma_{ip}\sigma_{jq}\sigma_{kr} \dots \sigma_{nu}d_{pqr\dots u} \quad (6.7b)$$

$$d_{ijk\dots n} = (-1)\sigma_{ip}\sigma_{jq}\sigma_{kr} \dots \sigma_{nu}d_{pqr\dots u} \quad (6.7c)$$

$$d_{ijk\dots n} = (-1)|\sigma|\sigma_{ip}\sigma_{jq}\sigma_{kr} \dots \sigma_{nu}d_{pqr\dots u}, \quad (6.7d)$$

Table 6.3: Symmetry operations allowed for ferromagnetic (001) surface of *fcc* crystal.

$\vec{M} = 0$	$\vec{M} \parallel [001]$	$\vec{M} \parallel [100]$	$\vec{M} \parallel [110]$	$\vec{M} \parallel [hk0]$
				
C_{4v} $4mm$	$C_{4v}(C_4)$ $4mm$	$C_{2v}(C_{1h})$ $2mm$	$C_{2v}(C_{1h})$ $2mm$	$C_{1h}(C_1)$ m
E	E	E	E	E
C_{2z}	C_{2z}	\underline{C}_{2z}	\underline{C}_{2z}	\underline{C}_{2z}
C_{4z}^+	C_{4z}^+			
C_{4z}^-	C_{4z}^-			
σ_x	$\underline{\sigma}_x$	σ_x		
σ_y	$\underline{\sigma}_y$	$\underline{\sigma}_y$		
σ_{xy}	$\underline{\sigma}_{xy}$		σ_{xy}	
$\sigma_{\bar{x}y}$	$\underline{\sigma}_{\bar{x}y}$		$\underline{\sigma}_{\bar{x}y}$	

where σ is the matrix corresponding to a particular permissible symmetry operation for the crystal class.

It is worth to note that in non-magnetic crystallography one considers only the first two equations (6.7a) and (6.7b), where the latter one is used for improper rotations and axial tensors, and the former is valid otherwise. This is due to the fact that some tensors do not change sign under the space inversion (polar tensors, true tensors), while other do (axial tensors, pseudotensors). In particular it says, that the magnetization vector being an axial tensor of first rank (true vector) is not influenced by space inversion, which means that the SHG process is forbidden within the electric-dipole approximation (described by a polar tensor of 3-rd rank $\chi^{(2\omega)}$) in the systems possessing a center of inversion (element $\bar{1}$ is in the point group) and this process becomes allowed if this symmetry is broken, giving rise to the sensitivity of SHG to surfaces.

The situation is changed if we consider magnetically ordered crystals. In this case an additional symmetry operation (reversal of magnetic moments) appears. Keeping in mind the special meaning of this operation (time-reversal) we may classify all tensors as being either even or odd in respect to the time-reversal. Following Birss [60] each tensor is either an *i*-tensor and keeps its sign under time-reversal or a *c*-tensor which changes it. Additionally, with respect to time-reversal all the processes may be divided into two classes: static processes, for which two directions of time are equivalent and Neumann's principle keeps its validity in four-dimensional space-time (all the symmetry operations present in the magnetic point group may be used to simplify the tensors); and dynamical

Table 6.4: Symmetry operations allowed for AF (001) surface of *fcc* crystal. Each symmetry operation is present in the group twice with and without time-inversion (C_2 means both C_2 and \underline{C}_2).

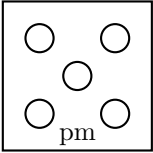
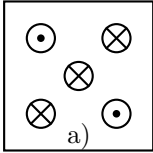
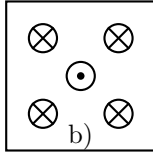
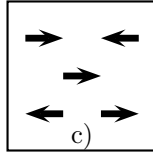
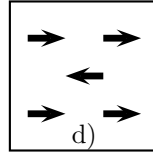
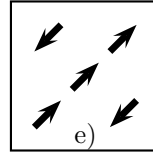
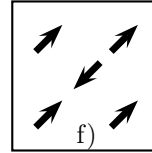
$\vec{L} = 0$ $\vec{A} = 0$	$\vec{L} \parallel [001]$ $\vec{A} \parallel [110]$	$\vec{L} \parallel [001]$ $\vec{A} \parallel [100]$	$\vec{L} \parallel [100]$ $\vec{A} \parallel [110]$	$\vec{L} \parallel [100]$ $\vec{A} \parallel [100]$	$\vec{L} \parallel [110]$ $\vec{A} \parallel [110]$	$\vec{L} \parallel [110]$ $\vec{A} \parallel [100]$
						
C_{4v} $4mm$	C_{2v} $2mm$	C_{4v} $4mm$	C_2 2	C_{2v} $2mm$	C_{2v} $2mm$	C_2 2
E C_{2z} C_{4z}^+ C_{4z}^- σ_x σ_y σ_{xy} $\sigma_{\bar{x}y}$	E C_{2z}	E C_{2z} C_{4z}^+ C_{4z}^- σ_x σ_y σ_{xy} $\sigma_{\bar{x}y}$	E C_{2z}	E C_{2z} σ_x σ_y	E C_{2z} σ_{xy} $\sigma_{\bar{x}y}$	E C_{2z}

Table 6.5: Form of the third rank polar tensors for different symmetries

Magnetic symmetry group	Unitary subgroup	Orientation of reference axis	Generating matrices	Form of $\chi_{ijk}^{(2\omega)}$	Example of configuration
$4mm$	$4mm$	$4//z, \bar{2}//y$	$\sigma^{(4)}, \sigma^{(7)}$	I_3	
$4mm$	4	$4//z$	$\sigma^{(7)}$	F_3	
$2mm$	m	$\bar{2}//z$	$\sigma^{(5)}$	C_3	
$2mm$	$mm2$	$\bar{2}//x, \bar{2}//y$	$\sigma^{(3)}, \sigma^{(4)}$	E_3	
2	2	$2//z$	$\sigma^{(3)}$	B_3	

processes, in which a unique flow of time is assumed. For the latter case only the unitary subgroup of the corresponding magnetic point group has to be employed in the symmetry analysis. At this point it is important to note that quantum mechanical models are time-symmetric, however this symmetry is broken by the presence of an externally applied magnetic field. The only physical principle which breaks this symmetry is the second law of thermodynamics (unique flow of entropy in the system).

Time- and space-reversal properties of (6.4) yields for $\chi^{(2\omega)}$ being the polar i -tensor of 3-rd rank. The particularization of matrices, given in [60] for the polar tensor of 3-rd rank is presented in Table 9.6

For the material under consideration the form of different third rank tensors is summarized in Table 6.5. This table also shows the generating matrices for each of the groups. These matrices (used in the Neumann equations) give the simplest form of any tensor. Thus, it is possible to simplify a tensor with the help of the few only generating matrices, which is sometimes done with the help of the excessive direct inspection method (in which all the symmetry operations are substituted in the Neumann equations).

In order to make it more clear we have to note that each magnetic point group has its own orientation of axis, and those orientations do not necessarily correspond to the crystallographic axis, defined for paramagnetic configuration. To find the form of tensors in the crystallographic coordinate system one has to define a coordinate system transformation which transforms the magnetic coordinate system (x_m, y_m, z_m) into the crystallographic one (x_c, y_c, z_c) , and use the relations

$$d'_{ijk\dots n} = \sigma_{ip}\sigma_{jq}\sigma_{kr}\dots\sigma_{nu}d_{pqr\dots u} \quad (6.8a)$$

$$d'_{ijk\dots n} = |\sigma|\sigma_{ip}\sigma_{jq}\sigma_{kr}\dots\sigma_{nu}d_{pqr\dots u} \quad (6.8b)$$

$$d'_{ijk\dots n} = (-1)\sigma_{ip}\sigma_{jq}\sigma_{kr}\dots\sigma_{nu}d_{pqr\dots u} \quad (6.8c)$$

$$d'_{ijk\dots n} = (-1)|\sigma|\sigma_{ip}\sigma_{jq}\sigma_{kr}\dots\sigma_{nu}d_{pqr\dots u}, \quad (6.8d)$$

where the tensor $d_{pqr\dots u}$ is defined in the magnetic coordinate system (its form for different symmetries is presented in Table 6.5), tensor $d'_{ijk\dots n}$ is defined in the crystallographic one and σ is the matrix of the symmetry operation transforming the magnetic coordinate system to the crystallographic one.

In the paramagnetic state the form of third rank polar i -tensor is (existence of c -tensors is forbidden by the presence of $\underline{1}$ in the group)

$$\begin{pmatrix} 0 & 0 & 0 & 0 & xzx & 0 \\ 0 & 0 & 0 & xzx & 0 & 0 \\ zxx & zxx & zzz & 0 & 0 & 0 \end{pmatrix}. \quad (6.9)$$

In the ferromagnetic configuration with $\vec{M} \parallel z$ third rank polar i -tensor has the form

$$\begin{pmatrix} 0 & 0 & 0 & xyz & xzx & 0 \\ 0 & 0 & 0 & xzx & -xyz & 0 \\ zxx & zxx & zzz & 0 & 0 & 0 \end{pmatrix}. \quad (6.10)$$

Such an orientation of \vec{M} allows two domains with $\vec{M} \uparrow\uparrow z$ and $\vec{M} \downarrow\downarrow z$, which gives parity of tensors under the domain operation

$$\begin{pmatrix} 0 & 0 & 0 & xyz^- & xzx^+ & 0 \\ 0 & 0 & 0 & xzx^+ & -xyz^- & 0 \\ zxx^+ & zxx^+ & zzz^+ & 0 & 0 & 0 \end{pmatrix} \quad (6.11)$$

6.3 Microscopic theory

For the calculation of SHG on the microscopic level we use the theory presented in [61]. Authors derived an expression for calculating the electric-dipole non-linear optical susceptibility tensor $\chi_{ijk}^{(2\omega)}$, based on the quantum mechanical characteristics of the system. The

general formula is

$$\begin{aligned} \chi_{ijk}^{(2\omega)}(2\mathbf{q}, 2\omega) &= \frac{-ie^3}{2q^3\Omega} \cdot \sum_{\mathbf{k}, l, l', l''} \langle \mathbf{k} + 2\mathbf{q}, l'' | e^{2i\mathbf{q}\cdot\mathbf{r}} | \mathbf{k}, l \rangle \langle \mathbf{k}, l | e^{-i\mathbf{q}\cdot\mathbf{r}} | \mathbf{k} + \mathbf{q}, l' \rangle \\ &\quad \langle \mathbf{k} + \mathbf{q}, l' | e^{-i\mathbf{q}\cdot\mathbf{r}} | \mathbf{k} + 2\mathbf{q}, l'' \rangle \\ &\quad \times \frac{\frac{f(\mathbf{E}_{\mathbf{k}+2\mathbf{q}, l''}, t) - f(\mathbf{E}_{\mathbf{k}+\mathbf{q}, l'}, t)}{E_{\mathbf{k}+2\mathbf{q}, l''} - E_{\mathbf{k}+\mathbf{q}, l'} - \hbar\omega + i\hbar\alpha} - \frac{f(\mathbf{E}_{\mathbf{k}+\mathbf{q}, l'}, t) - f(\mathbf{E}_{\mathbf{k}, l}, t)}{E_{\mathbf{k}+\mathbf{q}, l'} - E_{\mathbf{k}, l} - \hbar\omega + i\hbar\alpha}}{E_{\mathbf{k}+2\mathbf{q}, l''} - E_{\mathbf{k}, l} - 2\hbar\omega + 2i\hbar\alpha} \end{aligned}$$

It is clearly seen from this equation that incident laser light should be adjusted to the energy levels presented in the system (denominators $E_{l''} - E_{l'} - \hbar\omega$ and $E_{l'} - E_l - \hbar\omega$ require the resonance between the incoming photons energy and energies of the electronic states). Transition matrix elements $\langle l | \mathbf{d} | l' \rangle$ describe electric-dipole transitions between the one-particle states. The quantity α in the denominators describes life-time of excited levels and corresponds to the instrumental resolution in the experiment.

All the values which enter the equation (6.12) are provided by our Crystal Field Calculations, except the transition matrix elements, which are taken from [62].

This equation is modified towards a CFT basis set. Summation over one-particle states is replaced by the summation over many-particle states and corresponding transition matrix elements are expressed in the new basis set as follows

$$\langle l_1 | \hat{d} | l_2 \rangle = \sum_{r, s} c_r c_s \langle \Phi_{1r} | \hat{d} | \Phi_{2s} \rangle \quad (6.12)$$

where Φ_r and Φ_s are Slater determinants corresponding to many-particle states r and s respectively. The element $\langle \Phi_r | \hat{d} | \Phi_s \rangle$ may be easily expressed using standard form of one-particle operators in many-particle basis sets.

Chapter 7

SHG Results

At this point we are ready with the quantum-mechanical description of the system and the way to apply it for computation of its optical properties. The wavefunctions and the energy levels for NiO, CoO, and FeO are provided by CFT. Because CFT fails to give acceptable results for FeO, we concentrate here on both the NiO and CoO. In the paramagnetic states both TMMO have symmetry O_h and C_{4v} for the metal ion in the bulk and surface environments respectively. The tensor $\chi^{(2\omega)}$ which describes SHG within electric-dipole approximation being a polar tensor of 3-rd rank vanishes for system having space inversion in the group (O_h in our case), while on the surface the space-inversion symmetry is broken which leads to the form of this tensor

$$\begin{pmatrix} 0 & 0 & 0 & 0 & xzx & 0 \\ 0 & 0 & 0 & xzx & 0 & 0 \\ zxx & zxx & zzz & 0 & 0 & 0 \end{pmatrix} \quad (7.1)$$

Since on the paramagnetic surface the directions x and y are equivalent some of the tensor elements are equal ($zxx = zyy$ and $xzx = yzy$). All the elements of this tensor have a crystallographic origin and are also allowed if the symmetry is lowered by the presence of magnetization.

The symmetry of these systems in the antiferromagnetic state (below the Néel temperature) is necessarily lower than in the paramagnetic one. Even the lowest symmetry of the bulk NiO (described by C_i symmetry group) does contain the space-inversion, which forbids the existence of $\chi^{(2\omega)}$ tensor within the electric-dipole approximation. However, for the (001) surface this symmetry is broken even in the paramagnetic state. Depending on the orientation of magnetic moments there are (except the trivial symmetry group C_1 which corresponds to the arbitrary direction of \vec{L}) two possible magnetic point groups for out-of-plane orientation of magnetic moments and four ones for \vec{L} lying in the xy -plane.

Setting the time t equal to zero and choosing ground state occupancies in Eq. (6.12) we are able to study the frequency-dependent response of the sample. According to Eq. (6.12), there are three components needed for our calculations of the nonlinear susceptibility tensor elements: the wavefunctions of the NiO many-body eigenstates, the transition matrix

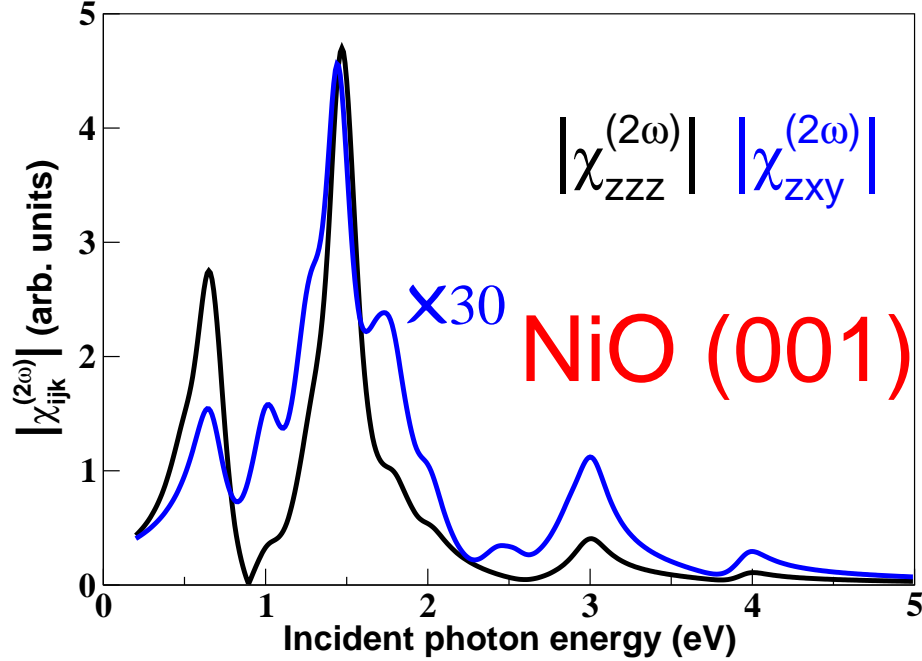


Figure 7.1: Static dependence of $\chi_{ijk}^{(2\omega)}$ on the frequency of the incident laser for the NiO(001) surface

elements between these states, and the energy levels of these states. The wavefunctions and the corresponding energies were derived in the previous sections. However, a reliable calculation of the transition matrix elements would require an *ab initio* theory of static and dynamic optical phenomena, which is unfeasible so far (transition metal oxides constitute the most difficult case due to their strong electronic correlations). Instead, we will use the approximations for the transition matrix elements obtained by Hübner *et al.* [62], which constitute simple selection rules allowing for distinguishing the tensor elements.

Here, we present the spectra of two tensor elements: the prototypic paramagnetic tensor element $\chi_{zzz}^{(2\omega)}$ and the prototypic antiferromagnetic (AF) tensor element $\chi_{zxy}^{(2\omega)}$ in Fig. 7.1. In both spectra, all the features fall within the gap, which we assume at 4.0 eV. The dominant structure in both spectra corresponds to the transitions from the ground state to the states located near 3.0 eV, see Tab. 3.5. The position of the peak around 1.5 eV corresponds to the fact that the tensor describes SHG. Other, smaller peaks related to transitions between various states are also present. Another feature of the calculated spectra is that the tensor elements are complex and their phases vary. This has important consequences for the AF domain imaging using SHG.

The main distinctive features of the spectrum of the AF tensor element $\chi_{zxy}^{(2\omega)}$ are additional peaks at 1.02 eV, 1.73 eV, and 2.46 eV where at best shoulders exist in the spectrum of the paramagnetic tensor element $\chi_{zzz}^{(2\omega)}$. Consequently, this is an “antiferromagnetic”

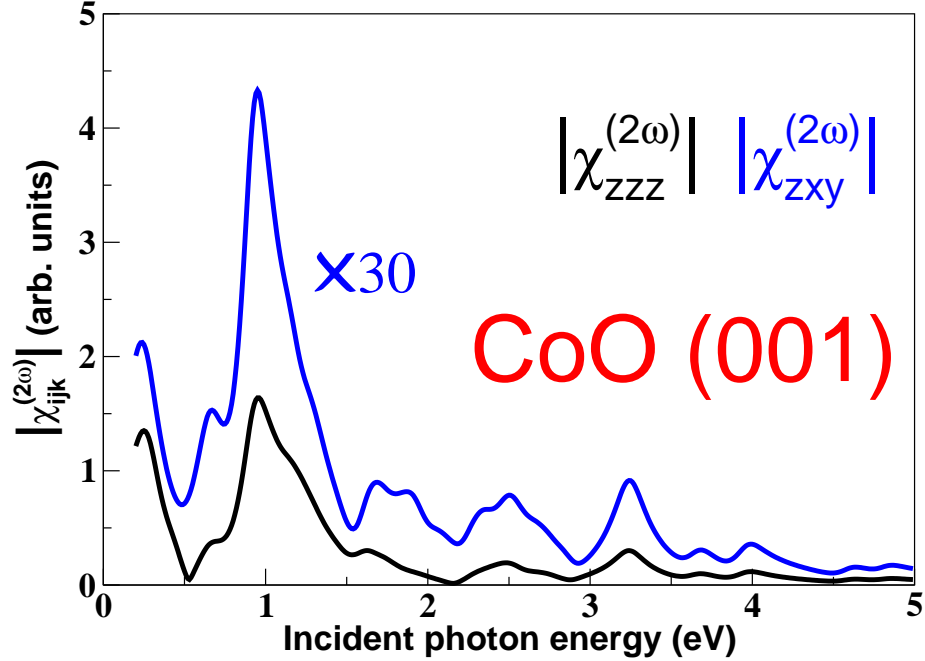


Figure 7.2: Static dependence of $\chi_{ijk}^{(2\omega)}$ on the frequency of the incident laser for the CoO(001) surface

spectral line which we suppose is especially suitable for nonlinear magneto-optics. Note that the AF SHG tensor element $\chi_{zxy}^{(2\omega)}$ is *linear* in the AF order parameter. Another interesting result is that both tensor elements are of similar magnitude. This is a favorable condition for AF domain imaging. Taking into account the magnitudes of both tensor elements presented in this section, the domain contrast should be as large as in ferromagnets (where it is of the order of *unity* in SHG, as opposed to the small domain contrast in MOKE). This large contrast provides a large driving force for the dynamics of the nonlinear magneto-optical response.

Using the results provided by CFT for the CoO we have computed in the same way the prototypical paramagnetic and antiferromagnetic tensor elements for this system. The results are shown in Fig. 7.2. Due to the bigger number of levels within the gap the structure of these tensors elements is more complicated. However, there are characteristic features which allows to distinguish the contributions of χ_{zzz} from those of χ_{zxy} . Most of these features appear above the main peak (around 1 eV) which make them more difficult to access them experimentally.

Next, we turn to the calculation of the AF spin dynamics on the femtosecond time scale for the NiO. The initial excitation is assumed to be infinitesimally short in time (the excitation pulse is already completed when our dynamics starts) but its energy distribution follows a Gaussian profile, centered at 2 eV and 20 eV wide (truncated at 0 eV, so that no

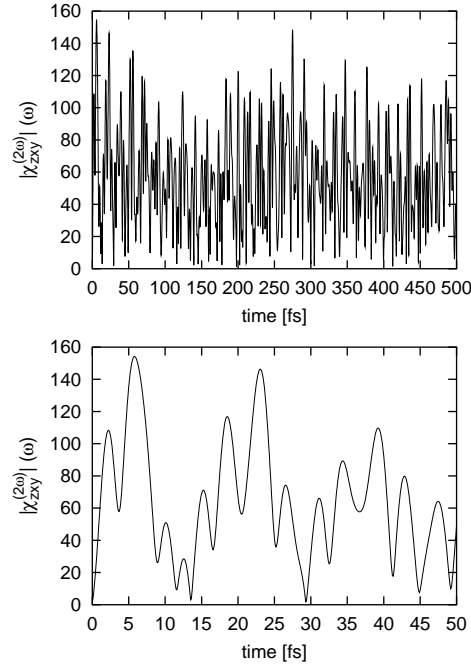


Figure 7.3: Time evolution of the tensor element $\chi_{zyx}^{(2\omega)}$ within the first 50 fs after the excitation. The inset shows the evolution of the same tensor element within the first 500 fs.

negative energies appear). Such a strong excitation will be distributed in a real experiment among many atoms, but here we confine it to one atom without any loss of generality. The chosen width of excitation allows us to probe the fast limit of the dynamics, since all the energy levels (including the highest) are populated and consequently all de-excitation channels are open. Restricting the Hamiltonian to electronic on-site interactions complies with this limit. The initial excitation causes a strong redistribution of charges among the energy levels, visible as a drop (to a value close to zero at time $t = 0$, because all the states are nearly equally populated) of the observed signal compared to its value in a static experiment. The time evolution of the excited system then results from the quantum phase factors and has no classical analogue.

Fig. 7.3 shows the dynamics of the AF tensor element $\chi_{zxy}^{(2\omega)}(t)$ within the first 50 fs. Such a dynamics can be probed in an interferometric SHG experiment. The inset shows its evolution up to 500 fs, at the fundamental photon energy 0.64 eV (This frequency corresponds to the low lying AF line in the SHG spectrum of NiO (001)). There is no decay of the envelope of $\chi_{zxy}^{(2\omega)}(t)$, unlike for metallic systems [63]. The coherence is preserved for a long time (until phenomena neglected here, such as electron-phonon coupling that is of particular relevance in dielectrics take place), which manifests itself by beats repeated regularly every 20 fs. The spin dynamics takes place within femtoseconds, thus being

as fast as in metals. Consequently, we predict coherence times that are four orders of magnitude longer than the ultimate speed of the spin and charge dynamics. This allows for many read-write cycles during the intrinsic life-time of the excitation. Besides, it fulfills one of the important conditions for quantum information [64]. This finding is in line with the experimentally determined widths of spectral lines in oxides [2] (tens of μeV , which corresponds to tens of picoseconds coherence times) and bears a similarity to the optical effects used for coherent control in semiconductor quantum dots [65].

Chapter 8

Conclusions

This work is devoted to the investigations of electronic and magnetic properties of transition metal ions positioned in bulk and within interfacial layers of transition metal monoxides (TMMO). The description of the electronic structure is based on Crystal Field Theory (CFT), which efficiently handles the systems whose behavior is mostly determined by strongly correlated electrons of the outermost incomplete shell, in our case $3d$ -electrons. These electrons do not only define the electronic structure of the system, but are also responsible for its magnetic properties, being an origin of the fact that transition metals exist in the ferromagnetic state below the Curie temperature while their oxides usually have antiferromagnetic ordering below the Néel temperature. There are two basic approaches to account for magnetism, the method of localized magnetic moments and the method of itinerant magnetic moments. The choice of a particular approach depends on the nature of the material and in many cases is a difficult one to make. The first method is based on the current distributions which are localized within a lattice cell. Well pronounced states of ionic character found in different kinds of experiment on TMMO assume this method to be appropriate for insulating TMMO. However, ferromagnetic metals are usually described by the second method, in which the current distributions are those associated with free electrons.

Although CFT is sketched in many of the textbooks as an example to show multiplet splitting due to the interaction with the field of ligands, its complete many-particle realization is rather complicated and requires a careful treatment. In this work we completely take into account all the crystal field effects. Three materials of interest (NiO, CoO, and FeO) are described and their electronic states have been computed within this theory. Expressions for the field produced by surrounding ligands for both bulk and (001) surface symmetries are derived. Approximate eigenfunctions of the angular momentum operator \hat{L} (cubic harmonics) are replaced by the exact wavefunctions which completely diagonalize the Hamiltonian matrix. Angular parts of the wavefunctions for different states of the system assumed to be defined by ligands are found in the equivalent directions, and are calculated exactly. Localization of the electrons on the metal site allows to reduce the task of finding the radial parts of the wavefunctions to the one of fitting few contributing

integrals to get the best convergence to the already known energies of the system. In case of “true” eigenfunctions of the Hamiltonian this is a task of non-linear least-squares fitting in many dimensions (dimension for each energy level is equal to the number of times it appears in the given symmetry for a given electronic configuration). This task is successfully solved by employing the Powell’s method of minimization in multidimensions. The way to include spin-orbit coupling effects and label the resulting levels is presented.

The description of the system, provided by CFT gives a possibility to compute its characteristics which can be measured in experiment allowing to confirm the applicability of the theory and make some predictions. In order to prove our results we applied CFT data to compute the response of the system to the external laser light. The interaction of ions with the light created in the medium by the initial laser field gives rise to many physical phenomena, of which one considered here is Second Harmonic Generation (SHG). The effect of Sum Frequency Generation (and in particular SHG) represents one of a broad variety of non-linear optical effects, which start to appear if the laser field is strong enough. The definition of the field strength depends on the particular process and may be stated as follows: a field can be called strong when, during the time of its action, processes involving more than one photon become significant. Already from this definition, it becomes clear that the non-linear optical effects, although require special experimental conditions, may give information about the system which is not accessible in other methods. Although some experiments are able to detect the magnetism of the sample, it is often difficult to identify the domains or determine the orientations of magnetic moments in the material. We have chosen the Second Harmonic Generation as an exemplary method to give such information. SHG is a non-destructive method which can be used to control the state of the system *in situ*. Moreover, a typical SHG experiment has tunable parameters which allow to precisely extract the information about microscopic properties. Choosing an appropriate geometry one may assure the output signal to be defined by one or another tensor $\chi^{(2\omega)}$ element (this tensor is an origin of SHG). Optical SHG is clearly sensitive to the interfaces. Additionally, an elementary process of SHG includes two photons; this extends the ability of this method to extract the structural information. Taking into account magnetic ordering one may try to use this technique to detect the magnetic structure. Symmetry analysis of optical SHG for different magnetic states of the same system shows a strong dependence of the output SHG signal on the particular magnetic structure of the system. Magnetic optical SHG experiments discriminate different types of magnetism and in many cases visualize magnetic domains existing in the sample which are not seen in other experiments.

The symmetry of the SHG process for materials having different crystal structures and/or set of domains follows from the well known Neumann’s principle. There are two basic approaches to account for magnetism. In the first approach the tensor $\chi^{(2\omega)}$ is expanded in the series of powers of the order parameter, while in the second one the magnetic point group of the sample has to be identified. The existence of the magnetic order parameter is defined in the Landau theory of phase transitions. This is a quantity which: (1) is invariant under all symmetry operations from the corresponding magnetic point group, and

(2) has different values for equivalent orderings of individual magnetic moments. Although the order parameter is unambiguously defined for ferromagnets, its form for antiferromagnetic configurations is complicated. In such cases the second approach of magnetic point groups seems to be simpler. The extension of Neumann's principle to the 90 magnetic point groups has been performed by R. Birss. Due to the existence of time-reversal in these groups the mathematical formulation of Neumann's principle is different for c - and i -tensors and for unitary and antiunitary symmetry operations. Special attention should be paid to the process itself which may be a static or dynamical one. In the second case time-reversal symmetry of the process is broken and the unitary subgroup only of the corresponding magnetic point group has to be considered.

Since the metal ions in TMMO are ordered antiferromagnetically, we use the magnetic point groups to find the symmetry of the tensor $\chi^{(2\omega)}$ for the materials under consideration. Although such an analysis for (001), (110), and (111) surfaces of *fcc* materials was done before by M. Trzeciecki *et al.*, magnetic point groups were not identified because the time-reversal operation was not included. It is worth to note that the definition of magnetic space groups is based on time-reversal and each such group contains an even number of symmetry operations of which half is unitary symmetry operations and the other half is operations augmented by the time-reversal. The antiunitary subgroup should be removed from the analysis of the tensors for dynamical (as SHG) processes, but it must be used in the symmetry (structural) analysis of magnetic media. Inclusion of the time-reversal in the symmetry analysis allows to replace excessive direct inspection method (matrices for each symmetry operations sequentially substituted in the Neumann formula) by the very elegant concept of generating matrices (for each point group only one or two symmetry operations define the form of any tensor) and greatly simplify the analysis. The form of any other tensor (describing magnetic-dipole, quadrupole, . . . contributions) may be easily found. Thus, the symmetry analysis of magnetic (001) surface is generalized. Because antiunitary symmetry operations play no role in the dynamical processes, this does not change the results obtained before. Different concepts of symmetry analysis of SHG process are compared and a comprehensive overview is presented.

The microscopic theory of SHG derived by W. Hübner *et al.* is used in this work to compute the elements of the tensor $\chi^{(2\omega)}$. Because TMMO have discrete energy levels, the laser pulse parameters have to fit the energy differences between them. In order to find the appropriate laser frequency we compute dependence of typical magnetic and crystallographic elements of $\chi^{(2\omega)}$ on the frequency of the incident light. There exist frequencies for which these tensor elements have different behaviors, which means that the laser pulse of a specially chosen frequency allows to identify the magnetic state of the surface.

Another intriguing feature of TMMO is their dynamical behavior. Based on the results of CFT, we tried to find dynamics of the system after applying the pump laser pulse. In this case levels are simultaneously excited and these excitations propagate in time. Dynamical SHG of antiferromagnetic spectral lines shows ultrafast spin dynamics. Long lasting coherence together with the possibility of ultrafast (of the order of femtoseconds)

spin switching makes these materials very promising for technological applications, such as permanent magnetic storage devices and quantum computing. Until now, among solids, only semiconductors and nuclear spins have been known to exhibit the combination of these features, suffering however from a much slower dynamics. Moreover, NiO possesses a high density of permanent magnetic moments (like metals) which is an option for device size reduction.

Chapter 9

Supplementary materials

Table 9.1: Numerical values of $c^k(lm, l'm') = (-1)^{m-m'} c^k(l'm', lm)$ for $l \leq 3, l' \leq 3$

l	l'	m	m'	$k = 0$	$k = 2$	$k = 4$
$l + l' = \text{even}$						
s	s	0	0	+1		
s	d	0	± 2		$+1/\sqrt{5}$	
		0	± 1		$-1/\sqrt{5}$	
		0	0		$+1/\sqrt{5}$	
p	p	± 1	± 1	+1	$-1/5$	
		± 1	0		$+\sqrt{3}/5$	
		0	0	+1	$+2/5$	
		± 1	∓ 1		$-\sqrt{6}/5$	
d	d	± 2	± 2	+1	$-2/7$	$+1/21$
		± 2	± 1		$+\sqrt{6}/7$	$-\sqrt{5}/21$
		± 2	0		$-2/7$	$+\sqrt{15}/21$
		± 1	± 1	+1	$+1/7$	$-4/21$
		± 1	0		$+1/7$	$+\sqrt{30}/21$
		0	0	+1	$+2/7$	$+6/21$
		± 2	∓ 2			$+\sqrt{70}/21$
		± 2	∓ 1			$-\sqrt{35}/21$
		± 1	∓ 1		$-\sqrt{6}/7$	$-2\sqrt{10}/21$

Table 9.3: Explicit Forms of the $\Theta_{lm}(\theta)$

$\Theta_{lm}(\theta) = (-1)^m \left(\frac{(2l+1)(l-m)}{2(l+m)!} \right)^{1/2} \sin^m \theta \frac{d^m}{(d \cos \theta)^m} P_l(\cos \theta),$
$\Theta_{lm}(\theta) = (-1)^m \Theta_{lm}(\theta), m \geq 0$
$\Theta_{00} \quad 1/\sqrt{2}$
$\Theta_{10} \quad (\sqrt{3}/\sqrt{2}) \cos \theta$
$\Theta_{1\pm 1} \quad \mp(\sqrt{3}/2) \sin \theta$
$\Theta_{20} \quad (\sqrt{5}/2\sqrt{2})(2 \cos^2 \theta - \sin^2 \theta)$
$\Theta_{2\pm 1} \quad \mp(\sqrt{15}/2) \cos \theta \sin \theta$
$\Theta_{2\pm 2} \quad (\sqrt{15}/4) \sin^2 \theta$
$\Theta_{30} \quad (\sqrt{7}/2\sqrt{2})(2 \cos^3 \theta - 3 \cos \theta \sin^2 \theta)$
$\Theta_{3\pm 1} \quad \mp(\sqrt{21}/4\sqrt{2}) \sin \theta (4 \cos^2 \theta - \sin^2 \theta)$
$\Theta_{3\pm 2} \quad (\sqrt{105}/4) \cos \theta \sin^2 \theta$
$\Theta_{3\pm 3} \quad \mp(\sqrt{35}/4\sqrt{2}) \sin^3 \theta$
$\Theta_{40} \quad (3/8\sqrt{2})(8 \cos^4 \theta - 24 \cos^2 \theta \sin^2 \theta + 3 \sin^4 \theta)$
$\Theta_{4\pm 1} \quad \mp(3\sqrt{5}/4\sqrt{2}) \cos \theta \sin \theta (4 \cos^2 \theta - 3 \sin^2 \theta)$
$\Theta_{4\pm 2} \quad (3\sqrt{5}/8) \sin^2 \theta (6 \cos^2 \theta - \sin^2 \theta)$
$\Theta_{4\pm 3} \quad \mp(3\sqrt{35}/4\sqrt{2}) \cos \theta \sin^3 \theta$
$\Theta_{4\pm 4} \quad (3\sqrt{35}/16) \sin^4 \theta$

Table 9.4: Cubic harmonics

free ion	cubic state	cubic harmonics		
S	A_{1g}	S_0		
P	T_{1g}	P_{-1}	P_0	P_1
D	E_g	D_0	$\sqrt{\frac{1}{2}}(D_{-2}+D_2)$	
	T_{2g}	$\sqrt{\frac{1}{2}}(D_{-2}-D_2)$	D_{-1}	D_1
F	A_{2g}	$\sqrt{\frac{1}{2}}(F_{-2}-F_2)$		
	T_{1g}	F_0	$\sqrt{\frac{3}{8}}F_{-3}+\sqrt{\frac{3}{8}}F_1$	$\sqrt{\frac{5}{8}}F_3+\sqrt{\frac{3}{8}}F_{-1}$
	T_{2g}	$\sqrt{\frac{1}{2}}(F_{-2}+F_2)$	$\sqrt{\frac{3}{8}}F_{-3}-\sqrt{\frac{5}{8}}F_1$	$\sqrt{\frac{3}{8}}F_3-\sqrt{\frac{5}{8}}F_{-1}$
G	A_{1g}	$\sqrt{\frac{5}{24}}(G_{-4}+G_4)+\sqrt{\frac{7}{12}}G_0$		
	E_g	$\sqrt{\frac{7}{24}}(G_{-4}+G_4)-\sqrt{\frac{5}{12}}G_0$	$\sqrt{\frac{1}{2}}(G_{-2}+G_2)$	
	T_{1g}	$\sqrt{\frac{1}{2}}(G_{-4}-G_4)$	$\sqrt{\frac{1}{8}}G_{-3}+\sqrt{\frac{7}{8}}G_1$	$\sqrt{\frac{1}{8}}G_3+\sqrt{\frac{7}{8}}G_{-1}$
	T_{2g}	$\sqrt{\frac{1}{2}}(G_{-2}-G_2)$	$\sqrt{\frac{7}{8}}G_{-3}-\sqrt{\frac{1}{8}}G_1$	$\sqrt{\frac{7}{8}}G_3-\sqrt{\frac{1}{8}}G_{-1}$
H	E_g	$\sqrt{\frac{1}{2}}(H_{-2}-H_2)$	$\sqrt{\frac{1}{2}}(H_{-4}-H_4)$	
	T_{1g}	H_0	$\sqrt{\frac{63}{128}}H_{-5}+\sqrt{\frac{35}{128}}H_3+\sqrt{\frac{15}{64}}H_{-1}$	$\sqrt{\frac{63}{128}}H_5+\sqrt{\frac{35}{128}}H_{-3}+\sqrt{\frac{15}{64}}H_1$
	T_{1g}	$\sqrt{\frac{1}{2}}(H_{-4}+H_4)$	$\sqrt{\frac{5}{128}}H_{-5}-\sqrt{\frac{81}{128}}H_3+\sqrt{\frac{21}{64}}H_{-1}$	$\sqrt{\frac{5}{128}}H_5-\sqrt{\frac{81}{128}}H_{-3}+\sqrt{\frac{21}{64}}H_1$
	T_{2g}	$\sqrt{\frac{1}{2}}(H_{-2}+H_2)$	$\sqrt{\frac{15}{32}}H_{-5}-\sqrt{\frac{3}{32}}H_3-\sqrt{\frac{7}{16}}H_{-1}$	$\sqrt{\frac{15}{32}}H_5-\sqrt{\frac{3}{32}}H_{-3}-\sqrt{\frac{7}{16}}H_1$
I	A_{1g}	$\sqrt{\frac{7}{16}}(I_{-4}+I_4)-\sqrt{\frac{1}{8}}I_0$		
	A_{2g}	$\sqrt{\frac{5}{32}}(I_{-6}+I_6)-\sqrt{\frac{11}{32}}(I_{-2}+I_2)$		
	E_g	$\sqrt{\frac{1}{16}}(I_{-4}+I_4)+\sqrt{\frac{7}{8}}I_0$	$\sqrt{\frac{11}{32}}(I_{-6}+I_6)+\sqrt{\frac{5}{32}}(I_{-2}+I_2)$	
	T_{1g}	$\sqrt{\frac{1}{2}}(I_{-4}-I_4)$	$\sqrt{\frac{11}{32}}I_{-5}+\sqrt{\frac{15}{32}}I_3-\sqrt{\frac{3}{16}}I_{-1}$	$\sqrt{\frac{11}{32}}I_5+\sqrt{\frac{15}{32}}I_{-3}-\sqrt{\frac{3}{16}}I_1$
	T_{2g}	$\sqrt{\frac{1}{2}}(I_{-2}-I_2)$	$\sqrt{\frac{165}{256}}I_{-5}-\sqrt{\frac{81}{256}}I_3+\sqrt{\frac{5}{128}}I_{-1}$	$\sqrt{\frac{165}{256}}I_5-\sqrt{\frac{81}{256}}I_{-3}+\sqrt{\frac{5}{128}}I_1$
	T_{2g}	$\sqrt{\frac{1}{2}}(I_{-6}-I_6)$	$\sqrt{\frac{3}{256}}I_{-5}+\sqrt{\frac{55}{256}}I_3+\sqrt{\frac{99}{128}}I_{-1}$	$\sqrt{\frac{3}{256}}I_5+\sqrt{\frac{55}{256}}I_{-3}+\sqrt{\frac{99}{128}}I_1$

Table 9.5: Generating matrices

$$\begin{array}{lcl}
\sigma^{(0)} = [1] = & \begin{bmatrix} 1 & 0 & 0 \\ 0 & 1 & 0 \\ 0 & 0 & 1 \end{bmatrix} & \sigma^{(1)} = [\bar{1}] = \begin{bmatrix} -1 & 0 & 0 \\ 0 & -1 & 0 \\ 0 & 0 & -1 \end{bmatrix} \\
\sigma^{(2)} = [2_y] = & \begin{bmatrix} -1 & 0 & 0 \\ 0 & 1 & 0 \\ 0 & 0 & -1 \end{bmatrix} & \sigma^{(3)} = [2_z] = \begin{bmatrix} -1 & 0 & 0 \\ 0 & -1 & 0 \\ 0 & 0 & 1 \end{bmatrix} \\
\sigma^{(4)} = [\bar{2}_y] = & \begin{bmatrix} 1 & 0 & 0 \\ 0 & -1 & 0 \\ 0 & 0 & 1 \end{bmatrix} & \sigma^{(5)} = [\bar{2}_z] = \begin{bmatrix} 1 & 0 & 0 \\ 0 & 1 & 0 \\ 0 & 0 & -1 \end{bmatrix} \\
\sigma^{(6)} = [3_z] = \frac{1}{2} & \begin{bmatrix} -1 & \sqrt{3} & 0 \\ -\sqrt{3} & -1 & 0 \\ 0 & 0 & 1 \end{bmatrix} & \sigma^{(7)} = [\bar{4}_z] = \begin{bmatrix} 0 & 1 & 0 \\ -1 & 0 & 0 \\ 0 & 0 & 1 \end{bmatrix} \\
\sigma^{(8)} = [\bar{4}_z] = & \begin{bmatrix} 0 & -1 & 0 \\ 1 & 0 & 0 \\ 0 & 0 & -1 \end{bmatrix} & \sigma^{(9)} = \begin{bmatrix} 0 & 1 & 0 \\ 0 & 0 & 1 \\ 1 & 0 & 0 \end{bmatrix}
\end{array}$$

Table 9.6: Possible tensors of 3-rd rank ($T_3 = 0$)

A_3	$\begin{pmatrix} xxx & xyy & xzz & xyz & xzx & xyx \\ yxx & yyy & yzz & yzy & yzx & yxy \\ zxx & zyy & zzz & zyz & zxz & zxy \end{pmatrix}$	$I_3 = Q_3$	$\begin{pmatrix} 0 & 0 & 0 & 0 & xzx & 0 \\ 0 & 0 & 0 & xzx & 0 & 0 \\ zxx & zxx & zzz & 0 & 0 & 0 \end{pmatrix}$
B_3	$\begin{pmatrix} 0 & 0 & 0 & xyz & xzx & 0 \\ 0 & 0 & 0 & yzy & yzx & 0 \\ zxx & zyy & zzz & 0 & 0 & zxy \end{pmatrix}$	J_3	$\begin{pmatrix} 0 & 0 & 0 & xyz & 0 & 0 \\ 0 & 0 & 0 & 0 & xyz & 0 \\ 0 & 0 & 0 & 0 & 0 & zxy \end{pmatrix}$
C_3	$\begin{pmatrix} xxx & xyy & xzz & 0 & 0 & xyx \\ yxx & yyy & yzz & 0 & 0 & yxy \\ 0 & 0 & 0 & zyz & zxz & 0 \end{pmatrix}$	K_3	$\begin{pmatrix} xxx & -xxx & 0 & xyz & xzx & -yyy \\ -yyy & yyy & 0 & xzx & -xyz & -xxx \\ zxx & zxx & zzz & 0 & 0 & 0 \end{pmatrix}$
D_3	$\begin{pmatrix} 0 & 0 & 0 & xyz & 0 & 0 \\ 0 & 0 & 0 & 0 & yzx & 0 \\ 0 & 0 & 0 & 0 & 0 & zxy \end{pmatrix}$	L_3	$\begin{pmatrix} 0 & 0 & 0 & xyz & 0 & -yyy \\ -yyy & yyy & 0 & 0 & -xyz & 0 \\ 0 & 0 & 0 & 0 & 0 & 0 \end{pmatrix}$
E_3	$\begin{pmatrix} 0 & 0 & 0 & 0 & xzx & 0 \\ 0 & 0 & 0 & yzy & 0 & 0 \\ zxx & zyy & zzz & 0 & 0 & 0 \end{pmatrix}$	M_3	$\begin{pmatrix} xxx & -xxx & 0 & 0 & xzx & 0 \\ 0 & 0 & 0 & xzx & 0 & -xxx \\ zxx & zxx & zzz & 0 & 0 & 0 \end{pmatrix}$
$F_3 = N_3$	$\begin{pmatrix} 0 & 0 & 0 & xyz & xzx & 0 \\ 0 & 0 & 0 & xzx & -xyz & 0 \\ zxx & zxx & zzz & 0 & 0 & 0 \end{pmatrix}$	O_3	$\begin{pmatrix} xxx & -xxx & 0 & 0 & 0 & -yyy \\ -yyy & yyy & 0 & 0 & 0 & -xxx \\ 0 & 0 & 0 & 0 & 0 & 0 \end{pmatrix}$
G_3	$\begin{pmatrix} 0 & 0 & 0 & xyz & xzx & 0 \\ 0 & 0 & 0 & -xzx & xyz & 0 \\ zxx & -zxx & 0 & 0 & 0 & zxy \end{pmatrix}$	R_3	$\begin{pmatrix} xxx & -xxx & 0 & 0 & 0 & 0 \\ 0 & 0 & 0 & 0 & 0 & -xxx \\ 0 & 0 & 0 & 0 & 0 & 0 \end{pmatrix}$
$H_3 = P_3$	$\begin{pmatrix} 0 & 0 & 0 & xyz & 0 & 0 \\ 0 & 0 & 0 & 0 & -xyz & 0 \\ 0 & 0 & 0 & 0 & 0 & 0 \end{pmatrix}$	$S_3 = U_3$	$\begin{pmatrix} 0 & 0 & 0 & xyz & 0 & 0 \\ 0 & 0 & 0 & 0 & xyz & 0 \\ 0 & 0 & 0 & 0 & 0 & xyz \end{pmatrix}$

Bibliography

- [1] J. de Boeck and G. Borghs, “Magneto-electronics,” *Phys. World*, vol. April, p. 27, 1999.
- [2] M. Fiebig, D. Fröhlich, B. B. Krichevstov, and R. V. Pisarev, “Second harmonic generation and magnetic-dipole–electric-dipole interference in antiferromagnetic Cr₂O₃,” *Phys. Rev. Lett.*, vol. 73, p. 2127, 1994.
- [3] V. N. Muthukumar, R. Valentí, and C. Gros, “Microscopic Model of Nonreciprocal Optical Effects in Cr₂O₃,” *Phys. Rev. Lett.*, vol. 75, p. 2766, 1995.
- [4] M. Trzeciecki, A. Dähn, and W. Hübner, “Symmetry analysis of second-harmonic generation at surfaces of antiferromagnets,” *Phys. Rev. B*, vol. 60, p. 1144, 1999.
- [5] M. Trzeciecki and W. Hübner, “Group-theoretical analysis of second harmonic generation at (110) and (111) surfaces of antiferromagnets,” *Appl. Phys. B*, vol. 68, p. 473, 1999.
- [6] M. Trzeciecki, O. Ney, G. P. Zhang, and W. Hübner, “Laser-Control of Ferro- and Antiferromagnetism,” *Adv. Solid State Phys.*, vol. 41, p. 547, 2001.
- [7] O. Ney, M. Trzeciecki, and W. Hübner, “Femtosecond dynamics of spin-dependent SHG response from NiO (001),” *Appl. Phys. B*, vol. 74, no. 7-8, pp. 741–744, 2002.
- [8] P. A. Franken, A. E. Hill, C. W. Peters, and G. Weinreich, “Generation of Optical Harmonics,” *Phys. Rev. Lett.*, vol. 7, no. 4, pp. 118–119, 1961.
- [9] F. Brown, R. E. Parks, and A. M. Sleeper, “Nonlinear Optical Reflection from a Metallic Boundary,” *Phys. Rev. Lett.*, vol. 14, no. 25, pp. 1029–1031, 1965.
- [10] G. Racah, “Theory of Complex Spectra. I,” *Phys. Rev.*, vol. 61, no. 3-4, pp. 186–197, 1942.
- [11] G. Racah, “Theory of Complex Spectra. II,” *Phys. Rev.*, vol. 62, no. 9-10, pp. 438–462, 1942.

- [12] G. Racah, "Theory of Complex Spectra. III," *Phys. Rev.*, vol. 63, no. 9-10, pp. 367–382, 1943.
- [13] G. Racah, "Theory of Complex Spectra. IV," *Phys. Rev.*, vol. 76, no. 9, pp. 1352–1365, 1949.
- [14] J. C. Slater, "The Theory of Complex Spectra," *Phys. Rev.*, vol. 34, no. 10, pp. 1293–1322, 1929.
- [15] S. Sugano, Y. Tanabe, and H. Kamimura, *Multiplets of Transition-Metal Ions in Crystals*. Academic Press, 1970.
- [16] M. Tinkham, *Group Theory and Quantum Mechanics*. McGraw-Hill, Inc., 1964.
- [17] D. A. Varshalovich, A. N. Moskalev, and V. K. Khersonskii, *Quantum theory of angular momentum : irreducible tensors, spherical harmonics, vectors coupling coefficients, 3nj symbols*. Singapore: World Scientific, 1989.
- [18] J. A. Gaunt, "The Triplets of Helium," *Phil. Trans. Roy. Soc. A (London)*, vol. 228, pp. 151–196, 1928.
- [19] W. H. Press, *Numerical recipes in Fortran 90: the art of parallel scientific computing*, vol. 2. Cambridge: Cambridge Univ. Press, 2 ed., 1996.
- [20] M. Trzeciecki, *Second Harmonic Generation from Antiferromagnetic Interfaces*. PhD thesis, Martin-Luther-Universitaet Halle-Wittenberg, 2000.
- [21] M. Klintonberg, *Rare-earth polarized absorption spectra as a structural tool*. PhD thesis, Uppsala University, Sweden, 1997.
- [22] C. W. Ufford and G. H. Shortley, "Atomic Eigenfunctions and Energies," *Phys. Rev.*, vol. 42, no. 2, pp. 167–175, 1932.
- [23] C. E. Moore, *Atomic Energy Levels*. Natl. Bur. Stand. (U.S.), U.S. GPO, Washington DC, 1971.
- [24] G. A. Sawatzky and J. W. Allen, "Magnitude and Origin of the Band Gap in NiO," *Phys. Rev. Lett.*, vol. 53, no. 24, pp. 2339–2342, 1984.
- [25] A. Fujimori and F. Minami, "Valence-band photoemission and optical absorption in nickel compounds," *Phys. Rev. B*, vol. 30, no. 2, pp. 957–971, 1984.
- [26] J. van Elp, J. L. Wieland, H. Eskes, P. Kuiper, G. A. Sawatzky, F. M. F. de Groot, and T. S. Turner, "Electronic structure of CoO, Li-doped CoO, and LiCoO₂," *Phys. Rev. B*, vol. 44, no. 12, pp. 6090–6103, 1991.

- [27] B. E. F. Fender, A. J. Jacobson, and F. A. Wegwood, "Covalency parameters in MnO, Alpha-MnS, and NiO," *J. Chem. Phys.*, vol. 48, no. 3, p. 990, 1968.
- [28] A. K. Cheetham and D. A. O. Hope, "Magnetic ordering and exchange effects in the antiferromagnetic solid solutions $\text{MnxNi}_{1-x}\text{O}$," *Phys. Rev. B*, vol. 27, no. 11, pp. 6964–6967, 1983.
- [29] V. Fernandez, C. Vettier, F. de Bergevin, C. Giles, and W. Neubeck, "Observation of orbital moment in nio," *Phys. Rev. B*, vol. 57, no. 13, pp. 7870–7876, 1998.
- [30] W. Neubeck, C. Vettier, V. Fernandez, F. de Bergevin, and C. Giles, "Observation of orbital moment in NiO using magnetic X-ray scattering," *J. Appl. Phys.*, vol. 85, no. 8, pp. 4847–4849, 1999.
- [31] A. P. Cracknell, "Crystal Field Theory and Magnetic Groups: Spin-Orbit Coupling," *Aust. J. Phys.*, vol. 20, pp. 189–192, 1967.
- [32] A. P. Cracknell, "Crystal Field Theory and the Shubnikov Point Groups," *Adv. in Phys.*, vol. 17, p. 367, 1968.
- [33] H. L. Schäfer and G. Gliemann, *Einführung in die Ligandenfeldtheorie*. Leipzig: Geest & Portig, 1967.
- [34] A. Freitag, V. Staemmler, D. Cappus, C. A. Ventrice Jr., K. Al Shamery, H. Kuhlenbeck, and H.-J. Freund, "Electronic surface states of NiO(100)," *Chem. Phys. Lett.*, vol. 210, pp. 10–14, 23 July 1993.
- [35] P. A. Cox and A. A. Williams, "The observation of surface optical phonons and low-energy electronic transitions in NiO single crystals by electron energy loss spectroscopy," *Surf. Sci.*, vol. 152/153, pp. 791–796, 1985.
- [36] A. Gorschlüter and H. Merz, "Localized $d-d$ excitations in NiO(100) and CoO(100)," *Phys. Rev. B*, vol. 49, pp. 17293–17302, 15 June 1994.
- [37] V. Propach, D. Reinen, H. Drenkhahn, and H. Müllerbuschbaum, "Different colors of NiO," *Z. Naturforsch. b*, vol. 33, no. 6, pp. 619–621, 1978.
- [38] R. Newman and R. M. Chrenko, "Optical Properties of Nickel Oxide," *Phys. Rev.*, vol. 114, pp. 1507–1513, 15 June 1959.
- [39] B. Fromme, M. Möller, Th. Anschütz, C. Bethke, and E. Kisker, "Electron-Exchange Processes in the Excitations of NiO(100) Surface d States," *Phys Rev. Lett.*, vol. 77, pp. 1548–1551, 19 August 1996.
- [40] B. Fromme, Ch. Koch, R. Deussen, and E. Kisker, "Resonant Exchange Scattering in Dipole-Forbidden $d-d$ Excitations in NiO(100)," *Phys. Rev. Lett.*, vol. 75, pp. 693–696, 24 July 1995.

- [41] W. C. Mackrodt and C. Noguera, "Bulk and (100) surface d→d excitations energies in NiO from first-principles Hartree-Fock calculations," *Surf. Sci.*, vol. 457, pp. L386–L390, 2000.
- [42] C. de Graaf, R. Broer, and W. C. Nieuwpoort, "Electron correlation effects on the d-d excitations in NiO," *Chem. Phys.*, vol. 208, pp. 35–43, 1996.
- [43] M. Gelejins, C. de Graaf, R. Broer, and W. C. Nieuwpoort, "Theoretical study of local electronic transitions in the NiO(100) surface," *Surf. Sci.*, vol. 421, pp. 106–115, 1999.
- [44] B. Fromme, M. Schmitt, E. Kisker, A. Gorschlüter, and H. Merz, "Spin-flip low-energy electron-exchange scattering in NiO(100)," *Phys. Rev. B*, vol. 50, pp. 1874–1878, 15 July 1994.
- [45] A. F. Wells, *Structural inorganic chemistry*. Oxford: Clarendon Press, 5 ed., 1984.
- [46] D. C. Khan and R. A. Erickson, "Magnetic Form Factor of Co^{++} Ion in Cobaltous Oxide," *Phys. Rev. B*, vol. 1, no. 5, pp. 2243–2249, 1970.
- [47] R. J. Powell and W. E. Spicer, "Optical Properties of NiO and CoO," *Phys. Rev. B*, vol. 2, no. 6, pp. 2182–2193, 1970.
- [48] G. W. Pratt, Jr. and Roland Coelho, "Optical Absorption of CoO and MnO above and below the Néel Temperature," *Phys. Rev.*, vol. 116, no. 2, pp. 281–286, 1959.
- [49] F. C. von der Lage and H. A. Bethe, "A Method for Obtaining Electronic Eigenfunctions and Eigenvalues in Solids with An Application to Sodium," *Phys. Rev.*, vol. 71, no. 9, pp. 612–622, 1947.
- [50] C. de Graaf, W. A. de Jong, R. Broer, and W. C. Nieuwpoort, "Theoretical study of the crystal field excitations in CoO," *Chem. Phys.*, vol. 237, no. 1-2, pp. 59–65, 1998.
- [51] M. Haßel, H. Kühlenbeck, H.-J. Freund, S. Shi, A. Freitag, V. Staemmler, S. Lütkehoff, and M. Neumann, "Electronic surface states of CoO(100): an electron energy loss study," *Chem. Phys. Lett.*, vol. 240, no. 1-3, pp. 205–209, 1995.
- [52] W. L. Roth, "Magnetic Structures of MnO, FeO, CoO, and NiO," *Phys. Rev.*, 1958.
- [53] Ru-Pin Pan, H. D. Wei, and Y. R. Shen, "Optical second-harmonic generation from magnetized surfaces," *Phys. Rev. B*, vol. 39, no. 2, p. 1229, 1989.
- [54] A. Dähn, W. Hübner, and K. H. Bennemann, "Symmetry Analysis of the Nonlinear Optical Response: Second Harmonic Generation at Surfaces of Antiferromagnets," *Phys. Rev. Lett.*, vol. 77, no. 18, pp. 3929–3932, 1996.

- [55] N. Bloembergen, W. K. Burns, and C. L. Tang, "Symmetry of Non-linear Optical Susceptibilities in Absorbing media and Conservation of Angular Momentum," *Int. J. Quant. Chem.*, vol. 5, pp. 555–562, 1971.
- [56] L. D. Landau, E. M. Lifshitz, and L. P. Pitaevskii, *Electrodynamics of Continuous Media*, vol. 8 of *Course of Theoretical Physics*. Butterworth-Heinemann, 2 ed., 1998.
- [57] F. P. Netzer and M. Prutton, "LEED and electron spectroscopic observations on NiO (100)," *J. Phys. C*, vol. 8, pp. 2401–2412, 1975.
- [58] S. J. Joshua, *Symmetry Principles and Magnetic Symmetry in Solid State Physics*. IOP Publishing Ltd., 1991.
- [59] W. Opechowski and R. Guccione, *Magnetic Symmetry*, vol. IIA. Academic Press: New York, 1965. ed. by G. T. Rado and H. Suhl.
- [60] R. R. Birss, *Symmetry and Magnetism*. North-Holland Publishing Company, 1966.
- [61] W. Hübner and K.-H. Bennemann, "Nonlinear magneto-optical Kerr effect on a nickel surface," *Phys. Rev. B*, vol. 40, no. 9, pp. 5973–5979, 1989.
- [62] W. Hübner, K. H. Bennemann, and K. Böhmer, "Theory for the nonlinear optical response of transition metals: Polarization dependence as a fingerprint of the electronic structure at surfaces and interfaces," *Phys. Rev. B*, vol. 50, no. 23, pp. 17597–17605, 1994.
- [63] G.P. Zhang and W. Hübner, "Femtosecond electron and spin dynamics probed by nonlinear optics," *Appl. Phys. B*, vol. 68, no. 3, pp. 495–499, 1999.
- [64] D. P. DiVincenzo and D. Loss, "Quantum computers and quantum coherence," *J. Magn. Magn. Mat.*, vol. 200, no. 1-3, pp. 202–218, 1999.
- [65] N. H. Bonadeo, J. Erland, D. Gammon, D. Park, D. S. Katzer, and D. G. Steel, "Coherent Optical Control of the Quantum State of a Single Quantum Dot," *Science*, vol. 282, pp. 1473–1476, 1998.

Zusammenfassung

Diese Arbeit ist den Erforschungen von elektronischen und magnetischen Eigenschaften der Metall-Ionen, die im Inneren und an der Oberfläche der Monoxide der Übergangsmetalle liegen, gewidmet. Die Beschreibung der Elektronenstruktur solcher Ionen basiert auf der Kristallfeldtheorie (KFT). Diese Theorie beschreibt effektiv die Systeme, dessen Verhalten sich hauptsächlich durch die stark korrelierten Elektronen der äußeren unvollständigen Schale, in diesem Fall $3d$ -Elektronen, definieren lässt. Diese Elektronen definieren nicht nur die Elektronenstruktur des Systems, sondern auch ihre magnetische Eigenschaften. Sie sind die Ursache dafür, dass die Übergangsmetalle im ferromagnetischen Zustand unterhalb der Curie-Temperatur existieren, während deren Oxide gewöhnlich eine antiferromagnetische Ordnung unterhalb der Néel-Temperatur besitzen. Es gibt zwei grundlegende Ansätze für die Beschreibung des Magnetismus: die Methode der lokalisierten magnetischen Momente und die Methode der itineranten magnetischen Momente. Die Wahl des Ansatzes hängt von der Beschaffenheit des Materials ab und ist in vielen Fällen schwer zu treffen. Die erste Methode basiert auf der Verteilung der in der Gitterzelle lokalisierten Ströme. Die gut ausgeprägten Zustände ionischen Zustände, die in vielen Experimenten gefunden wurden, gestatten uns diese Methode auf die isolierenden Übergangsmetallmonoxide anzumerken. Allerdings wurden gewöhnlich die ferromagnetischen Metalle durch die zweite Methode beschrieben, worin die Ströme von freien Elektronen getragen werden.

Die KFT wurde in vielen Lehrbüchern als Beispiel, das die Spaltung der durch Zusammenwirkung mit dem Ligandenfeld entstandenen Schichten zeigt, angesprochen. Ihre vollendete Verwirklichung ist eine komplizierte Aufgabe und erfordert ein spezielles Herangehen. In dieser Arbeit berücksichtigen wir alle Wirkungen des Kristallfeldes. Drei uns interessierte Stoffe NiO, CoO und FeO wurden im Rahmen dieser Theorie beschrieben und deren Elektronenzustände berechnet. Es werden die Ausdrücke für das durch die umgebenden Liganden gebildete Feld für die Volumen- und für die Oberflächensymmetrie ermittelt. Die Verwendung der annähernden Wellenfunktionen (Eigenfunktionen des Bahndrehimpulsoperators \hat{L} - kubische Harmonische) wurde durch die genauen Wellenfunktionen, die komplett die Hamilton'sche Matrix diagonalisieren, ersetzt. Die Winkel-Anteile der Wellenfunktionen für verschiedene Zustände sind durch die sich in äquivalenten Richtungen befindenden Liganden definiert und werden exakt berechnet. Die Elektronenlokalisierung auf den Metall-Ionen erlaubt uns die Aufgabe der Ermittlung der Radialteile von Wellenfunktionen auf die Berechnung nur weniger Integrale zu reduzieren und so die optimale Konvergenz zu den schon bekannten Energien des Systems zu erhalten. Im Fall der "wahren" Eigenfunktionen des Hamilton-Operators wird eine nichtlineare Fit-Prozedur in vielen Dimensionen erforderlich (die Dimension für jede Energieniveau ist mit der Häufigkeit des Vorkommens des Energieniveaus in der gegebenen Symmetrie für die gegebene Elektronenkonfiguration identisch). Diese Aufgabe wurde dank der Powell-Methode erfolgreich gelöst, was uns die Möglichkeit gibt, die Mehrelektronenzustände, die durch die Außenelektronen der Ionen geprägt sind, für das Volumen sowie für die Oberfläche zu berechnen. In der vorliegenden Arbeit stellen wir die Methode dar, die die Effekte der Spin-Bahn Kopplung

umfasst und die resultierende Zustände bezeichnet.

Die KFT-Beschreibung der Systeme gibt uns die Möglichkeit, experimentell zugängliche Größen zu Berechnen, was die Anwendbarkeit der Theorie bestätigt und uns einige Vorhersagen erlaubt. Um unsere Ergebnisse zu kontrollieren, verwenden wir die Resultate von KFT für die Berechnung der Antwort des Systems auf das äußere Laserfeld. Die Zusammenwirkung von Ionen mit dem Laserfeld führt zu verschiedenen physikalischen Phänomenen. Wir konzentrieren uns nur auf einer, auf die Frequenzverdopplung (SHG - Second Harmonic Generation). Der Effekt der SHG ist einer der vielen nichtlinearen Effekte, die nur im ausreichend Laserfeld entstehen. Die Bestimmung der Stärke des Feldes hängt vom Prozess ab und kann auf folgende Weise definiert sein: Ein Feld heißt stark, wenn die Prozesse, die mehr als ein Photon enthalten, während der Feldwirkung bedeutend werden. Schon aus der Definition ist klar, dass die nichtlinearen optische Effekte Informationen über das System geben, die man durch andere Methoden nicht erhält, obwohl jene spezielle experimentelle Bedingungen benötigen. So sind viele Experimente in der Lage die magnetische Phase zu bestimmen. Jedoch ist es oft unmöglich die Domänen zu identifizieren oder die Orientierung der magnetischen Momente zu bestimmen. Wir haben die Frequenzverdopplung als Beispiel, das uns solche Informationen liefert und viele Vorteile hat, ausgewählt. Erstens ist SHG eine nichtdestruktive Methode, die zur Kontrolle des Systemzustandes *in situ* benutzt werden kann. Zweitens hat ein typisches SHG-Experiment einstellbare Parameter, was genaue Informationen über die mikroskopische Eigenschaften zu erhalten ermöglicht. Je nach der Geometrie kann das ausgehende Signal durch verschiedene Tensorelemente von $\chi^{(2\omega)}$ bestimmt werden. Die optische SHG ist grenzflächenempfindlich, da in jedem Elementarprozess eine ungerade Anzahl von Photonen involviert ist. Dieses Verfahren kann auch für die Bestimmung der magnetischen Ordnung auf der Oberfläche verwendet werden. Die Symmetrie-Analyse der optischen SHG für die verschiedenen magnetischen Zustände eines Systems zeigt die starke Abhängigkeit des ausgehenden SHG-Signals von der magnetischen Struktur des Systems. Ein optisches SHG-Experiment unterscheidet verschiedene Arten des Magnetismus und in mehreren Fällen kann es magnetische Domänen sichtbar machen.

Die Symmetrie des SHG-Prozesses für die Stoffe, die unterschiedliche Kristall- und Domänenstruktur haben, lässt sich durch das wohlbekannten Neumannprinzip ermitteln. Es gibt hauptsächlich zwei Wege zur Berücksichtigung des Magnetismus. Im ersten Fall wird der Tensor in die Ordnungsparameter zerlegt, im zweiten muss die magnetische Punktgruppe gefunden werden. Die Existenz der Ordnungsparameter wurde in der Landau-Theorie der Phasenübergänge bewiesen. Diese Größe muss (1) unverändert bei allen Symmetrioperationen aus der entsprechenden magnetischen Gruppe sein und (2) verschiedene Werte für die äquivalenten Domänen haben. Der Ordnungsparameter wurde eindeutig für die Ferromagnetika definiert, für die Antiferromagnetika allerdings hat er eine sehr komplizierte Form. In solchen Fällen ist der zweite Weg wesentlich einfacher. Die Erweiterung des Neumannprinzips auf 90 magnetische Punktgruppen gelang R. Birss. Die Existenz der Zeitreversion in diesen Gruppen führt zu den verschiedenen mathematischen Formulierungen des Neumannsprinzips für *c*- und *i*-Tensoren und für die unitäre und antiunitäre Symmetrie-

operationen. Eine spezielle Aufmerksamkeit soll auf den Prozess selbst gerichtet werden, welcher statisch oder dynamisch sein kann. Im zweiten Fall wird die Zeitumkehrsymmetrie des Prozesses gebrochen und nur die unitäre Subgruppe betrachtet.

Weil die Metall-Ionen im Übergangsmetallmonoxid antiferromagnetisch geordnet sind, verwenden wir für die Ermittlung der Symmetrie des Tensors $\chi^{(2\omega)}$ magnetische Punktgruppen. Abgesehen davon, dass eine solche Analyse für die (001), (110) und (111) Oberflächen der *fcc*-Festkörper von M. Trzeciecki schon durchgeführt wurde, wurden die magnetischen Punktgruppen nicht ermittelt, da die Zeitumkehr-Operation nicht mitbetrachtet war. Man muss sagen, dass die Definition der magnetischen räumlichen Gruppen auf der Zeitinversion basiert und jede solche Gruppe eine gerade Anzahl der Symmetrieeoperationen enthält, von denen eine Hälfte unitäre Symmetrieeoperationen und die andere antiunitäre mit der Zeitumkehr beinhaltet. Die antiunitäre Subgruppe wird in der Analyse der Tensoren für die dynamischen SHG-Prozesse nicht betrachtet, aber sie muss bei der Strukturanalyse des Kristalls verwendet werden. Die Einbeziehung der Zeitumkehr in die Symmetrieanalyse erlaubt uns, die exzessive Methode der direkten Inspektion gegen die elegante Konzeption der generierten Matrizen auszutauschen. Die Formen der anderen Tensoren können leicht gefunden werden. So ist die Symmetrieanalyse der (001)-Oberfläche verallgemeinert. Da die antiunitäre Symmetrieeoperationen bei den dynamischen Prozessen keine Rolle spielen, bleiben die früher erhaltenen Ergebnisse unverändert. Die unterschiedliche Konzeptionen der Symmetrieanalyse der SHG sind verglichen und in einem ausführlichen Überblick dargestellt.

Es wurde die mikroskopische Theorie der SHG (ausgearbeitet von W. Hübner und anderen) für die Ermittlung der Tensorelemente $\chi^{(2\omega)}$ benutzt. Da die Übergangsmetallmonoxide diskrete Energiezustände haben, müssen die Parameter des Lasers dem entsprechend ausgewählt werden. Dafür haben wir die Abhängigkeit der typischen magnetischen und kristallographischen Elemente der Tensoren $\chi^{(2\omega)}$ von der Frequenz des fallenden Lichtes berechnet. Wir haben festgestellt, dass die Tensorelemente für bestimmte Frequenzen unterschiedliche Charakteristiken haben, was uns erlaubt, die SHG für die Bestimmung des magnetischen Zustandes der Oberfläche zu verwenden.

Noch eine tiefliegende Besonderheit der Übergangsmetallmonoxide ist ihr dynamisches Verhalten. Wir haben die in der KFT erhaltenen Resultate verwendet und haben versucht, die Dynamik des Systems nach der Einwirkung des Laserimpulses zu finden. In diesem Fall werden die Zustände angeregt und diese Anregungen sind zeitabhängig. Die dynamische SHG der antiferromagnetischen spektralen Linien zeigt die ultraschnelle Spindynamik. Die langanhaltende Kohärenz und die Möglichkeit der ultraschnellen (im Bereich von Femtosekunden) Änderung der Spinorientierung macht diese Materialklasse für die technologische Anwendungen (z.B. magnetische Bauelemente für eine permanente Datenspeicherung und Quantencomputer) sehr vielversprechend. Bis heute waren unter den harten Stoffen nur Halbleiter und Kernspins als Träger solcher Besonderheiten bekannt, dabei zeigten sie eine wesentlich langsamere Dynamik. Überdies besitzen die Übergangsmetallmonoxide eine hohe Dichte von permanenten magnetischen Momenten (wie auch Metalle), was die Ver-

kleinerung der Bauelementgröße ermöglicht.

Acknowledgements

Since the first day of my work as a PhD student at the Max-Planck Institute of Microstructure Physics (Halle), I have been receiving a large amount of support and inspiration from many people. Here are a few to whom I should like to deliver my special thanks.

I would like to thank Professor Jürgen Kirschner for allowing me to undertake the research for this degree.

I would also like to thank my supervisor Professor Wolfgang Hübner for all his help and support, for his creative influence, inspiration and valuable advice, and I feel very fortunate to have been one of his students. With his encouragement and guidance, I have kept on the right way.

The other members of our group, Dr. Yaroslav Pavlyukh, Dr. Ricardo Gómez-Abal, and Dr. Torsten Andersen, provided much advice and feedback on my research at different stages.

I am also grateful to all other staff at the Institute who have made my working time more pleasant.

Another very special thank you must go to my mother Nelli Ney without whom I would never have got this far. Very special thanks go to my wife, Natalia Ney, who offered her time to give me all her love and understanding.

Finally, I acknowledge the financial support provided by the Forschergruppe "Oxidische Grenzflächen" (project number 404) and Deutsche Forschungsgemeinschaft.

Publikationsliste

- M. Trzeciecki, O. Ney, G. P. Zhang, and W. Hübner, Laser-Control of Ferro- and Antiferromagnetism, *Adv. in Solid State Phys.* **41** (2001), pp.547-555.
- O. Ney, M. Trzeciecki, and W. Hübner, Femtosecond dynamics of spin-dependent SHG response from NiO (001), *Appl. Phys. B.* **74** (2002), pp.741-744

Erklärung

Hiermit erkläre ich, dass ich diese Dissertation selbstständig und ohne fremde Hilfe verfasst habe. Ich habe keine anderen als die angegebenen Quellen und Hilfsmittel benutzt. Die den benutzten Werken wörtlich oder inhaltlich entnommen Stellen habe ich als solche kenntlich gemacht.

Halle (Saale), den 07. April 2003

Oleksandr Ney

Lebenslauf

25.06.1976	geboren in Odessa, Ukraine
1983-1993	Schule in Odessa
1993-1998	Universitätsstudium an der Südkrainischen Staatlichen Universität für Pädagogik, Physikalisch-Mathematische Fakultät
1998	Masterarbeit "Influence of the intergrains interaction on mechanical properties of polycrystals"
1998	Diplom mit Auszeichnung
1998	Masterdiplom
1998-2000	Doktorandenstudium an der SUSUP
08.09.2000-2003	Doktorand am Max-Planck-Institut für Mikrostrukturphysik in Halle (Saale)